

**ANATOMICAL EVIDENCE FOR SEGREGATED PROCESSING STREAMS IN THE  
CAT'S VISUAL CORTEX**

by

**JAMIE D. BOYD**

B.Sc., Dalhousie University, 1988

**A THESIS SUBMITTED IN PARTIAL FULFILLMENT OF  
THE REQUIREMENTS FOR THE DEGREE OF**

**DOCTOR OF PHILOSOPHY**

in

**THE FACULTY OF GRADUATE STUDIES**

**NEUROSCIENCE**

**We accept this thesis as conforming to the required standard**

**THE UNIVERSITY OF BRITISH COLUMBIA**

**April 1995**

**© Jamie D Boyd, 1995**

In presenting this thesis in partial fulfillment of the requirement for an advanced degree at The University of British Columbia, I agree that the Library shall make it freely available for reference and study. I further agree that permission for extensive copying of this thesis for scholarly purposes may be granted by the Head of my Department or by his or her representatives. It is understood that copying or publication of this thesis for financial gain shall not be allowed without my written permission.

Graduate Program in Neuroscience  
The University of British Columbia  
2075 Wesbrook Place  
Vancouver, Canada  
V6T 1Z4  
Date: April 3, 1995

## ABSTRACT

Studies in primates suggest the existence of at least three separate systems operating in parallel and specialized to process information about : 1) shape; 2) colour; and 3) motion. In visual cortex, these systems are segregated into either the "blobs" staining densely for cytochrome oxidase (CO), or the less densely staining interblobs. Recent reports of CO blobs in the cat led to this investigation to determine whether CO blobs in this species also act to segregate inputs and outputs.

LGN inputs to cat V1 arise from three classes of cells, known as X, Y, and W cells. W cell input was found in different layers of areas 17 and 18 than the X and Y cell input and was localized to CO blobs but not interblobs. The Y cell input from layer C was also found to be confined to the blobs.

Area 17 has five major output pathways; to areas 18, 19, 20a, 21a, and the posterior medial lateral suprasylvian area (PMLS). In areas 17 and 18, PMLS-projecting cells were clustered within the CO blobs. Labeling from injections in PMLS was also observed in other cortical areas, and was always clustered, most notably in area 19, where clusters of labeled cells were much wider than in other areas, and often elongated in a direction perpendicular to the 18/19 border.

Large injections of tracers into area 19 labeled both blobs and interblobs in areas 17 and 18 while small injections often labeled either only blobs, or only interblobs.

Labeling of the callosal pathway, while dense and uniform at the 17/18 border, showed, at the edges of the labeling pattern in areas 17 and 18, regular fluctuations of labeling density that aligned with the CO blobs.

Together, these results provide the first demonstration of segregated visual processing streams in a non-primate species. Such an organization may be a general characteristic of mammalian visual cortical organization and not a primate specialization, as was once thought. Knowledge of these pathways in cats, a frequently used system for many developmental and physiological studies, should prove valuable.

## TABLE OF CONTENTS

Abstract.....	ii
Table of Contents .....	iii
List of Figures.....	vi
Acknowledgement .....	ix
Forward.....	x
<b>1 General Introduction.....</b>	<b>1</b>
Organization Of Parallel Visual Pathways In The Cat .....	3
Retina.....	3
Lateral Geniculate Nucleus.....	5
Primary Visual Cortex.....	6
Geniculocortical Inputs.....	6
Corticocortical Outputs .....	7
Extrastriate Visual Cortex .....	9
Organization Of Parallel Visual Pathways In Primates .....	13
Magno, Parvo, and Koniocellular Streams .....	13
Processing in Primate Extrastriate Cortex.....	14
From Enzymes to Segregated Streams .....	15
Parallel Streams in the Cat's Visual Cortex: Hypothesis .....	17
<b>2 Methods and Materials .....</b>	<b>22</b>
Surgery.....	22
Tracer Injections.....	22
Electrophysiology.....	23
Perfusion and Sectioning.....	24
Histology.....	25
Horseradish Peroxidase .....	25
Biotinylated Dextran Amine.....	25
Cholera Toxin .....	26
Cytochrome Oxidase.....	26
Data Analysis .....	27
<b>3 Laminar and Columnar Patterns of Geniculocortical Projections .....</b>	<b>29</b>
Methods and Materials.....	30
Results.....	31



	Cytochrome Oxidase Staining .....	37
	Laminar Organization of Geniculocortical Projections.....	46
	Tangential Organization of Geniculocortical Projections .....	57
	Discussion .....	58
	Laminar Pattern of Geniculocortical Terminations .....	65
	Geniculate Inputs and Cytochrome Oxidase Staining.....	66
	Relationship of C-laminae patches to Ocular Dominance	
	Columns.....	70
	Geniculocortical Projections in Area 18 .....	73
<b>4</b>	<b>Cortical Afferents to a Lateral Suprasylvian Area.....</b>	<b>76</b>
	Methods and Materials:.....	77
	Results.....	78
	Tangential organization of PMLS-projecting neurons .....	78
	Correspondence of PMLS-Projecting Cells and CO Staining .....	85
	Labeling in Other Cortical Areas .....	88
	Discussion .....	93
	Role of Y-cells in Tangential Organization of CO Blobs .....	93
	Tangential Organization of Area 18 .....	98
	LS-projecting Cells in Area 19 .....	99
<b>5</b>	<b>Organization of Cortical Afferents from Areas 17 and 18 to Area 19.....</b>	<b>100</b>
	Methods and Materials.....	101
	Results.....	102
	Both Blobs and Interblobs Project to Area 19 .....	102
	Segregation of Projections to Area 19 .....	103
	Relationship to Cytochrome Oxidase Blobs .....	114
	Intrinsic Connectivity in Area 19.....	115
	Discussion .....	124
	Are the Area 19 Connections Truly Soft Patterned? .....	124
	Segregated Processing Streams through Area 19? .....	129
	Columnar Organization of Area 19.....	132
<b>6</b>	<b>Tangential Organization of Callosal Connectivity.....</b>	<b>134</b>
	Methods and Materials.....	135
	Results.....	136
	The callosal pathway is patchy .....	136
	Uniformity and size of the zone of effective tracer uptake .....	139
	Computer reconstructions of callosally labeled cells.....	142

Distribution of callosal terminals .....	148
Callosal stripes in areas 18 and 19 .....	151
Relationship of Callosal Labeling to CO Staining.....	151
Discussion .....	154
Patchy callosal labeling at the 17/18 border.....	159
Callosal connections and CO staining in areas 17 and 18.....	160
The callosal stripes.....	161
<b>7 General Discussion .....</b>	<b>163</b>
Segregation of Pathways in Area 17: A Comparison with Primates .....	164
Comparison of Area 18 and Area 17.....	168
Continuation of Segregated Streams Through Area 19.....	169
The Organization of Inputs to PMLS .....	170
Do Functional Correlates Exist?.....	171
Conclusions and Future Directions .....	174
<b>8 References.....</b>	<b>178</b>

## LIST OF FIGURES

Figure 1.1	The arrangement of the visual cortical areas on the surface of the cerebral cortex of the cat.....	11
Figure 1.2	A tangential section through the visual cortex of a cat, stained to visualize cytochrome oxidase activity.....	20
Figure 3.1	Schematic diagram of the isoelevation map in the geniculate and how aspects of its organization were utilized to obtain topographically separated labeling from different geniculate lamina.....	33
Figure 3.2	Results from tracer studies demonstrating the mapping outlined in Figure 3.1.....	36
Figure 3.3	Laminar pattern of CO staining in areas 17 and 18.....	39
Figure 3.4	CO blobs in coronal and tangential planes of section.....	42
Figure 3.5	A series of 50 $\mu$ m thick tangential sections through area 17 stained for CO.....	45
Figure 3.6	Labeling from the A laminae in areas 17 and 18.....	49
Figure 3.7	Labeling from the C-laminae in area 17.....	51
Figure 3.8	Labeling from the C-laminae in area 18.....	54
Figure 3.9	Labeling from the parvocellular C laminae.....	56
Figure 3.10	Comparison of cytochrome oxidase blobs and C-laminae labeling in layer 3 of area 17.....	60
Figure 3.11	Comparison of cytochrome oxidase blobs and C-laminae labeling in layer 4a of area 17.....	62
Figure 3.12	Comparison of cytochrome oxidase blobs and C-laminae labeling in area 18.....	64
Figure 3.13	Diagram of the X, Y, and W pathways of the cat's visual system.....	72
Figure 4.1	Examples of injection sites in PMLS typical of those used in this study.....	80
Figure 4.2	A tangential section through area 17 showing cells retrogradely labeled from a large injection in PMLS.....	83

Figure 4.3	Computer-generated plot of PMLS-projecting cells in areas 17 and 18 .....	87
Figure 4.4	Photograph of two superimposed serial tangential sections through area 17, one reacted for CO to show the blobs and one reacted for HRP to show the patches of PMLS-projecting cells.....	90
Figure 4.5	Computer-generated plot of PMLS-projecting cells in areas 17 and 18 superimposed onto a digitally captured image of CO staining .....	92
Figure 4.6	A computer generated plot of PMLS-projecting cells labeled with CTB-Au in four alternate tangential sections.....	95
Figure 4.7	The pattern of PMLS-projecting cells in area 19 .....	97
Figure 5.1	Labeling in areas 17 and 18 from a large injection in area 19.....	105
Figure 5.2	A computer generated plot of area 19-projecting cells labeled with CTB-Au in the full one-in-two series of sections from the same experiment shown in Figure 5.1.....	107
Figure 5.3	Another example of labeling in areas 17 and 18 from a large injection in area 19.....	109
Figure 5.4	A computer generated plot of area 19-projecting cells labeled with CTB-Au in the full one-in-two series of sections from the same experiment shown in Figure 5.3.....	111
Figure 5.5	Computer-generated plots of area 19-projecting cells in areas 17 and 18 .....	113
Figure 5.6	Dark field photomicrographs of two different patterns of labeling in visual cortex following similarly-sized small, focal injections of CTB-Au in area 19.....	117
Figure 5.7	A computer generated plot of area 19-projecting cells labeled with CTB-Au in the full one-in-two series of sections from the same experiments shown in Figure 5.6.....	119
Figure 5.8	A computer generated plot showing the results of paired injections of unconjugated CTB and CTB-Au in area 19.....	121

Figure 5.9	A computer generated plot showing the results of another example of paired injections of unconjugated CTB and CTB-Au in area 19.....	123
Figure 5.10	Relationship of patches of area 19-projecting cells and CO blobs in area 17 .....	126
Figure 5.11	Relationship of patches of area 19-projecting cells and CO blobs in areas 17 and 18 .....	128
Figure 5.12	Patchy intrinsic labeling in areas 17 and 19.....	131
Figure 6.1	Callosal labeling in a tangential section through the 17/18 border region of case 1 .....	138
Figure 6.2	Labeling in the LGN at three different A-P levels following injection of WGA-HRP at the 17/18 border (case 2) .....	141
Figure 6.3	Three different representations of the same data (case 2), same scale and vertically aligned .....	145
Figure 6.4	The complete pattern of callosal labeling from case 1.....	147
Figure 6.5	Anterograde callosal labeling from a BDA injection .....	150
Figure 6.6	Retrograde labeling and CO staining from case 5 .....	153
Figure 6.7	Reconstruction of retrograde labeling for case 6 .....	156
Figure 6.8	Alignment of callosal labeling and CO staining for case 6 .....	158
Figure 7.1	A summary diagram showing the contributions of this study towards understanding the columnar organization of some of the inputs and outputs of cat visual cortical areas and a comparison with the columnar organization of some macaque monkey visual areas. ....	177

## ACKNOWLEDGMENT

I am deeply indebted to many individuals for their contribution to the work which is represented by this manuscript.

First and foremost, I thank my wife Allyson for her love, understanding, and support through it all, even the days-long separations due to the many all night experiments.

I thank my supervisor and mentor, Dr. Joanne Matsubara, whose enthusiasm (and patience) in explaining things to an undergraduate part-time technician with no neuroscience background was truly the impetus for my eventual decision to do graduate studies.

Many thanks are due to Dr. Robert Douglas for assistance with the computing and imaging facilities used in producing much of this thesis, to Dr. Nicholas Swindale for helpful discussions of various types of data analysis, and to Dr. Max Cynader for creating within the research group a positive working atmosphere with a minimum of friction and a maximum of co-operation.

Excellent technical and surgical support was provided by Virginia Booth, Michael Boyd, Eleanor To, and Jin Zhang.

Many fellow graduate students and post-doctoral fellows in the laboratory over the years have contributed to my experience here. I would like to especially acknowledge the contributions of Clermont Beaulieu, Avi Chaudhuri, Paul Finlayson, Debbie Giaschi, Qiang Gu, Yu-Lin Liu, Glen Prusky, Stuart Marlin, and Hasan Yücel.

The research presented here was supported by research grants from the Medical Research Council of Canada to Dr. Joanne Matsubara.

## **FORWARD**

The experiments described in Chapter 6 have been published in *The Journal of Comparative Neurology* (1994) **347**: 197-210.

The authors, in order, are:

Jamie Boyd and Joanne Matsubara

The contribution of each author to this publication is:

Matsubara: Provision of laboratory, supplies and insight.

Boyd: The remainder.

*"If one were to study the distribution of the efferent cortical projections from area 17, one might well suppose that ... one of its major functions might be to segregate out the information coming over the retinogeniculate cortical pathways and parcel this information out to different cortical areas for further analysis"*

(Semir Zeki, 1975).

# 1 GENERAL INTRODUCTION

In mammals, visual information is processed in several consecutive stages by a hierarchically organized group of interconnected structures: the retina, which performs the actual transformation of light energy into neural activity; the lateral geniculate nucleus (LGN), which is the main thalamic relay between the retina and the visual cortex; primary visual cortex, which receives the bulk of the inputs from the LGN; and a host of extrastriate areas, some of which receive direct inputs from primary visual cortex and all of which are richly interconnected amongst themselves. This complexly interconnected system of eyes and brain is the machinery that allows us to perceive and react to all manner of visual stimuli.

As with the study of any complex neural system, one of the goals of visual neuroscience is to learn "...what takes place along the way-how the information arriving at a certain group of cells is transformed and then sent on...." (Hubel, 1988). Hubel and Wiesel showed that the ascension through the hierarchy, from retinal ganglion cells through the LGN to striate and extrastriate cortex, was marked by increasingly complex receptive field properties and increasing specificity of neuronal responses for stimulus parameters (Hubel and Wiesel, 1962;



Hubel and Wiesel, 1965; Hubel, 1988). Although this implies a rather serial, hierarchical organization of visual pathways, each local portion of visual space is not analyzed by a single chain of neurons extending from the retina, through the LGN and striate cortex, and then through each extrastriate area in turn. Rather, multiple pathways originate at each level of the hierarchy. In cats and primates three separate, functionally distinct pathways can be traced from the retina to the LGN, and thence to the cortex; for review, see Stone et al. (1979), Sherman, (1985), and Casagrande and Norton (1991). Although information is not as complete for other species, it has been suggested that "...three pathways from the retina to striate cortex appear ubiquitous in mammals.." (Casagrande, 1994); for review, see Stone (1983). Moreover, each cortical area has connections with several other areas, so a single hierarchical sequence of visual processing cannot be identified in the cortex either (Symonds and Rosenquist, 1984a; Zeki and Shipp, 1988; Felleman and Van Essen, 1991).

It has been suggested that the individual pathways "...independently analyze different aspects of the same visual scene, and that these different analyses are combined to form the neural representation of the visual environment" (Sherman, 1985). The notion of "parallel pathways", as they have come to be called, has become a popular concept, helpful towards organizing the plethora of anatomical and physiological data recently uncovered on the visual pathways.

The cat has been used extensively as a model system for the study of visual pathways. As reviewed below, the first evidence for parallel pathways in the visual system was from electrophysiological recordings in the retina of the cat (Enroth-Cugell and Robson, 1966); the first demonstration of visual responses in an area outside of the geniculorecipient primary visual cortex was also in the cat (Marshall et al., 1943; Clare and Bishop, 1954). In light of these facts, it is somewhat surprising that relatively little is known about the organization of parallel pathways in the primary visual cortex and the extrastriate visual areas of this species. In contrast, a complex and precisely detailed organization of parallel pathways through the primary

visual cortex and extrastriate areas has been exhaustively documented in several species of primates. This leads to the following question: **"Can parallel pathways of information flow be traced through striate and extrastriate areas of visual cortex of the cat?"**

In the following paragraphs, the current knowledge of the organization of parallel pathways from the retina to the visual cortex in the cat will be reviewed. This organization will then be compared to that of primates, and the detailed organization of parallel pathways through primate extrastriate visual areas will be briefly discussed. Finally, the hypothesis will be discussed that information flow through the visual cortex of the cat may be organized into identifiable parallel pathways, as has been found to be the case in primates.

## **Organization Of Parallel Visual Pathways In The Cat**

### **Retina**

In the 1950's, Kuffler showed that the receptive fields of cat ganglion cells (the output cells of the retina) consisted of roughly circular centers and annular surrounds which had antagonistic responses to visual stimulation (Kuffler, 1953). In some cells, changes in firing rate were sustained as long as the receptive field was stimulated, while other cells responded to prolonged stimulation with only a transient burst of spikes at light onset. Enroth-Cugell and Robson (Enroth-Cugell and Robson, 1966) showed that the sustained cells, which they called X-cells, summed visual stimulation across their receptive fields in a nearly linear fashion; thus, a flickering grating of the proper spatial frequency could be so positioned that stimulation of the mutually antagonistic center and surround counterbalanced to give little or no response. For the transient cells, dubbed Y-cells, no such "null" position could be found and it was concluded that these cells summed inputs from the center and surround in a non-linear fashion.

From this beginning, a whole host of characteristics in which X-cells and Y-cells differed were discovered; for review see Sherman and Spear, (1982), Stone (1983) and

Sherman, (1985). It was found that X-cells have smaller receptive fields, and respond to higher spatial frequencies, while Y-cells have larger receptive fields and respond to lower spatial frequencies, at a given retinal eccentricity. Y-cells respond to higher velocities of a moving stimulus and with a shorter latency than do X-cells. X-cells are relatively more concentrated in the area centralis versus the periphery than Y-cells. X-cells and Y-cells have different morphologies as well. Y-cells correspond to the alpha class of retinal ganglion cells and are characterized by larger soma size, thicker axon, and a more widespread dendritic arborization than the X-cells, which correspond to the beta class of ganglion cells. Both cell types project to the LGN.

It has been suggested that X- and Y-cells are concerned with different aspects of visual processing, with X-cells being well suited for visual tasks requiring high acuity, and Y-cells being more fit for the detection of visual motion. This dichotomy between X- and Y-cells was the first example of parallel processing in the visual system. As will be seen, this theme of a "division of labor" is repeated at all levels in the visual system.

Not all ganglion cells in the cat retina could be classified as X-cells or Y-cells. Some cells lacked a concentric center-surround receptive field organization and often had unusual requirements for effective stimulation; again, see Sherman and Spear (1982), Stone (1983) and Sherman (1985), for review. All of these cells, termed W-cells, responded more slowly than X- or Y-cells, and had more slowly conducting axons. This heterogeneous class of cells included: cells with continuously maintained activity that were suppressed by contrast of any sign; cells that preferred a contrasting border of a size smaller than the receptive field; cells with a preferred direction of movement. Several different morphological classes corresponding to different subtypes of W-cells have been described as well. What aspect of visual processing these cells might be specialized for is not clear, but W cells of all kinds make up at least 20% of all retinal ganglion cells, and, as will be shown, their projections can be traced through several levels of the visual system.

### Lateral Geniculate Nucleus

The LGN is the principle thalamic relay between the retina and the visual cortex; see Stone et al. (1979), Sherman (1985) and Casagrande and Norton (1991) for review. There does not appear to be a great deal of elaboration of visual receptive field properties at the level of the LGN; rather, the same classes of X-, Y, and W-cells encountered in the retina are also found in the LGN. Thus, the three parallel streams of information that originate in the retina are maintained in the LGN.

The LGN in most mammals is a laminated structure, with different laminae receiving input from either the contra- or ipsilateral eye, and/or containing cells of different receptive field class. In the cat LGN, X-, Y-, and W-cells are only partially segregated into different lamina. The two largest geniculate layers, layers A and A1, contain a mixture of X and Y cells and receive inputs from the contra- and ipsilateral eye, respectively. Electrophysiological studies show that there is little or no convergence of X- and Y-retinal cells onto the same cells in the LGN (Cleland et al., 1971; Hoffmann et al., 1972).. Thus, although X- and Y-cells are intermingled spatially in these layers, they are kept functionally distinct by virtue of their different patterns of synaptic connectivity. The C layers, ventral to the A layers, can be subdivided into an upper, magnocellular division (layer C) containing both Y and W cells, and a lower, parvocellular division (layers C1 and C2) containing mostly W cells (Guillery, 1970; Hickey and Guillery, 1974; Guillery and Oberdorfer, 1977). Cats and other carnivores also possess a medial interlaminar nucleus (MIN) adjacent medially to the LGN, which contains mostly Y-cells, with W-cells in the lower part of the nucleus, adjacent to the W cells in layers C1 and C2 of the LGN (Kratz et al., 1978; Dreher and Sefton, 1979; Rowe and Dreher, 1982).

As in the retina, there are anatomical correlates of the X-, Y-, and W-cell classes shown physiologically (Friedlander et al., 1979; Friedlander et al., 1981). Y-cells are larger than X-

cells, and possess many stout, radially arranged dendrites that may cross laminar boundaries. X-cells, on the other hand, are smaller and have fewer, thinner dendrites that are more restricted spatially. W-cells have the smallest cell bodies in the LGN, but can have extensive dendrites; often these are arranged parallel to the thin C laminae in which these cells are found (Hitchcock and Hickey, 1983; Stanford et al., 1983; Raczkowski et al., 1988).

## **Primary Visual Cortex**

### **Geniculocortical Inputs**

X-, Y-, and W-cells in the LGN project to the visual cortex. Circuitry within the cortex produces novel physiological classes of cells from these LGN inputs. The two main categories of cells in primary visual cortex, termed simple and complex (Hubel and Wiesel, 1962), can be differentiated from LGN cells by the fact that they respond best to slits of light of a particular orientation. The simple cell has separate on- and off- subfields with summation within each subfield and antagonism between adjacent subfields. Complex cells differ from simple cells in not having separate on- and off-subfields. Simple cells are found most commonly in cortical layers 4 and 6, the layers that receive the bulk of the inputs from the LGN, while complex cells are found most commonly outside of layer 4 (Gilbert, 1977; Bullier and Henry, 1979a; Bullier and Henry, 1979c; Bullier and Henry, 1979b). It should be noted that there are different subclasses of simple and complex cells, and that these can correlate with laminar position; see Henry (1988) for review.

In the cat, it is not completely clear whether inputs from the three classes of cells in the LGN are kept separate in the visual cortex, or at what stage they might be integrated. There is some physiological evidence, mainly differences in latency, suggesting that simple cells in the visual cortex that are monosynaptically activated from the LGN receive inputs from either X- or

Y-cells, but not from both. Anatomically, however, different classes of LGN terminations are only partially segregated into separate layers of the cortex. Thus, in area 17, intracellular fills of single, physiologically characterized LGN afferents have shown that, while Y afferents are mostly confined to the upper half of layer 4, X afferents terminate throughout the depth of this layer (Freund et al., 1985; Humphery et al., 1985a; Humphery et al., 1985b). Both X and Y axons make collaterals to layer 6. In area 18, where X afferents are rare or absent, Y afferents terminate throughout the depth of layer 4, but still appear to terminate most heavily in the upper part of the layer (Humphery et al., 1985b; Friedlander and Martin, 1989).

No W afferents have been intracellularly filled, probably due to their smaller axonal diameter. Bulk injections of tracers in the C layers of the LGN, which contain both Y and W cells, resulted in labeling at the layer 3/4 and the layer 4/5 borders in area 17 and throughout layer 4 in area 18 (LeVay and Gilbert, 1976). The projection of the C-layers to layers 3 and 5, but not layer 4, of area 17 was also suggested by small injections of tracers restricted to individual cortical layers (Leventhal, 1979). Interestingly, LeVay and Gilbert noted that the labeling from the C laminae had a patchy distribution in the cortex, being present in some cortical columns but not others, suggesting that there may be a tangential, as well as a laminar, segregation of the different classes of geniculate inputs.

### Corticocortical Outputs

In addition to the parallel inputs from the X, Y, and W-cell classes of geniculate cells, area 17 has multiple parallel outputs to other visual cortical areas (Symonds and Rosenquist, 1984a). These include areas 18, 19, 20, 21, and the posterior medial lateral suprasylvian area (PMLS). With few exceptions, each projection neuron in area 17 targets a single visual area, and populations of cells projecting to the individual extrastriate areas have unique laminar or sublaminar distributions, (Symonds and Rosenquist, 1984b; Salin, 1989; Einstein and Fitzpatrick,

1991). This suggests that different information is being sent in parallel to each of the extrastriate visual areas.

Another feature of these corticocortical connections which may suggest the existence of parallel pathways from area 17 is that many of these connections are patchy. That is, a single injection of a tracer substance into an extrastriate area gives rise to multiple, separate patches of labeling in area 17 (see review by LeVay and Nelson (1991)). As described by Ferrer *et al.* (1988), there are at least two different ways by which patchy connections may be generated. The first way involves the whole extent of an area taking part in the connection, with any single small site in this area connecting to multiple separate sites in the target area. The second means by which patchy connectivity could be organized is with the distribution of cells projecting to a particular area in a genuinely discontinuous or uneven fashion. In order to distinguish this type of organization from the first, the injection site must be made larger than the divergence of the projection being investigated; if the labeled cells are no longer patchy, then the projection is not truly discontinuous. These two types of patchiness have been termed "soft-patterning" and "hard-patterning," respectively (Shipp and Grant, 1991).

In general, patchiness of a projection has been thought to reflect a specificity for some property that varies tangentially in a columnar fashion across the surface of the cortex. For instance, the projection from area 17 to area 18 has been shown to connect sites with the same orientation (Gilbert and Wiesel, 1989). Thus, the patches of labeling in area 17 following a small injection in area 18 must represent orientation columns matching that of the column injected in area 18. If orientation was the only variable governing the connectivity between these two areas, then when the injection site in area 18 is made large enough to cover a full range of orientation columns, the labeling in area 17 would be continuous. That this does not happen (Ferrer *et al.*, 1988) indicates that, in addition to orientation selectivity, some other variable that changes in a regular fashion across the surface of the cortex is governing the connectivity between area 17 and area 18.

In addition to the projections of area 17 to area 18, projections from area 17 to area 19 and to area PMLS have also been shown to be hard-patterned (Shipp and Grant, 1991; Ferrer et al., 1992). What variable might differ between projecting and non-projecting columns of area 17 is unknown, and it cannot be assumed that the same variable is involved in each of these projections. No connections between visual areas in the cat have been shown definitively to be soft-patterned. This is likely because most of the connections between visual cortical areas of the cat have only been examined using relatively small injections of tracers, so it is not known whether they are soft-patterned or hard-patterned.

### **Extrastriate Visual Cortex**

At least 19 retinotopically organized extrastriate visual areas have been described in the cat (Rosenquist, 1985; Updyke, 1986). Figure 1.1 shows the organization of visual areas on the surface of the cat's cerebral cortex, adapted from a summary of the work of Tusa and colleagues (Tusa et al., 1981). The boundaries of the visual areas shown in this figure are only approximate because of inter-animal variability, which is relatively minor for areas 17 and 18, but is likely greater for some of the extrastriate areas. Many of these areas have not been mapped extensively, and their boundaries (and even, in some cases, their very existence) are not agreed upon by all investigators (Sherk, 1988). Nevertheless, there is evidence that each of these areas has a different pattern of connections with subcortical nuclei and other cortical areas (Graybiel and Berson, 1981; Updyke, 1981; Raczkowski and Rosenquist, 1983; Symonds and Rosenquist, 1984a; Harting et al., 1992). Although few of these extrastriate areas have been closely examined physiologically, it would appear that differences also exist in the neuronal response properties for at least some of these areas. The PMLS, for example, responds well to rapidly moving stimuli and contains a high percentage (at least 80%) of neurons selective for direction of



Figure 1.1. Arrangement of the visual areas on the surface of the cerebral cortex of the cat. **A** shows the brain of a cat from a dorsal-lateral view. The approximate boundaries of the different visual cortical areas with respect to sulcal and gyral patterns, as obtained from (Tusa et al., 1981), are marked by dashed lines. Many of the visual areas are partially or completely hidden within the lateral sulcus (Lat) or the suprasylvian sulcus (SS). AMLS: Anterior Medial Lateral Suprasylvian area. ALLS: Anterior Lateral Lateral Suprasylvian area. PMLS: Posterior Medial Lateral Suprasylvian area. PLLS: Posterior Lateral Lateral Suprasylvian area. VLS: Ventral Lateral Suprasylvian area. DLS: Dorsal Lateral Suprasylvian area. PS: Posterior Suprasylvian area. The solid line shows the cuts that were made to remove a block of cortex similar to the one from which the section in **B** was taken. **B** shows a section through a block of cortex, as shown in **A**, that was unfolded, flattened, and sectioned tangentially. This section was stained for cytochrome oxidase, which stains densely through layer 4 of areas 17 and 18. The darkly stained oval corresponding to areas 17 and 18 is interrupted by a cut which was made to relieve the intrinsic curvature of the cortex while flattening. Approximate boundaries of cortical areas were marked with dashed lines as in **A**., using the maps of Tusa et al. (1981). The lips and the fundi of the lateral and the suprasylvian sulci are shown; the hatched areas correspond to the areas which were buried within these sulci prior to unfolding and flattening. Cortical areas buried within the sulci, such as the lateral suprasylvian areas, are now visible.

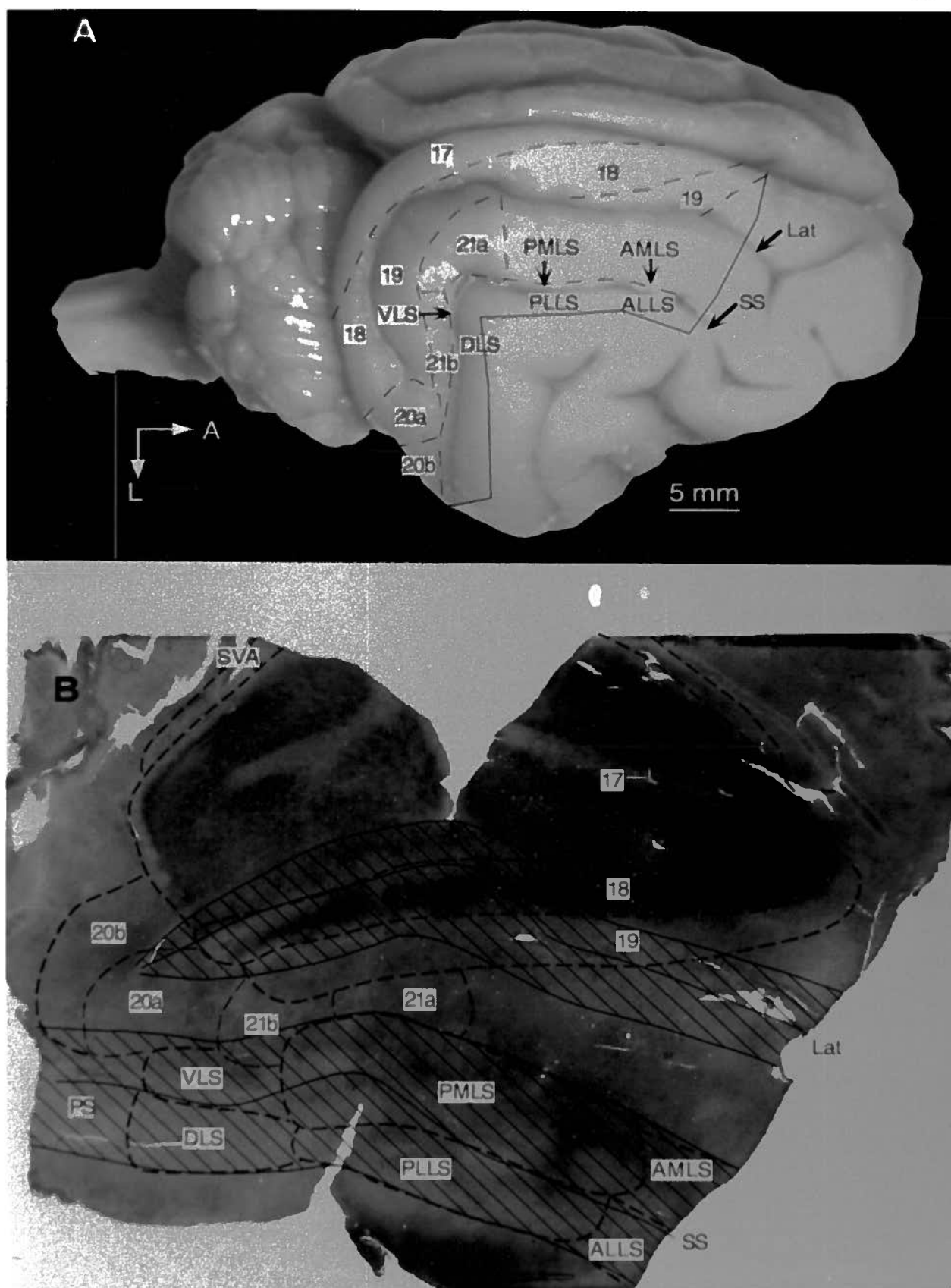


Figure 1.1

stimulus motion (Hubel and Wiesel, 1969b; Spear and Baumann, 1975; Camarda and Rizzolatti, 1976; von Grünau et al., 1987; Zumbroich and Blakemore, 1987) This physiological data, in addition with the facts that this area receives projections from area 17, 18, and 19, (Hubel and Wiesel, 1969b; Symonds and Rosenquist, 1984a; Sherk, 1986; Shipp and Grant, 1991) indicates that PMLS may be part of a processing stream important in the discrimination of moving stimuli.

In the extrastriate area 21a, on the other hand, only about 30% of neurons are direction selective, which is less than the percentage of direction selective neurons found in area 17. In addition, area 21a neurons have been shown to respond poorly to fast-moving stimuli (Wimborne and Henry, 1992; Dreher et al., 1993; Toyama et al., 1994), again unlike the cells in PMLS. Cells in this area do, however, possess orientation tuning that is sharper than in PMLS, even as sharp as is found in area 17 (Dreher et al., 1993).

Sensitivity to binocular retinal disparity is another response parameter that can differ between extrastriate areas. Cells in area 21a, for instance, have been tested and found insensitive to retinal disparity (Wieniawa-Narkiewicz et al., 1992), while disparity sensitive cells are not uncommon in area 19 (Guillemot et al., 1993). This property does not appear to have been tested in area PMLS. If the properties of these areas reflect the properties of their corticocortical inputs, these findings suggest that the different populations of cells projecting from primary visual cortex to these extrastriate areas may, indeed, be transmitting different information.

Are the segregated retinogeniculocortical pathways to visual cortex matched by a series of segregated parallel output pathways from primary visual cortex and terminating in different extrastriate visual cortical areas? It is just such a series of segregated input and output pathways that has been so well described in another mammalian group, the primates. Unlike cats, or any other mammalian group, for that matter, processing streams through primary visual cortex and extrastriate areas have been extensively studied in primates. Thus, when setting out to study the organization of parallel pathways in cats, the only mammalian system available for comparison is

the primate. For this reason, the organization of parallel pathways in primates will be reviewed and compared to what is currently known for the cat.

## **Organization Of Parallel Visual Pathways In Primates**

### **Magno, Parvo, and Koniocellular Streams**

As does the cat, the primate visual system contains three parallel pathways that begin at the retina and remain segregated until at least the first synapse in primary visual cortex. Parasol cells (magnocellular-projecting, or M-cells) are among the largest retinal ganglion cells, with widespread dendritic fields and thicker axons, while midget cells (Parvocellular-projecting or P-cells) have more restricted dendritic fields and narrower axons (Leventhal et al., 1981; Rodieck et al., 1985). M-cells have larger receptive fields, respond well to rapidly moving targets, and have transient responses to visual stimuli, while P-cells have smaller receptive fields, are sensitive to wavelength, respond poorly to rapidly moving targets, and have sustained responses to visual stimuli (Gouras, 1968; Gouras, 1969; DeMonasterio and Gouras, 1975). For a review of the physiology of primate retinal ganglion cells, see Rodieck and Brening (1983), and Kaplan (1991). As in the cat, the physiological types first generated in the retina are maintained in the LGN. Axons from M-cells and P-cells segregate into the two ventral, large cell (magnocellular, M) and the four dorsal, small cell (parvocellular, P) layers, respectively; see Casagrande and Norton (1991) for review. There is also a third class of LGN neurons, found in the smallest celled layers of the LGN, which may be ventral to the magno layers, or intercalated between the main layers of the LGN, depending on the species (Casagrande, 1994). These koniocellular (K) layers receive input from a separate class of cells possessing the smallest caliber retinal axons (Lachica and Casagrande, 1988; Rodieck, 1992); their physiology is also different from the magno and parvo layers, at least in the galago, the only primate species in which they have been

studied physiologically (Irvin et al., 1986). The segregation of the M, P, and K pathways continues in the striate cortex, where axons from the M and P layers terminate in different sublayers of layer 4 (Hubel and Wiesel, 1969a; Blasdel and Lund, 1983; Fitzpatrick et al., 1983), while the K pathway terminates within patches in layer 3 (Fitzpatrick et al., 1983; Livingstone and Hubel, 1987c). Thus, the general principles of organization of parallel pathways from the retina first described in the cat can also be identified in primates. In fact, segregation of the M, P and K pathways in the LGN and primary visual cortex is, spatially if not functionally, substantially more pronounced in primates than is the segregation of the W, X and Y pathways in the cat.

### **Processing in Primate Extrastriate Cortex**

In primates, as in cats, there are multiple extrastriate visual areas (certainly more than 20 in the macaque and the owl monkey, but the exact number is unclear) (Sereni and Allman, 1991; Felleman and Van Essen, 1991). Also as in cats, primary visual cortex (V1) has multiple major projections (to V2, V3, V4, and the mid-temporal area, MT), as well as minor projections to other areas. As in the cat, cells almost always project from primary visual cortex to a single extrastriate area, and cells projecting to different areas can be segregated into different layers and columns (Maunsell and Van Essen, 1983; Van Essen and Maunsell, 1983; Felleman and Van Essen, 1991). As first argued by Zeki in the 1975, "It would be difficult to imagine that the same small region of V1 sends identical signals to these different, functionally specialized, visual areas in these independent and parallel pathways" (Zeki, 1993). Thus, a crucial role of V1 is to direct the flow of different types of visual information to more specialized extrastriate visual areas. It has also been shown that area V2 of primates receives projections from all of the processing streams in V1 and that it too has segregated connections to specialized extrastriate

areas (Livingstone and Hubel, 1983; Livingstone and Hubel, 1984; Livingstone and Hubel, 1987a).

Clues to the specializations of the multiple processing streams from V1 to extrastriate areas were first gained by examination of the physiological specializations of the different extrastriate areas, themselves. Primate extrastriate visual cortex has the advantage of an extensive record of anatomical and physiological investigation, and functional specializations of different areas have been well documented. For a review of the functional organization of primate visual cortex, see Zeki (1993). Two areas in particular have received a great deal of attention. In an extrastriate area of the temporal lobe, the mid temporal area (MT), all of the cells are sensitive to motion, and over 90% are selective for a particular direction of motion (Albright, 1984; Girard et al., 1992; Zeki, 1974). Conversely, responses of cells in MT contain little information about stimulus color; a spot moving in the preferred direction could be black or white or any color against a background of any other color, and still be an effective stimulus for driving the cell. In the extrastriate area V4, on the other hand, most cells are color selective, in that they respond better to some wavelengths of light than to others (Zeki, 1973; Zeki, 1977; Desimone and Schein, 1987; Schein and Desimone, 1990). Together, the two areas make the best argument for a division of labor among extrastriate cortex, with different areas undertaking different tasks in parallel. As differences in receptive field properties in V4 and MT were likely a reflection of differences in their afferent input coming from V1 and V2, they provide indirect evidence as to what functions are being segregated by the anatomically-distinct processing streams through V1 and V2.

### **From Enzymes to Segregated Streams**

As in the cat, the connections of the various primate visual areas are patchy. In the cat, the difficult process of divining the relationships among these pathways has, for the most part,

not been attempted; in contrast, the spatial relationships between many of the patchy projections from primate areas V1 and V2 have been well established. A great aid to the establishment of these relationships was the discovery, originally by Margaret Wong-Riley (Hubel, 1988) of a discontinuous distribution within V1 and V2 of the metabolic enzyme cytochrome oxidase (CO) (Horton and Hubel, 1981; Humphery and Hendrickson, 1983; Horton, 1984). CO staining provided a needed system of cortical landmarks with which to compare the different distributions of labeling and also electrophysiological response properties. For a review of CO staining in primate visual cortex, see Wong-Riley (1994).

In V1, histochemical staining for this enzyme in layers 2 and 3 shows patches of dense staining, also known as blobs, which colocalize with the patchy koniocellular geniculate input (Fitzpatrick et al., 1983; Livingstone and Hubel, 1987c). The magno and parvo geniculate input zones of layer 4 are labeled densely and continuously. In V2, CO-rich compartments form an alternating cycle of thick and thin stripes separated by pale stripes (Tootell et al., 1983). These stripes extend across the thickness of V2, roughly at right angles to the V1/V2 border. The blobs of V1 and the thin stripes of V2 are interconnected, as are the interblobs and interstripes (Livingstone and Hubel, 1983; Livingstone and Hubel, 1984), while the thick stripes receive input from layer 4B of V1 (Livingstone and Hubel, 1987a). The thick stripes of V2 project to MT, while the thin stripes and interstripes project to V4 (DeYoe and Van Essen, 1985; DeYoe et al., 1990). The CO system thus marks processing streams originating in V1, passing through separate columns in V2, and terminating in V4 or MT (DeYoe and Van Essen, 1988).

It has often been pointed out (Martin, 1988) that the enzyme cytochrome oxidase is a very general metabolic enzyme found in different levels in all parts of the body. It does not appear to have a specific role in visual processing, but has only been used as an opportunistic marker. Nevertheless, it is easy to imagine how difficult the demonstration of such intricate patterns of connectivity would be if no simple marker for the various columns had existed. For

instance, the question of hard-patterning versus soft-patterning can be answered without the use of very large injections; if injections in one area (like MT) always produce labeling in the same CO compartment (thick stripes in V2), then that projection is hard patterned. (It is noteworthy that the terms "hard-patterned" and "soft-patterned" were coined for use in describing labeling patterns in cats, i.e., connectivity in the absence of CO architecture). Similarly, CO staining allowed the relationship between a column's inputs and its outputs (e.g., inputs from layer 4B and outputs to MT for thick CO stripes) to be demonstrated without the need for comparing labeling from multiple tracer injections in a single animal (for the example given above, one tracer in MT to label the thick stripes, and a different tracer in V2).

### **Parallel Streams in the Cat's Visual Cortex: Hypothesis**

Before the demonstration of parallel processing streams through primate visual areas V1 and V2, their existence was postulated by Semir Zeki based on several principles then known about visual cortical organization (Zeki, 1975). These were: the multiple inputs to V1 from the different LGN cell classes; the multiple outputs from V1 to the various extrastriate areas; the functional differences between the different extrastriate areas; and the divergent connections between visual areas. It is important to note that Zeki's hypothesis remained unproved (and untested) until CO staining provided a set of anatomical landmarks with which to correlate it. This has implications for the demonstration of similar organizations in other cortical systems.

As has been reviewed in the preceding paragraphs, the visual system of the cat possesses all of the organizational motifs that prompted Zeki's hypothesis of parallel processing streams: multiple inputs from X, Y, and W LGN cells; multiple outputs of area 17 to extrastriate areas 18, 19, area 21a and PMLS; physiological differences between extrastriate areas; and patchy connections of area 17 to extrastriate areas. However, the visual cortex of the cat has, until



recently, been described as lacking CO architecture (Horton, 1984). It is not surprising, then, that the segregation of connectivity and physiology characterized in the visual cortices of primates has not been shown in the cat. As CO is used merely as an opportunistic marker, it seems possible that segregated patterns of connectivity could exist in the visual cortex of other species "cryptically" without an attendant patchy pattern of CO staining to draw attention to it.

While these arguments were being developed, it was reported that CO blobs are, in fact, present in area 17 of cats (Murphy et al., 1990). By unfolding and flattening the cortex and cutting sections tangential to the cortical surface, it was possible to show patterns in CO labeling that were not apparent in sections cut in the coronal plane. An example of these blobs in a tangential section of cat visual cortex stained for CO is shown as Figure 1.2. Therefore, it was of great interest to compare the organization of corticocortical and geniculocortical labeling with the organization of CO blobs in the cat.

In this thesis, the relationship of CO staining to geniculocortical and corticocortical pathways is examined. Chapter 3 deals with inputs from the LGN; Chapter 4 with corticocortical projections to PMLS; Chapter 5 with projections to area 19; and Chapter 6 with the callosal projections of areas 17 and 18. A close relationship was found between the CO blobs and patterns of geniculocortical inputs and corticocortical outputs. Two components of the visual system known to be related to the Y-cell and/or W-cell stream, the C-layers of the LGN and PMLS, are connected preferentially with the CO blobs. Inputs from blob and interblob regions remain segregated within area 19, and output from this area to PMLS is also segregated. Callosal connections extended farther from the vertical meridian representation in CO blobs than in interblobs.

These results argue for a segregation of processing stream(s) within the CO blobs, and continuing through certain columns in area 19 and into the PMLS. These results are consistent with the notion that parallel pathways of information flow from the retina through to extrastriate areas in the visual system of the cat. It is concluded that different input and output pathways of




Figure 1.2. A tangential section through the visual cortex of a cat, stained to visualize cytochrome oxidase activity. The dashed outline indicates the extent of areas 17 and 18. The arrowheads mark the bottom of the lateral sulcus, which, at this AP level, marks the lateral border of area 19. Due to residual curvature in the cortical tissue present after flattening, the plane of section passes in an irregular fashion through the different cortical layers. Layer 3 is pale, and the blobs are not visible, or only faintly visible towards the bottom of the layer. Layer 4 stains darkly; the blobs are most visible in the upper part of layer 4. Scale bar: 5 mm.

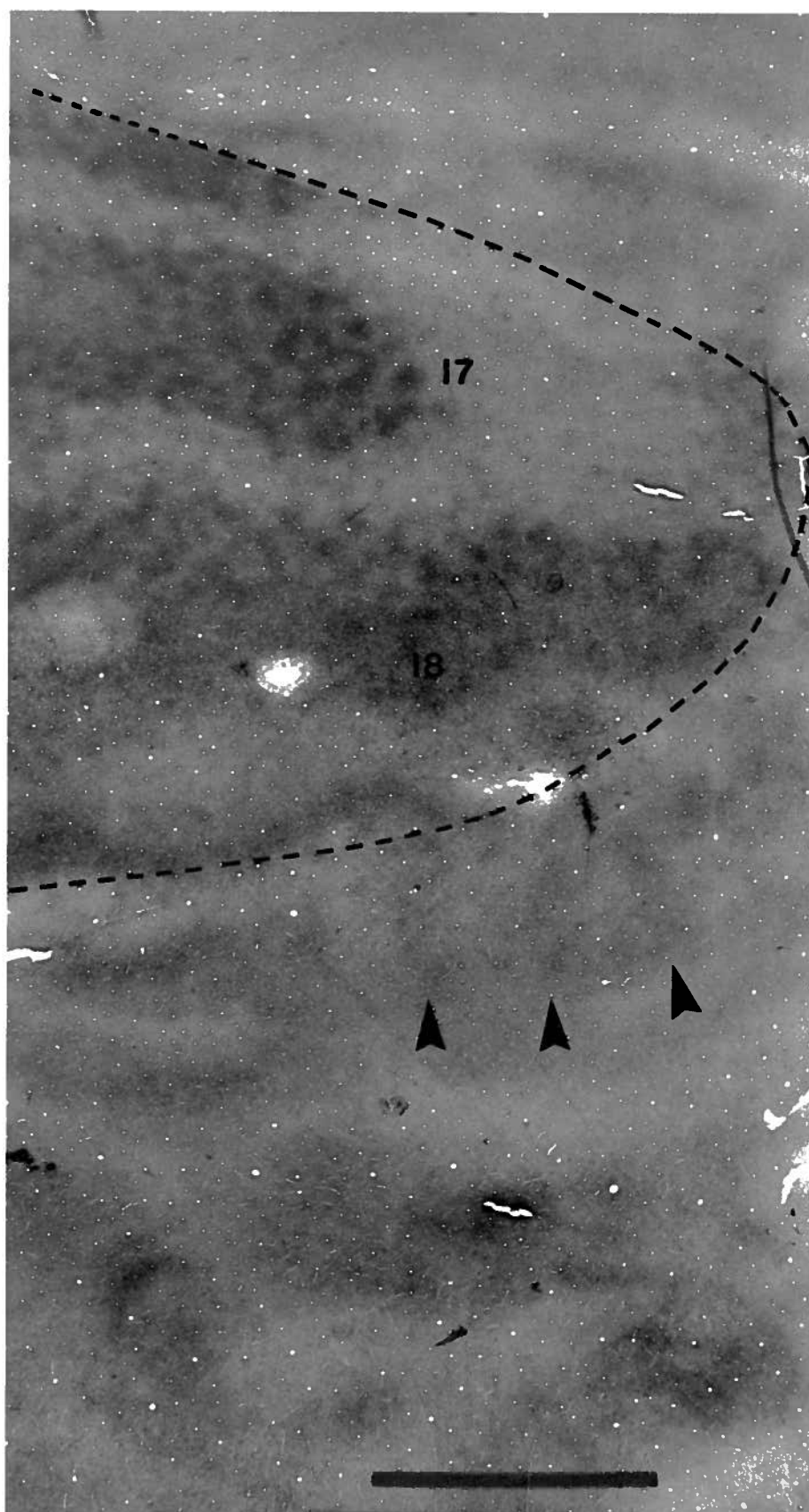


Figure 1.2

the cat's visual cortex are segregated in accordance with the general principles in which pathways are segregated in primates. These data show that parallel processing in the visual cortex is not specific to primates and suggest that it is, instead, a general principle of visual cortical organization that will likely be extended to other mammals as they have herein been extended to cats.

## **2 METHODS AND MATERIALS**

Many aspects of the experiments reported in subsequent chapters utilize similar techniques for the injection of tracers into LGN or visual cortex, and the subsequent histology to visualize the tracers. Therefore, procedures common to the various experiments have been gathered into one chapter. Only details which vary from experiment to experiment, such as tracer injected, number of animals used, location of injection, and survival time will be reported in the individual chapters.

### **Surgery**

#### **Tracer Injections**

In all of these experiments, adult cats of both sexes were used. Prior to surgery, animals were given a mixture of 0.5mg/kg acepromazine maleate (atravet; M.T.C. Pharmaceuticals) and 0.05 mg/kg atropine sulfate (M.T.C. pharmaceuticals) i.m. as a preanaesthetic. Animals were also given 0.1 mg/kg dexamethasone (Austin Laboratories) i.m. to reduce brain edema. Anesthesia was induced by sodium methohexital (Brietal; Eli Lilly Canada, Inc) i.v. and maintained by trifluoroethane (halothane; M.T.C. Pharmaceuticals) inhalation through an endotracheal tube. Expired CO<sub>2</sub> and EKG were continuously monitored. Animals were positioned in a stereotaxic frame and the site of the incision was injected with 3-5 ml of a long lasting local anesthetic, 0.25% bupivacaine hydrochloride (Marcaine; Winthrop Laboratories).

Under sterile surgical conditions, craniotomies and duratomies were performed over the relevant areas using the appropriate stereotaxic coordinates from the work of Tusa and coworkers (Tusa et al., 1981). Injections of tracers were made with micropipettes of tip diameter 10-20  $\mu\text{m}$ . Volume was calculated by measuring, with a dissecting microscope and eye-piece micrometer, the drop in the meniscus following application of a brief pulse of positive air pressure.

At the conclusion of the injections, the craniotomy was packed with saline soaked gelfoam, and the fascia and skin overlying the wound were sutured. The animals were then given antibiotics (Durapen, 0.2 cc/Kg) and allowed to recover from the anesthesia.

### **Electrophysiology**

For the injection of tracers into the LGN, it was necessary to first localize the injection sites using electrophysiology. The surgical procedures for these animals thus differed from the other experiments. Before surgery, animals were given a mixture of 0.5mg/kg acepromazine maleate (Atravet; M.T.C. Pharmaceuticals) and 0.05 mg/kg atropine sulfate (M.T.C. Pharmaceuticals) i.m as well as 0.05 mg/kg dexamethasone (Austin Laboratories) i.m. Anesthesia was maintained during surgery by sodium methohexital (Brietal; Eli Lilly Canada, Inc.) i.v. The sites of all incisions were injected with 3-5 ml of a long lasting local anesthetic, 0.25 % bupivacaine hydrochloride (Marcaine; Winthrop Laboratories). The saphenous vein was cannulated and a tracheotomy was performed. The animal was then positioned in a stereotaxic frame and a craniotomy and duratomy was performed.

After all surgery was completed, the animal was paralyzed with gallium triethiodide and artificially respired with a 70:30 mixture of nitrous oxide and oxygen. The animal was infused with 10 mg/kg/hr gallium triethiodide and 1.0 mg/kg/hr sodium pentobarbital dissolved in 5% dextrose in lactated Ringer's solution. The EEG and EKG were monitored and the end-tidal

pCO<sub>2</sub> was maintained near 4%. Contact lenses were inserted having 4 mm artificial pupils and the appropriate refractive power to focus the eyes on a tangent screen 1.3 m away.

Electrophysiological recording using glass insulated platinum-iridium electrodes (resistance 0.5-1.0 MW) was used to find the ipsilateral and contralateral eye layers of the LGN. Visual stimuli (bright spots 1-10° diameter on a dark background) were generated with a computer driven projector and neuronal responses were bandpass-filtered to remove 60 Hz noise. Signals were then amplified and displayed on an oscilloscope and an audio monitor. After the C-laminae were identified by observing reversals in eye dominance of evoked responses, the metal electrode was replaced with a glass pipette containing 2% WGA-HRP in saline. Electrical recordings could also be obtained through the glass pipette. Although no single units could be isolated, the background multi-unit "hash" showed clear shifts in eye dominance so that the position of the injection could be re-verified. When the appropriate injection site was found, polyethylene tubing was attached to the back of the pipette and air pressure from a syringe was used to inject 0.1 to 0.5 ml of tracer.

### **Perfusion and Sectioning**

After appropriate survival times, animals were euthanized with an overdose of barbiturate. They were then perfused through the aorta with 1500 ml phosphate buffer (0.1 M, pH 7.2 with 0.5% sodium nitrite), followed by 400 ml 0.25% glutaraldehyde and 4% paraformaldehyde in phosphate buffer delivered over 5-7 min by means of a perfusion pump.

In some experiments, visual cortex was sectioned coronally after cryoprotection in 30% sucrose. In other experiments, visual cortex was removed from the brainstem, unfolded and flattened before sectioning (Olavarria and Van Sluyters, 1985). The flattened cortex was then pressed between glass slides, left for several hours in 4% paraformaldehyde and 25% sucrose in

phosphate buffer, and then left overnight in 25% sucrose. A block of tissue through the posterior thalamus containing the lateral geniculate nucleus from each animal was also postfixed and cryoprotected with the same solutions.

Tangential sections of the visual cortex were cut at 50 $\mu$ m on a freezing microtome, while coronal sections were cut at 50 or 75 $\mu$ m. Coronal sections through the posterior thalamus were cut at 100  $\mu$ m.

## **Histology**

### **Horseradish Peroxidase**

Wheatgerm agglutinin-conjugated horseradish peroxidase (WGA-HRP; Sigma) was used as a 1-2% solution dissolved in sterile saline. Sections from experiments using WGA-HRP were processed by the standard tetramethylbenzidine (TMB) method (Mesulam, 1978) sometimes followed with stabilization in chilled ammonium heptamolybdate and cobalt-diaminobenzidine (Horn and Hoffman, 1987). Unstabilized sections, whether coronal or tangential, were always counterstained for Nissl substance with neutral red; stabilized sections were sometimes counterstained with cresyl violet.

### **Biotinylated Dextran Amine**

Biotinylated dextran amine (BDA; Molecular Probes, Inc) was used as a 10% solution in 0.9% saline. Sections from the BDA experiments were incubated for 48 hours in avidin-horseradish peroxidase (Vector Laboratories; 0.5% in 0.1 M phosphate buffer, pH 7.2), rinsed in



buffer, and then processed to visualize peroxidase activity with nickel and cobalt intensified diaminobenzidine (DAB) (Adams, 1981).

### **Cholera Toxin**

Cholera toxin subunit B, either unconjugated (CTB) or conjugated to 7nm colloidal gold particles (CTB-Au; List Biological) was used as a 1% solution in 0.9% sterile saline. CTB-Au was visualized by silver intensification (Jannsen IntenSE M) with incubation times ranging from one to two hours. Unconjugated CTB was localized using immunocytochemistry. Incubation for two days in goat anti-CTB (List Biological; 1:10, 000), was followed by two hours each in biotinylated rabbit anti-goat IgG (Vector Laboratories; 1:250) and avidin-biotin-HRP ("Elite" ABC kit; Vector Laboratories; 1:150). Incubations were separated by 45 minute rinses in buffer. Incubation solutions contained 1% Triton-X-100 and (excepting the ABC solution) 1% normal rabbit serum. Finally, a glucose oxidase-driven DAB (Itoh et al., 1979), without cobalt intensification, was used for visualization.

### **Cytochrome Oxidase**

Cytochrome Oxidase (CO) staining was performed in experiments using coronal sections as a guide to placement of laminar borders. More importantly, CO staining was used in tangential sections to show the pattern of CO blobs. Earlier studies have found nickel, alone or in combination with cobalt, to be very effective in enhancing CO staining (Silverman and Tootell, 1987; Crockett et al., 1993; Dyck and Cynader, 1993b; Liu et al., 1993). In these experiments, sections were reacted for cytochrome oxidase (CO) using either the protocol of Silverman and Tootel (Silverman and Tootell, 1987) adapted for free floating sections, or, in later experiments, modifications on this protocol. Of the various modifications tried, the CO reaction solution judged most sensitive consisted of 20-25 mg diaminobenzidine, 30 mg cytochrome C, 15mg catalase, and 1g sucrose dissolved in 100 ml 0.06 M phosphate buffer pH

7.2, to which was added 3-5 ml of a 1% nickel ammonium sulfate solution and 3-5 ml of a 1% cobalt chloride solution. Sometimes 250ml dimethyl sulfoxide was added as well. Incubation times ranged from two to four hours. In all of the coronally-sectioned brains and some of the tangentially-sectioned brains, sections were divided into two one-in-two series, one of which was reacted for the tracer, and the other was reacted for CO. In some of the tangentially-sectioned brains, only selected sections from the middle depths of the cortex were stained for CO.

## Data Analysis

Patterns of retrograde labeling were analyzed with a Nikon Optiphot compound microscope which was equipped with an x-y coordinate stage encoder. This was connected to a Compaq 386 computer running custom designed software. A drawing tube attached to the microscope was focused on the computer monitor. With the aid of a mouse, the image of the cursor as seen through the drawing tube was aligned with the image of the labeled neuron as seen through the microscope, and the x-y position of the labeled neuron was entered by selecting a symbol type and pressing a button. When a point was entered, a symbol on the monitor appeared which, through the drawing tube, overlay the labeled neuron. The image on the monitor was programmed to move in register with movements of the stage. In this way, large areas of the section could be scanned without missing any labeled neurons or entering the same neuron twice. In addition to labeled neurons, the positions of many radially-oriented blood vessels were also recorded. These could be recognized from section to section and were used as landmarks to align serial sections by means of custom designed software. The accuracy of this alignment was evidenced by the fact that the average distance between the centers of matching blood vessel profiles in two aligned serial sections was typically less than 50 $\mu$ m. This accuracy seemed quite adequate for examining fluctuations in labeling density on the scale of  $\cong$  1mm. The positions of

cells from an entire series of aligned tangential sections could then be displayed and plotted on the same axes, providing a “surface” view of the labeling pattern with labeling in different laminae collapsed onto a single plane.

Other software calculated and plotted the amount of labeling under each square of a superimposed grid of variable size (100 $\mu$ m was used in the figures shown). These density data were then displayed and manipulated using NIH *Image* v. 1.47 software running on a Macintosh IIfx computer. In order to illustrate periodic patterns in the data, images were averaged with a 0.25 mm radius convolution kernel (Callaway and Katz, 1991) and contrast could be enhanced by manipulating the look-up table.

Images of alternate sections stained for CO were digitally captured using a Cohu CCD camera (4915) and a Data Translation (DT-2255) frame grabber card with *Image* . Using radially-oriented blood vessels as landmarks, these images were aligned with the patterns of labeling by an *Image* module that allowed precise superimposition of successive images on line. By means of a slide processor, these computer images were copied onto black and white negative film (Ilford FP4), and then printed onto photographic paper. In other cases, computer images were printed on a Tektronix phaser IISDX dye sublimation printer.

### 3 LAMINAR AND COLUMNAR PATTERNS OF GENICULOCORTICAL PROJECTIONS

The lateral geniculate nucleus (LGN) is the main thalamic relay between the retina and the visual cortex. In the cat, three main classes of LGN cells, known as X, Y, and W, have been distinguished on both physiological and anatomical criteria (see Casagrande and Norton (1991) for review). These separate populations of LGN relay cells each receive input from corresponding classes of retinal ganglion cells (Boycott and Wässle, 1974; Leventhal et al., 1985). Thus, three parallel streams of information originate in the retina and are kept separate in the LGN. What is less clear is whether X, Y, and W inputs from the LGN are kept separate in the visual cortex, or at what stage they might be integrated.

The projections from the C laminae (C, C1, and C2) of the LGN, which include both Y- and W-cells, are at least partially segregated into different layers than the X- and Y-cell projection from the A laminae (A and A1) of the LGN (LeVay and Gilbert, 1976). Interestingly, these authors noted that the labeling from the C laminae had a patchy distribution in the cortex, which they incorrectly attributed to ocular dominance domains. As will be shown in this chapter, the C-laminae terminate in a patchy distribution and CO-localize with CO blobs in visual cortex.

In primates, the smallest cells in the LGN, the koniocellular geniculate cells, bear a certain resemblance to the W cells of the cat in their small size, projection outside of layer 4, and physiological responses; interestingly, koniocellular LGN cells project only to the CO blobs (Hendrickson et al., 1978; Fitzpatrick et al., 1983; Weber et al., 1983; Horton, 1984; Livingstone and Hubel, 1987c; Lachica and Casagrande, 1992). It was wondered whether W-cell terminations in the cat, which have a similar patchy projection to layer 3, might also show a relationship with CO staining.

The terminations of different geniculocortical projections in the cat were examined. These were compared to CO staining patterns to determine which classes of geniculate afferents are correlated with high levels of CO activity and, in particular, which classes of afferents provide input to the CO blobs. A preliminary account of this work has been previously presented (Boyd and Matsubara, 1993).

## **Methods and Materials**

Experiments were performed on eight cats. Some of these cats were also used for electrophysiological recordings unrelated to the present experiments. We also examined sections through the LGN and cortex from a separate series of experiments in this laboratory involving cortical injections of tracers. These were used to demonstrate the general topography of the geniculocortical projection. General details of the surgical procedures and electrophysiological techniques are found in Chapter 2.

The LGN was located by physiologically recording visual responses. The electrode was introduced into the brain at stereotaxic coordinates AP +9 to +4 and ML 7 to 12 mm. These coordinates, targeting the lower visual field representation, were chosen using Sanderson's map of the LGN (Sanderson, 1971a). The C laminae were located by following the shifts in eye dominance from contralateral to ipsilateral, and back to contralateral eye, as the electrode traversed the lamina A, A1, and C. It was not possible to record a shift to ipsilateral responses at the C/C1 border, probably because the low impedance of the electrodes precluded recording from the very small cells in layers C1 and C2, or because these cells were not responsive under the anesthetic regime used. Therefore, we centered the injections 0.5 - 1.0 mm below the last recorded visual response.

Injection sites were specifically chosen in areas where receptive field elevation changed rapidly along the penetration (see results). At such sites, the isoelevation projection lines of the

visual field run at steep angles to the coronal plane (Sanderson, 1971b). Therefore, although the injection site usually included layer A1 as well as all of the C layers of the LGN, labeling from the different layers was separated topographically in the cortex.

Twenty-four hours was allowed to pass from the time of the last injection until perfusion. In four cases, the cortex was sectioned coronally. In the remaining four cases, visual cortex was removed from the brainstem and unfolded and flattened. In all cases, the thalamus was sectioned coronally to verify injection site placement.

In all cases, one one-in-two series of sections was reacted for WGA-HRP and counter stained for Nissl substance with neutral red. The alternate series of sections was reacted for cytochrome oxidase.

## **Results**

We used the technique of injecting multiple geniculate lamina with a single injection, but at varying retinotopic locations. The rationale for this technique is illustrated in Figures 3.1 and 3.2. Figure 3.1 is a schematic diagram showing receptive field isoelevations for an injection site in the LGN and for the resulting labeling in the cortex and retina. As shown in Figure 3.1A, a vertically oriented pipette penetration into the curved region in the anterior part of the LGN traverses a 30° range of isoelevations. Elevation steadily decreases as the pipette passes from A through A1 and C and into the ventral C laminae. Differing elevation representations are thus injected in each layer. As elevation is also mapped across the surface of the retina (Fig. 3.1B) and the cortex (Fig. 3.1C), labeling from the different LGN layers will be separated across the surface of these structures. Retinotopic separation of labeling from different LGN layers following a single LGN injection has been previously noted by Illing and Wässle (Illing and Wässle, 1981). In a study of retinogeniculate projections, they injected the curved region in posterior part of the LGN and found separated sectors of labeling in the contralateral retina.

Figure 3.1. Schematic diagram of the isoelevation map in the geniculate and how aspects of its organization were utilized to obtain topographically separated labeling from different geniculate lamina. **A** shows a parasagittal section of the lateral geniculate with isoelevation lines marked for the lower visual field. An injection pipette in the coronal plane passing through the curved anterior part of the nucleus traverses a wide span of elevation, and each geniculate lamina is injected at a different, though slightly overlapping, range of elevations. Lamina A will be injected at representations of higher elevations, and lamina C1 and C2 at lower elevations. **B** shows the expected pattern of labeling in the retinae. A zone of labeling corresponding to each lamina is present, and these zones are separated across the retina. The X, Y, and W cell classes labeled from each geniculate lamina are shown as three different sizes of dots, W-cells being the smallest and Y-cells being the largest. **C** shows the expected distribution of labeling in the cortex. In this view of a flattened cortex, the border of the oval-shaped lower visual field representation of area 17 is outlined, and approximate isoelevations for the visual field map are indicated. As in the retina, labeling from the various geniculate layers is segregated according to the elevation representation injected in each geniculate lamina. Thus, labeling from layers C1 and C2 is found further anterior, and labeling from lamina A is found further posterior in area 17.



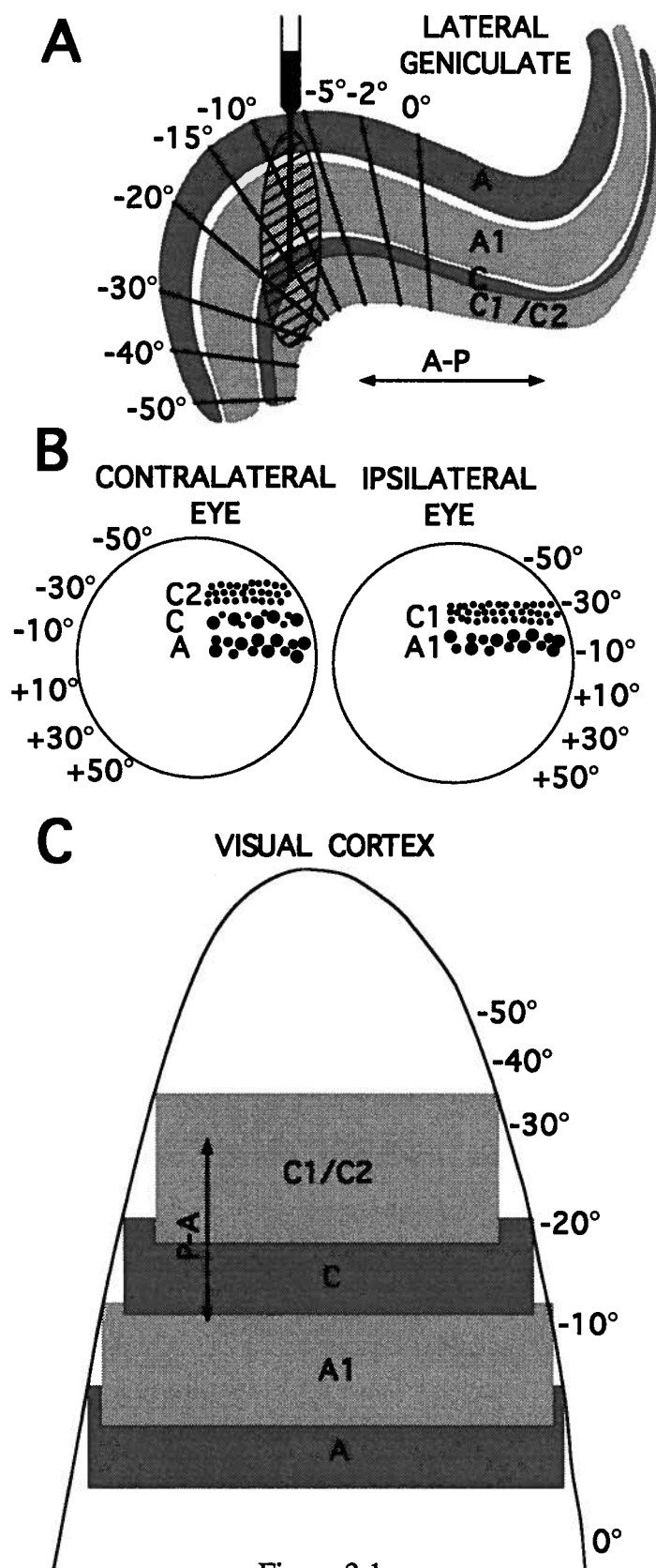


Figure 3.1

Figure 3.2 shows results from tracer injections illustrating the mapping of geniculocortical and retinogeniculate projections as outlined in Figure 3.1. Figures 3.2A and 2B show retrograde labeling in the LGN from the three small, widely separated injections of retrograde tracers in the visual cortex shown in Figure 3.2C. Figure 3.2B is at an A-P level where isoelevation lines are nearly parallel to the coronal plane; labeling from a single cortical injection site (the most posterior one) therefore appears throughout all of the geniculate laminae. This is in contrast to the situation in Figure 3.2A, which shows a section anterior to the one in Figure 3.2B. At this level, isoelevation projection lines run at steep angles to the coronal plane. Labeling from all three injection sites shown in Figure 3.2C are present in this one section, thus showing that the representation of elevation changes greatly from lamina A to lamina C2. The section in Figure 3.2A is at the approximate level where injections were made for this study, a typical example of which is shown in Figure 3.2D.

Topographical separation of labeling from the various LGN laminae was also seen in the retina. Labeling in topographically separated parts of the retina could be verified as arising from different layers of the LGN because different LGN laminae receive input from different classes of ganglion cells. Layers C1 and C2 (the parvocellular division of the C-laminae) receive mostly input from W retinal ganglion cells, layer C (the magnocellular division of the C-laminae) receives inputs from Y and W retinal ganglion cells, and layers A and A1 receive input from X and Y retinal ganglion cells (Guillery and Oberdorfer, 1977; Guillery et al., 1980; Leventhal, 1982; Leventhal et al., 1985). The fact that different classes of retinal ganglion cells were labeled at different elevations in the retina is evidence that we were successful in injecting different LGN layers at different elevation representations.

Figure 3.2E shows a low power photomicrograph of the flat-mounted retina ipsilateral to the LGN injection shown in Figure 3.2D. Lower visual field elevations are shown in the lower part of the figure. With progression from higher into lower representations of visual fields, the

Figure 3.2. Results from tracer studies demonstrating the mapping outlined in Figure 3.1. **A** and **B** show the coronal sections of the LGN at anterior-posterior levels +7.5 and +6.0, respectively. Approximate positions of isoelevation lines are shown (dashed lines) in **A**; the A-P level of **B** corresponds roughly to a plane of isoelevation at 0°. Scale bars in **A**, **B**: 500  $\mu\text{m}$ . A reverse contrast photograph of a flattened, tangential section of visual cortex from the same animal is shown in **C**. The outline of area 17 is shown in dashed white lines. Scale bar: 2 mm. Three injections of retrograde tracers, widely separated in the A-P dimension and thus with greatly differing isoelevations) were made into areas 17 and 18 of this animal. A single column of labeling, arising from only the most posterior injection site and extending across all of the geniculate layers, is present in **B**, but three separate clusters of labeling in different geniculate layers, each from a different injection site (arrowheads) is found in **A**. A bright field photomicrograph of a typical injection of WGA-HRP in the LGN is shown in **D**. The injection is at a similar A-P level as the section shown in 1A. Scale bar: 500  $\mu\text{m}$ . The injection site included all of the C layers, layer A1, and part of layer A. **E** shows a photomicrograph of the ipsilateral retina from this animal, flat-mounted, stained for HRP, and Nissl stained with neutral red. Lower elevations, corresponding to the part of the parvocellular C laminae injected, are represented at the bottom of the photograph. The arrowheads mark four retrogradely labeled Y ganglion cells, recognized by their large cell bodies and dendritic arborization. Above these cells, many other Y ganglion cells are labeled; below these cells, only small ganglion cells are labeled. Scale bar: 200  $\mu\text{m}$ . **F** and **G** show the area of small cell labeling at higher magnifications. Large ganglion cells stained with neutral red can be seen, arrowheads in **F**, but these do not contain HRP reaction product. Scale bar in **F**: 100  $\mu\text{m}$ . Scale bar in **G**: 25  $\mu\text{m}$ .

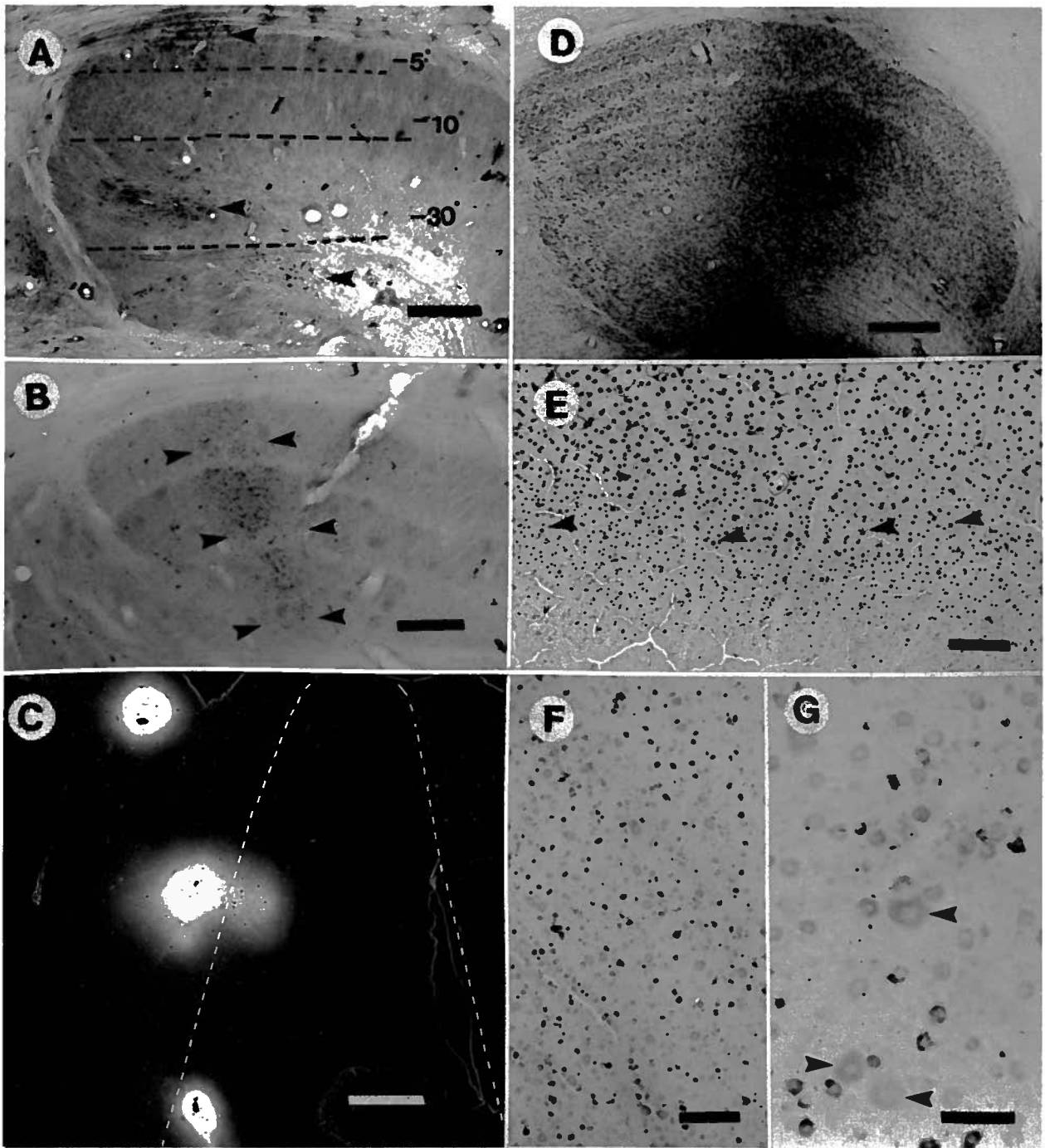


Figure 3.2

pattern of labeling changes such that only smaller retinal ganglion cells are labeled. Higher magnification photomicrographs of the area in the lower part of Figure 3.2E (Figs. 2F and 2G) show large, unlabeled ganglion cells intermixed with the smaller, retrogradely labeled cells. Thus, the portion of the injection site which extended into lamina A1 resulted in labeling of many large (X and Y) retinal ganglion cells, and only at higher receptive field elevations. In contrast, the part of the injection site extending into layer C1 resulted in the labeling of only the smaller (W) ganglion cells, and only at lower elevations. In this experiment, a relatively large amount of HRP was used, so that the visual field representations of the different LGN layers injected were relatively large and overlapped somewhat. The injected visual field representation of layer C (which receives input from the contralateral eye) was completely overlapped by the visual field representations injected in surrounding layers A1 and C1. An unlabeled region of ipsilateral retina sandwiched between lower elevations labeled from layer C1 and higher elevations labeled from layer A1 was thus not present.

### Cytochrome Oxidase Staining

As the goal of this study was to compare patterns of geniculocortical labeling to the pattern of CO staining, the laminar and columnar organization of the latter in area 17 and 18 will first be described (Figs. 3-5). The laminar terminology employed in this study was that of O'Leary (O'Leary, 1941), and as further expounded by Lund *et al.* (Lund et al., 1979). Although originally developed for area 17, this laminar scheme has also been used for area 18 (Friedlander and Martin, 1989), and we have done the same. In this scheme, the layer 3/4 border is at the level of the largest pyramidal cells in the upper layers- the so-called "border pyramids". Layer 4 is divided into sublayers 4a and 4b. Layer 4a has many large stellate cells in addition to smaller stellate cells and some pyramidal cells. Layer 4b is composed mostly of small stellates, and is more tightly packed than 4a. Figure 3.3A shows the border between areas 17 and 18 in a Nissl

Figure 3.3. Laminar pattern of CO staining in areas 17 and 18. The left and right panels of **A** show CO staining in coronal sections through areas 17 and 18, respectively. These photographs were matched to an adjacent section stained for Nissl substance with cresyl violet, in the middle panel. This section includes the 17/18 border, area 17 to the left, area 18 to the right. Arrowheads mark examples of large pyramidal cells at the layer 3/4 border, stained for Nissl or CO. Scale bar: 200  $\mu\text{m}$ . These sections were taken from the area between the dashed lines in **B**, which shows a low power drawing of the CO stained section (A-P -2). Layer 4 is shown as a thick black line. Scale bar = 2 mm. A high power photomicrograph of layer 4 at the 17/18 border, area 17 to the left, area 18 to the right is shown in **C**. Arrowheads mark three examples of large pyramidal cells at the layer 3/4 border. Scale bar: 200  $\mu\text{m}$ . The middle of these cells is shown at higher power in **D** (large arrowhead). Below this cell, in layer 4a, is a large cell, with dendrites (small arrowheads) radiating from the soma in the manner of a star-pyramid. Scale bar: 50  $\mu\text{m}$ .

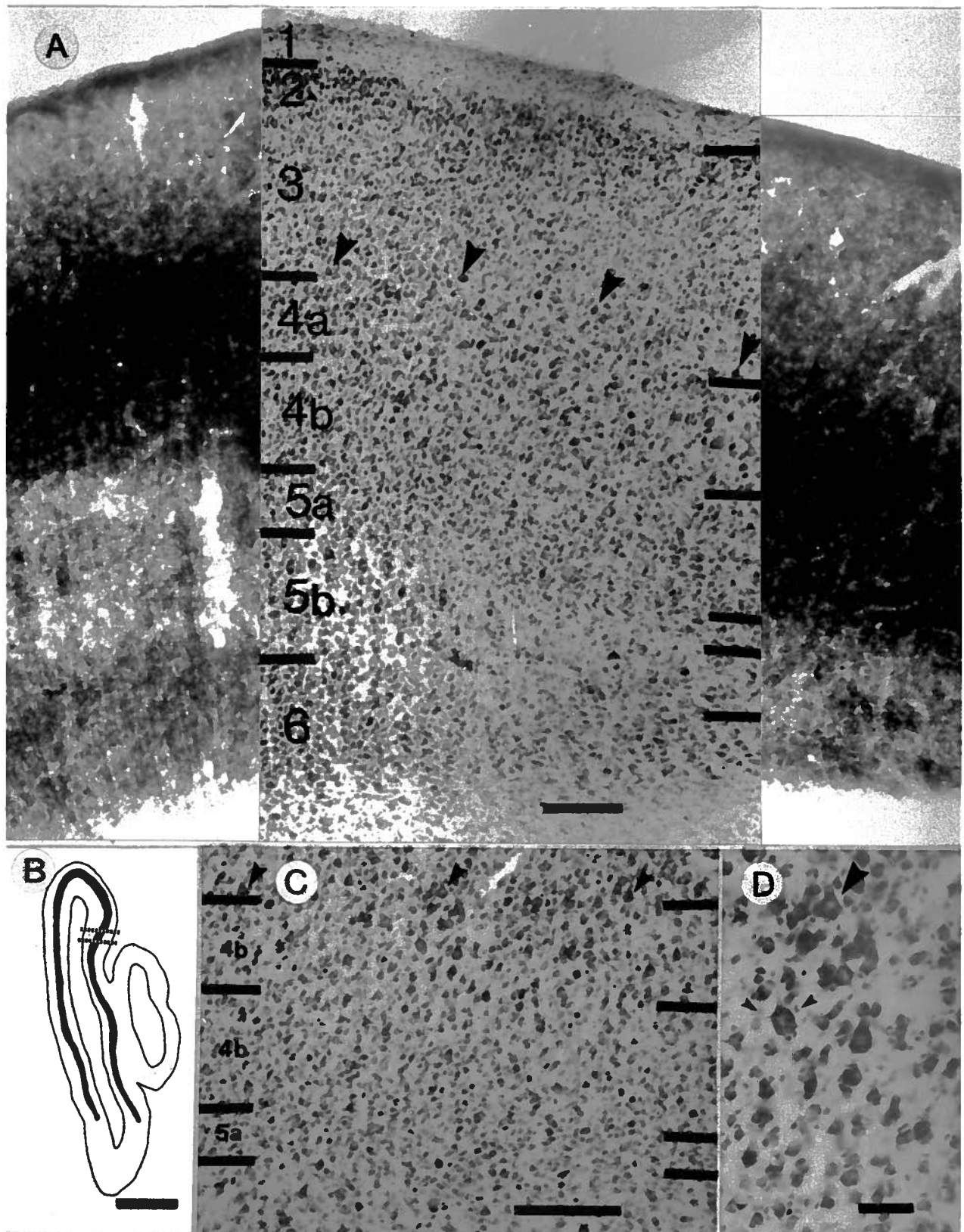


Figure 3.3

stained section, flanked by matched areas in an adjacent section stained for CO. The laminar pattern of CO staining was generally in agreement with previous studies (Wong-Riley, 1979; Kageyama and Wong-Riley, 1986). In both areas 17 and 18, a dense band of CO staining was coextensive with layer 4 as determined by cytoarchitecture. There was also moderately dense CO staining in layer 3. The border between this moderate level of staining in layer 3 and the dense band of layer 4 was usually quite sharp. In our material, the large pyramids at the layer 3/4 border often stained for CO. Below 4b is layer 5a, a thin layer of very small pyramids. This layer does not stain for CO. Layer 5b contains both large and medium pyramidal cells, and is very loosely packed. The largest pyramidal cells in area 17, the Meynert cells, are found at the 5a/5b border, and these cells were densely stained for CO. Often, a thin band of neuropil staining was coextensive with these large pyramids, giving layer 5 a trilaminar appearance, as the rest of layer 5b did not stain for CO. Layer 6 is composed of small and medium sized pyramidal cells, and can be differentiated from layer 5b by its more tightly packed cells. This layer stained moderately for CO.

An identical pattern of CO staining was found in area 18, in disagreement with a previous report that the dense band of CO staining in layer 4 in this area extended part way into layer 3 (Price, 1984). This discrepancy is probably due to a different assignation of the layer 3/4 border, rather than true differences in staining patterns. In particular, the large cells in layer 4a tend to be larger in area 18 than in area 17, as can be seen clearly in Figure 3.3C. Larger cells, such as these, have apparently been mistaken for "border pyramids" in area 18, resulting in deeper placement of the layer 3/4 border. We also noted that some of the large cells in layer 4a of area 18 were clearly not standard pyramidal cells. One of the cells shown in Figure 3.3D has a thin apical dendrite as well as other dendrites originating from various positions around the cell soma, giving it the appearance of a star-pyramid, a cell characteristic of layer 4 in area 17.

In addition to the laminar variation of CO staining, there was also a marked columnar organization, i.e., the CO "blobs". Figure 3.4 shows low power views of the CO blobs in the



Figure 3.4. CO blobs in coronal and tangential planes of section. **A** shows a low magnification photograph of a CO stained section near-adjacent to the one shown in **B**. The 17/18 border is marked by a large arrowhead. The small arrowheads mark examples of CO blobs, which appear as increases of labeling density in layers 3 and 4a, in area 17 and 18. CO blobs are clearly visible in the tangential section through layer 4a of area 17 shown in **B**. Scale bars in **A, B**: 1 mm. **C** shows a high power photomicrograph of layer 4. A CO blob is at the left, an interblob zone is at the right. Within the blob, layer 4a is much more densely stained than layer 4b. In the interblob, layer 4a is only slightly darker than layer 4b. The arrowheads mark two border pyramids staining for CO. Scale bar: 100  $\mu\text{m}$ . The border pyramids are also seen in tangential sections through the layer 3/4 border (**D**). Truncated apical dendrites can be seen arising from some of these cells (arrowheads). Scale bar: 50  $\mu\text{m}$ .

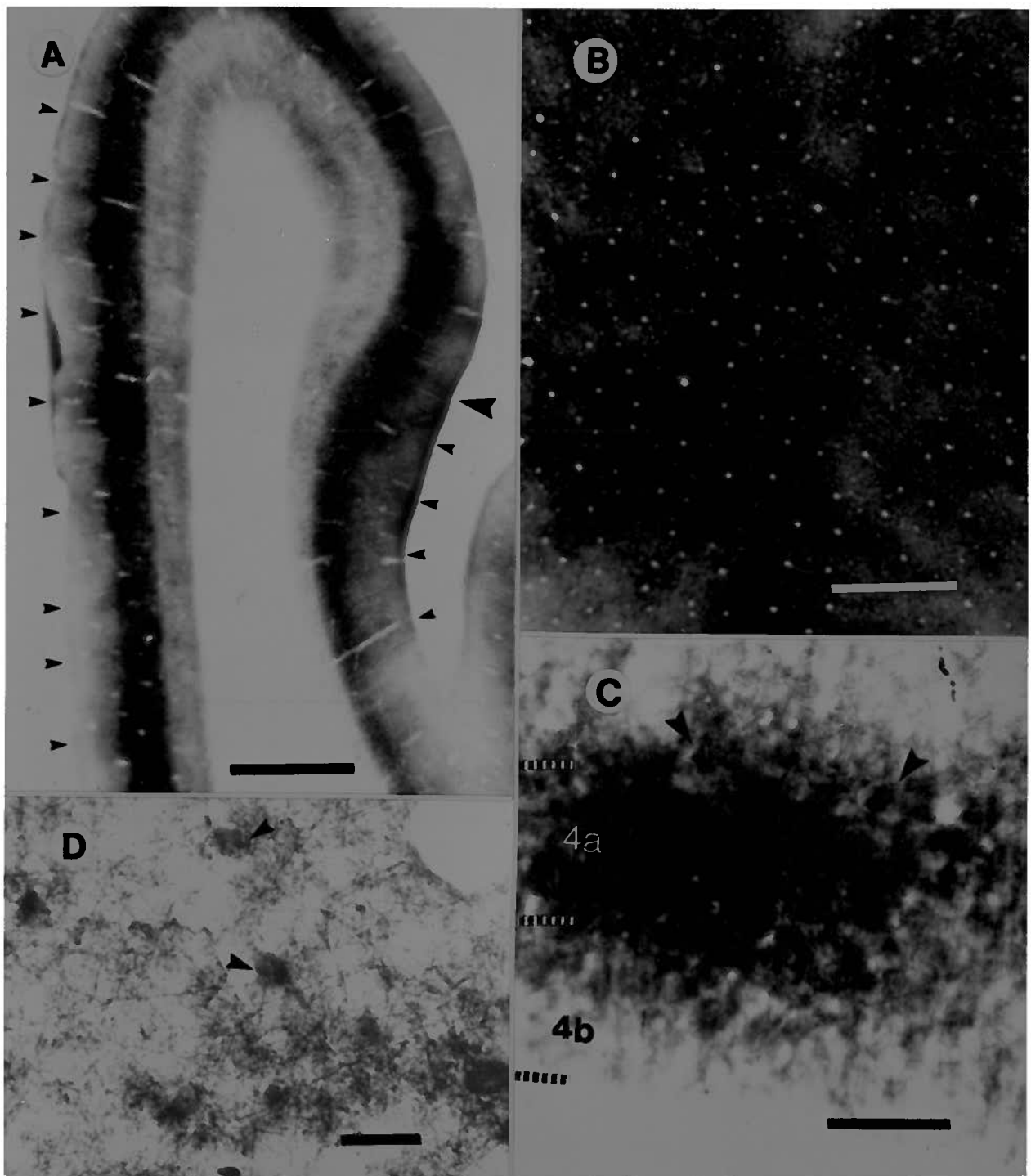


Figure 3.4

coronal and tangential planes. The center-to-center spacing of the blobs, uncorrected for shrinkage (estimated to be around 20%), was about 0.75 mm. In the tangential plane, the blobs were not arranged in orderly rows, as was found to be the case in some primates. Figure 3.4C shows a high power photomicrograph through layer 4. A CO blob to the left of the figure is marked by dense staining in layer 4a, with only moderate staining in 4b. To the right of the figure, in an interblob zone, there is little difference in the staining intensity of layers 4a and 4b. Note that, in addition to neuropil staining, several stained cell bodies are visible. Two large pyramidal cells at the layer 3/4 border are marked with arrow heads. These border pyramids were clearly seen in tangentially cut sections through the layer 3/4 border stained for CO. Several such cells can be seen in Figure 3.4D embedded in a meshwork of CO reactive processes. These cells can be identified as pyramidal cells by their apical dendrites, which are viewed face-on and thus appear fore-shortened. Basal dendrites can often be seen as well.

The photomicrographs of Figure 3.5 show nine alternate 50  $\mu$ m sections progressively deeper into the same zone of cortex in area 17. The first three sections (Figs. 4A-C) are mostly through layers 3. The CO blobs first appear, albeit faintly, in the middle part of this layer, becoming more visible towards the bottom of layer 3, as seen in Figure 3.5B and 5C. In Figures 3.5B-C, CO stained cell bodies can be seen as small dark spots which are more numerous within the CO blobs; these cells are the layer 3/4 border pyramids. Figures 3.5D-E contain mostly layer 4a, and it is in this layer where the blobs are most visible. Although Figures 3.5A-5B also show layer 4a, these prints were intentionally overexposed to show the faint staining of blobs in layer 3. Consequently, layer 4a in these sections appears densely and evenly stained which was not, in fact, the case. Figures 3.5F-5G contain mostly layer 4b. The blobs are not visible in this layer, and the CO staining has a fine mesh-work pattern to it, which differentiates it from layer 4a. This pattern may result from the tight packing of cells in this layer, which might constrain the positions of reactive dendrites and axon terminals. The darkly stained Meynert cells are clearly visible wherever the layer 5a/5b border is in the plane of section. A large expanse of

Figure 3.5. A series of 50  $\mu\text{m}$  thick tangential sections through area 17 stained for CO. Every other section, starting from the middle of layer 3 (5A) and continuing to layer 6 (5I) is shown. Cortical layers are numbered; "wm": white matter. Scale bar: 1 mm; applies to A-I.

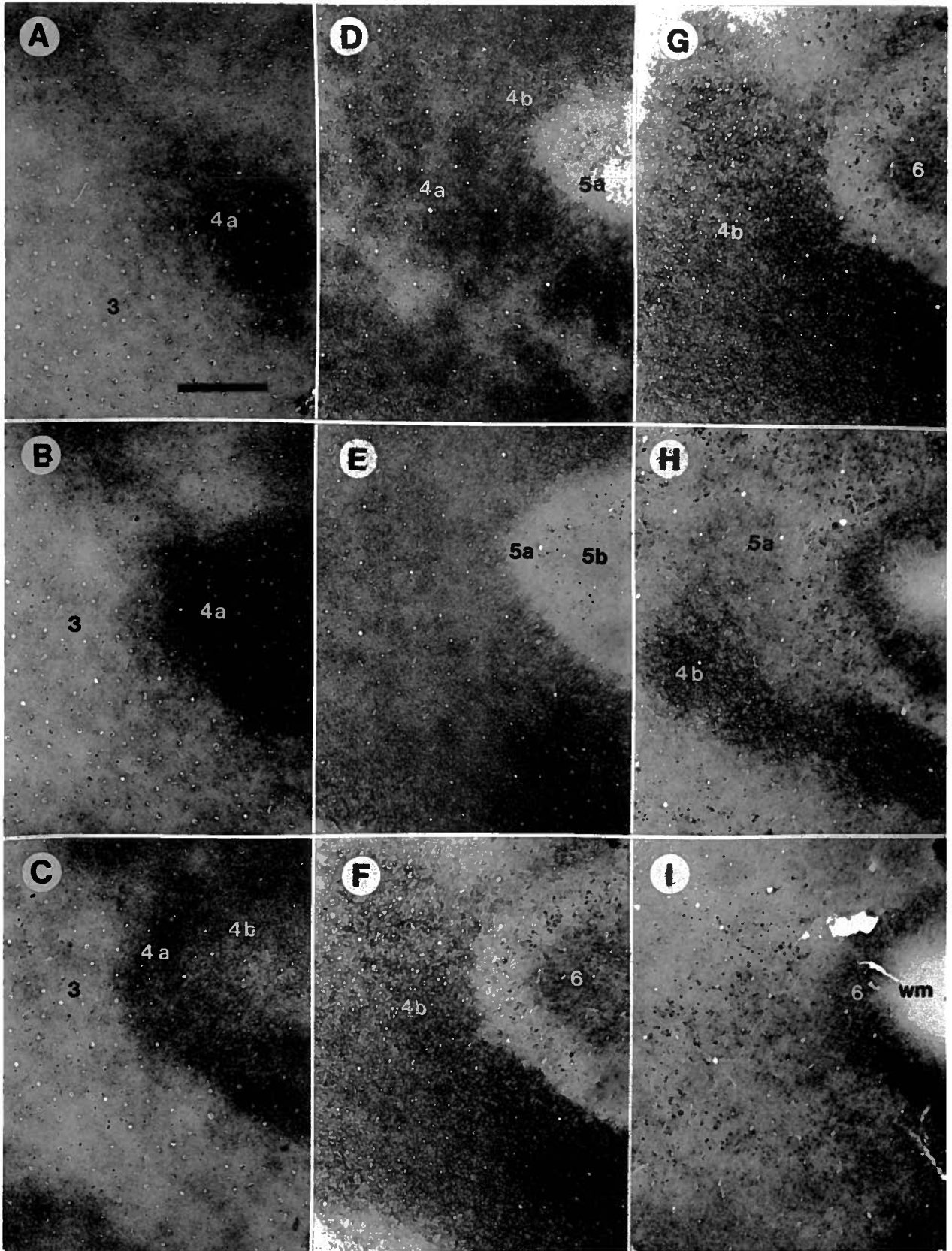


Figure 3.5

these cells is visible in Figure 3.5I. Layer 6, which can first be seen in Figure 3.4F, was found to be uniformly stained and the CO blobs were not visible in this layer.

### **Laminar Organization of Geniculocortical Projections**

Figures 3.6-9 present the results of the laminar distribution of geniculocortical projections from different layers of the LGN to cortical areas 17 and 18. As described in materials and methods, injections were made in such a way that different LGN laminae were injected at different isoelevation representations. As the pipette passed through representations of lower azimuths in the C laminae than in the A laminae, labeling from the C laminae was found more anteriorly in the visual cortex, and labeling from the A laminae was found more posteriorly. The position of coronal sections with respect to both the well established visual field map of areas 17 and 18 (Tusa et al., 1978; Tusa et al., 1979), and the overall extent of labeling, was recorded. With this information, it was possible to classify labeling in the cortex as arising from the A laminae versus arising from the C laminae. Labeling from the A laminae of the LGN is shown in Figure 3.6. Ocular dominance (OD) columns were often visible, as in Figure 3.6A, showing that labeling arising from a single lamina could be isolated. As this section was just slightly posterior to sections containing labeling from the C laminae, it is assumed that the labeling in Figure 3.6a arose from lamina A1. With slightly larger injections, labeling from both layer A and layer A1 could be obtained at some locations in the cortex, and in these cases, labeling was continuous in layers 4 and 6. Figure 3.6B and 6C show A laminae projections to areas 17 and 18, respectively. In both areas, terminal labeling extended throughout layers 4a and 4b, but did not extend appreciably into layer 3 or layer 5a. Adjacent sections stained for CO showed a band of heavy staining of CO in layers 4 and 6 that perfectly matched the terminal labeling in these layers. Layer 6 contained retrograde as well as anterograde labeling. In some experiments, many of the large cells at the border of layers 5a and 5b were also labeled, possibly due to the spread of the

injection into part of the lateral posterior/pulvinar nucleus (Mason, 1978; Lund et al., 1979). Although their labeling in this material was fortuitous, these cells provided a useful guide to the 5a/5b border in the dark-field photographs. The clear gap between these cells and the band of labeling showed that layer 5a was not labeled from the A laminae of the geniculate.

In area 18, other studies have shown that Y axons in area 18 extend well into the lower part of layer 3 (Humphery et al., 1985a; Humphery et al., 1985b). We found that, as in area 17, geniculate terminals from the A layers were nearly completely confined to layers 4 and 6. Figure 3.6D shows a bright field photomicrograph of the layer 3/4 border in area 18, in a section counterstained for Nissl substance with neutral red. Three large border pyramids are shown, and it can be seen that these are above the zone of heavy geniculate terminations. Viewing the same field with more sensitive dark field optics, very sparse terminal labeling could be seen extending to a level just above the border pyramids. The same result was observed in area 17. As was the case for the CO staining in area 18, the discrepancy between this study and previous ones probably involves differences in the assignment of the layer 3/4 border.

Labeling from the C laminae of the LGN in areas 17 and 18 had a different laminar pattern from labeling from the A laminae. Figure 3.7A shows a low power photomicrograph of labeling from the C laminae in area 17. Note that the labeling is patchy, with a spacing (after considering the slightly greater shrinkage that occurs during the TMB reaction) similar to that of the CO blobs (Fig. 3.4). As the labeling from the C-laminae was always patchy, and the injections used were certainly large enough to include laminae C, C1, and C2, these patches were not likely due to projections to one set of ocular dominance columns as might be expected from injections into a single eye-specific layer. Figures 3.7B-D are higher power photomicrographs of three examples of C laminae labeling in area 17. Labeling from the C laminae took the form of patches spanning the border of layers 3 and 4. The labeling in layer 4, which was often much more dense than the labeling in layer 3, extended to the bottom of layer 4b. This laminar pattern was confirmed by comparison to adjacent sections stained for CO, and by the Nissl

Figure 3.6. Labeling from the A laminae in areas 17 and 18. **A** shows a low magnification, dark field photomicrograph of ipsilateral ocular dominance columns in area 17 resulting from WGA-HRP transport from lamina A1 of the LGN. Scale bar: 500  $\mu\text{m}$ . **B** and **C** show higher magnification photomicrographs of A laminae labeling in areas 17 and 18, respectively. Laminar boundaries, using the criteria described in the text, are marked by dashed lines and laminae are numbered. Scale bar: 200  $\mu\text{m}$ ; applies to both **B** and **C**. **D** shows a bright field photomicrograph of the layer 3/4 border in area 18. The arrowheads mark 3 border pyramids counterstained with neutral red. Scale bar: 50  $\mu\text{m}$ .



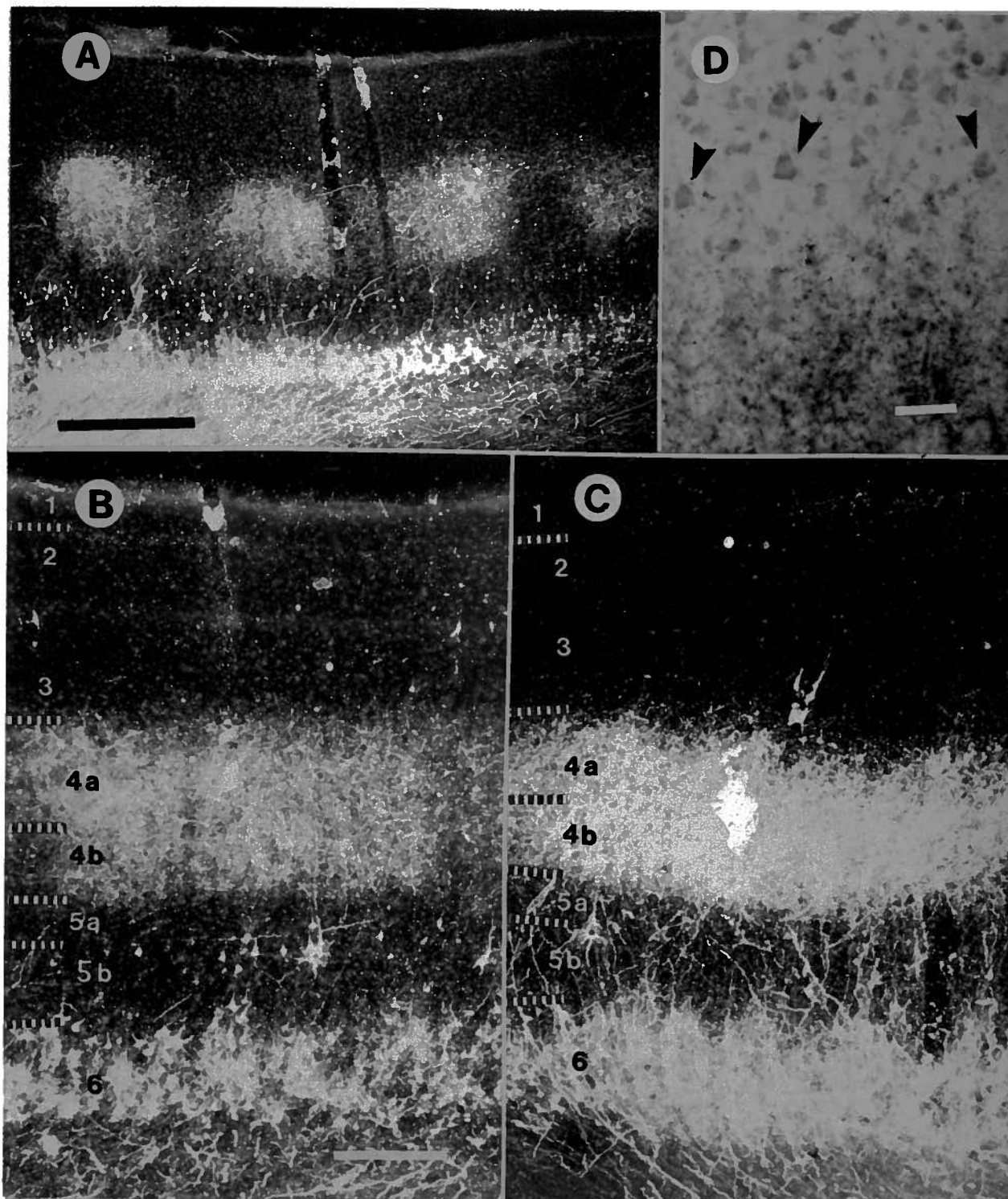


Figure 3.6

Figure 3.7. Labeling from the C-laminae in area 17. **A** shows a low magnification dark field photomicrograph of layer C labeling in area 17. The white arrows mark columns of anterograde labeling. The black arrowhead marks a labeled layer 5 pyramidal cell (see text). Scale bar: 500  $\mu\text{m}$ . **B-D** show examples of C-laminae labeling at higher magnification. Laminar boundaries are marked by dashed lines; see figure 3.6 for labeling scheme. Scale bar: 200  $\mu\text{m}$ ; applies to **B**, **C**, and **D**. **E** shows a bright field photomicrograph of a patch of labeling in layers 3 and 4 in a section counterstained with neutral red. The larger arrow marks a border pyramid at the layer 3/4 border and the smaller arrow marks the deepest large stellate cell, which roughly indicates the layer 4a/4b border. Scale bar: 100  $\mu\text{m}$ .

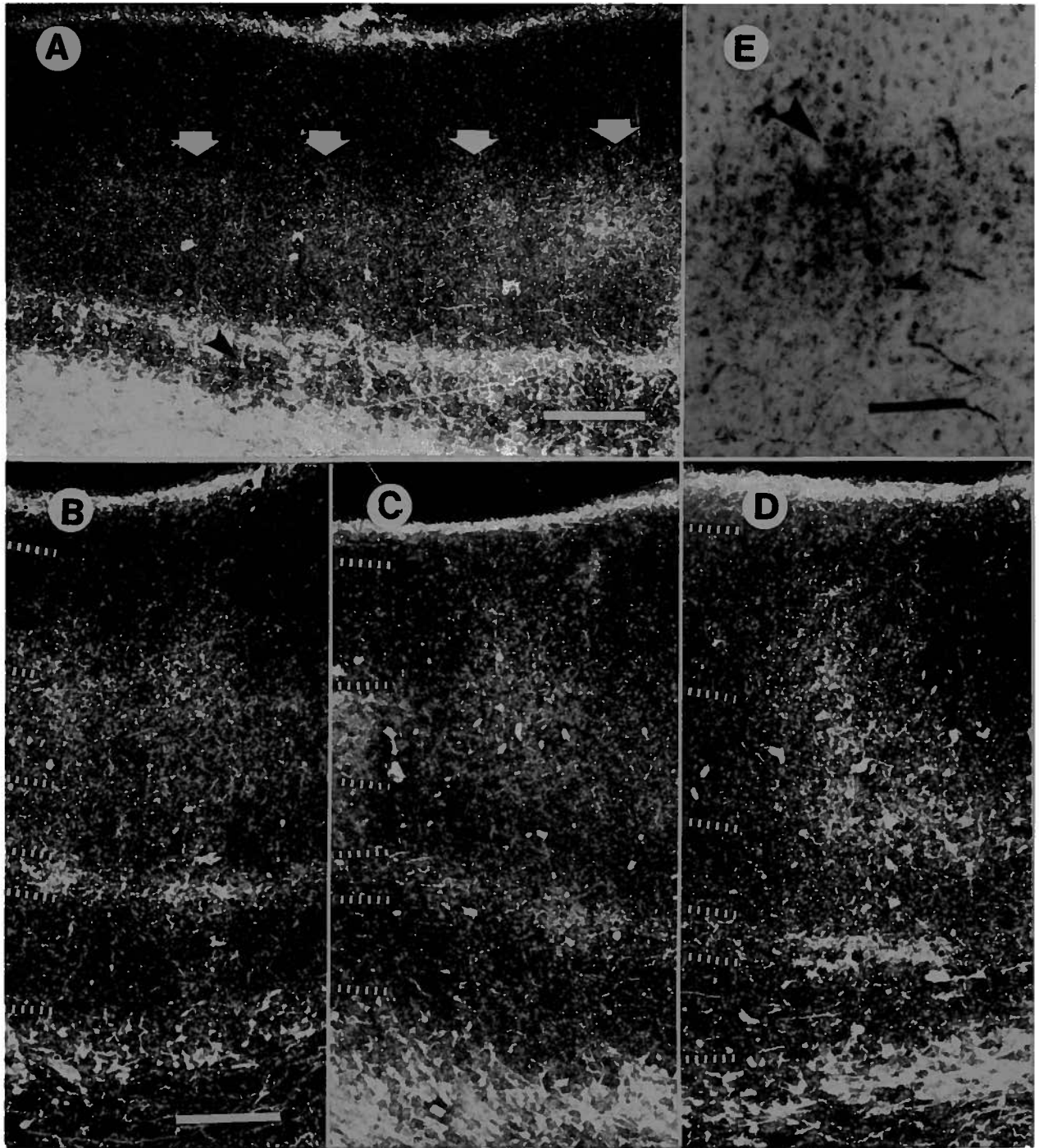


Figure 3.7

counterstaining (Fig. 3.7E). The extent of labeling in layer 3 varied from section to section, but in some cases extended to near the top of layer 3. A narrow band of labeling in layer 5a was also present, and this was patchy as well, although not always as clearly, with the layer 5a patches in register with those in layer 3/4. As well as the patchy labeling in other layers, there is a thin, continuous band of labeling confined to the top half of layer 1, and continuous, mostly retrograde, labeling in layer 6.

As in area 17, patches of terminals spanning layers 3 and 4 were also present in area 18 following C laminae injections (Fig. 3.8). However, in area 18 the dense labeling in layer 4 extended throughout the entire depth of the layer and was not confined to layer 4a. Moreover, while the terminal patches in layer 3 were as pronounced as those in area 17, the labeling in layer 4 tended to be less patchy than in area 17. When patches of increased labeling density were present in layer 4, however, they were always in register with patches in layer 3. The labeling in layer 5a in area 18 was also patchy, as in area 17, even when the labeling in the intervening layer 4 was nearly continuous, and these patches were also always in register with the patches in layer 3 (Fig. 3.8B).

The C-laminae are composed of a magnocellular layer C, which contains many Y-cells, and parvocellular layers C1 and C2 which contain mostly W-cells. The labeling in Figures 3.7 and 3.8 likely originated from both magnocellular and parvocellular subdivisions of the C-laminae. At the edge of the labeling pattern, at the most negative visual field elevation labeled in the cortex, a slightly different pattern was found. This is illustrated in Figure 3.9A for area 17. Here, only one component of the patches spanning the layer 3/4 border is present- the sparse labeling in layer 3. Because this pattern was found at the lowest iso-elevation representation labeled, it suggests that the labeling originated from the bottom of the C-laminae, where the lowest iso-elevation representations were injected. Thus, the small W cells of layers C1 and C2 appeared to project to patches in layer 3, while the large Y cells in the top part of the C layers projected to patches in layer 4a precisely in register with the projection to layer 3.

Figure 3.8. Labeling from the C-laminae in area 18. **A** and **B** show low magnification dark field photomicrographs of C-laminae labeling in area 18. The white arrows mark patches of labeling in layer 3. In **A** there are dense patches of labeling in layers 4a and 4b aligned with those in layer 3; in **B**, layer 4 is nearly continuously labeled. Scale bar: 500  $\mu\text{m}$ ; applies to both **A** and **B**. **C** shows the labeling pattern at higher magnification. Laminar boundaries are marked by dashed lines. Scale bar: 200  $\mu\text{m}$ .

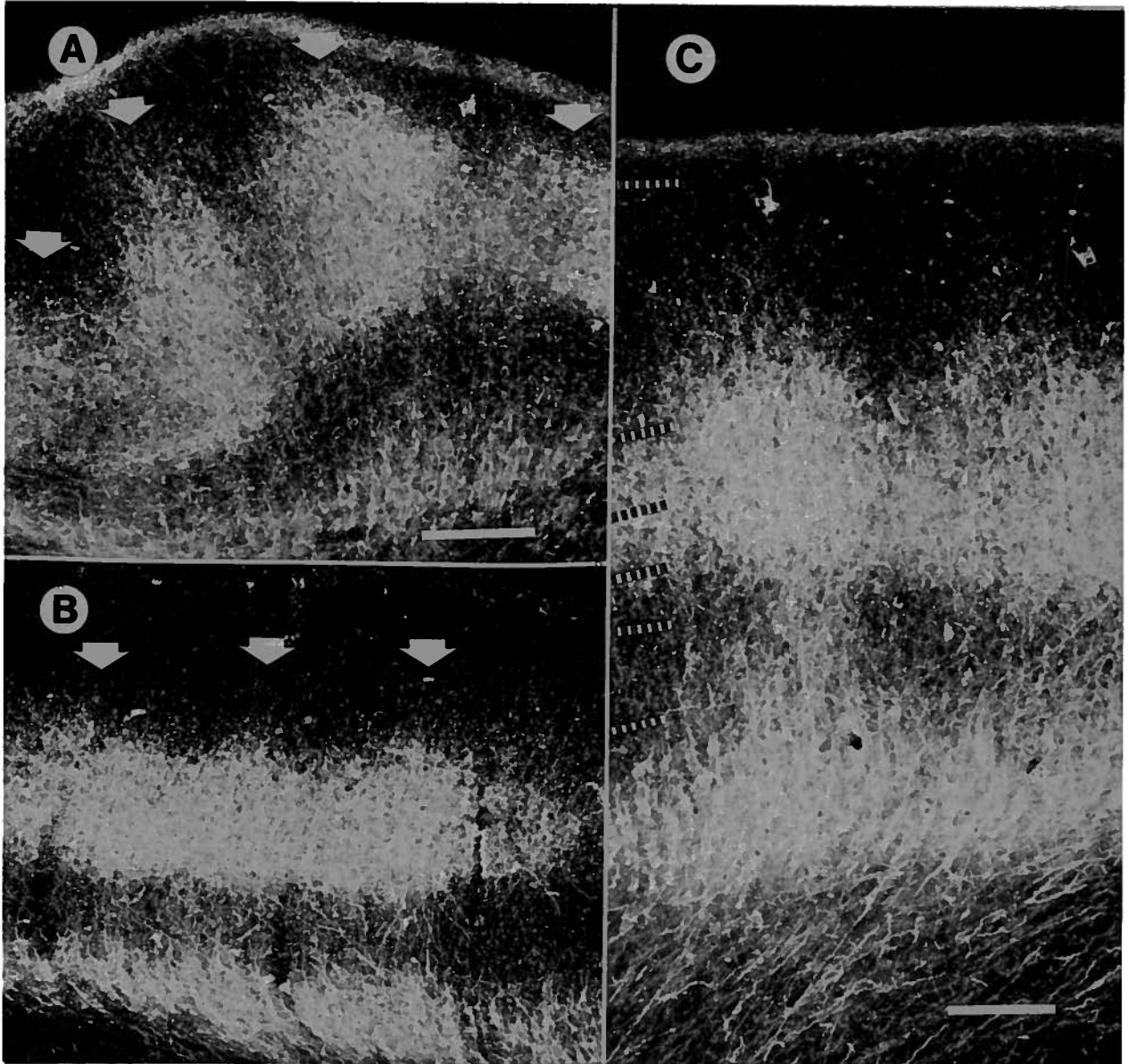


Figure 3.8

Figure 3.9 Labeling from the parvocellular C laminae (A) and from the MIN (B) in area 17. Laminar boundaries are marked by dashed lines. Scale bar: 500  $\mu\text{m}$ ; applies to both A and B. C and D show high magnification photomicrographs of layer 4 of the same section in dark field to show labeled terminals, and in bright field to show cytoarchitecture. The upper arrowhead marks a layer 3/4 border pyramid, the middle arrowhead marks the deepest large stellate cell in layer 4 in this section, approximately marking the layer 4a/4b border, and the bottom arrowhead marks a pyramidal cell in layer 5. Scale bar: 100  $\mu\text{m}$ ; applies to both C and D.



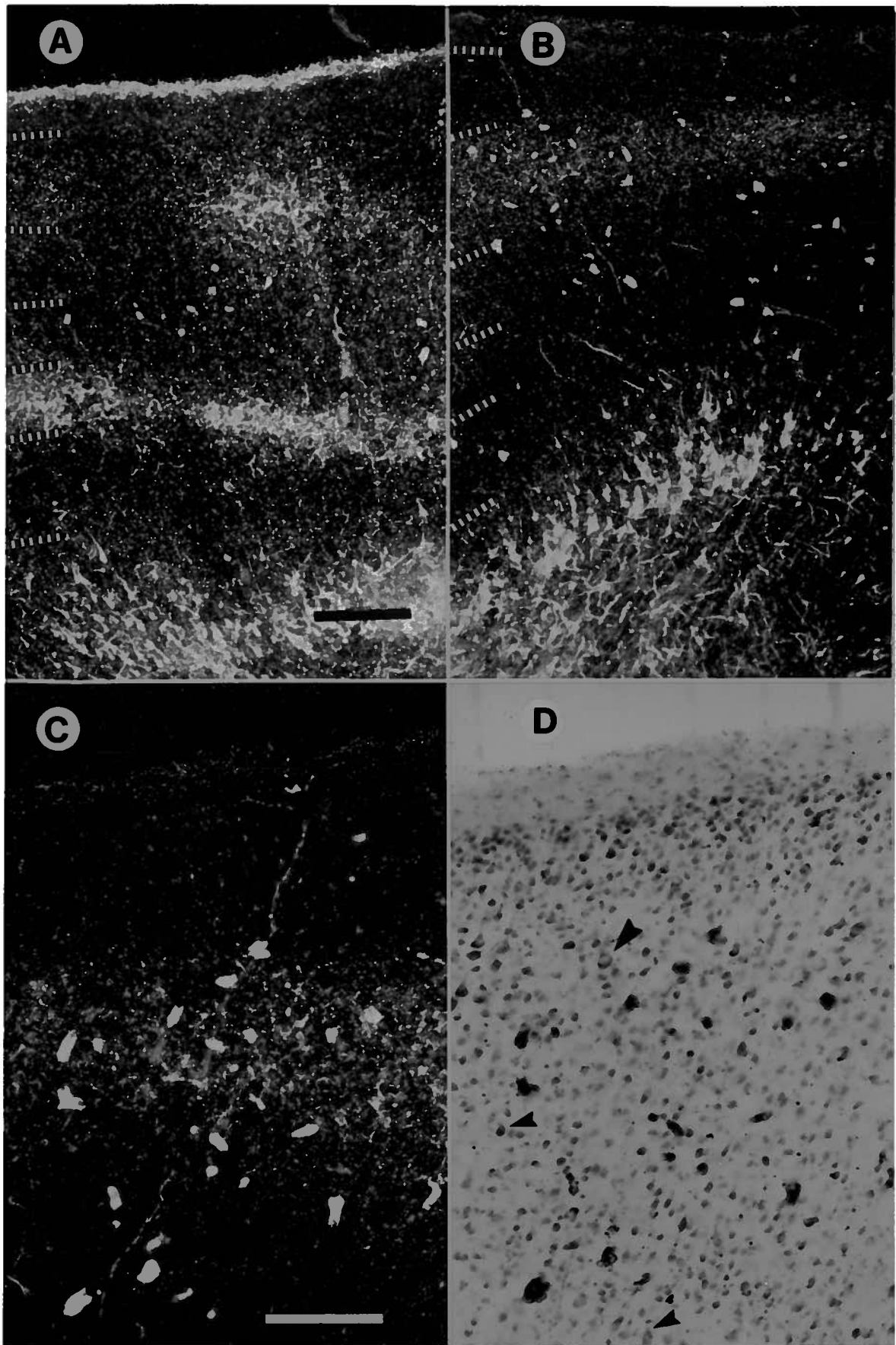


Figure 3.9



In some sections from one of our experiments, a different pattern of geniculate terminal labeling was found, in addition to the pattern described above. In this case, labeling in layer 4 was confined to sublayer 4a (Fig. 3.9B-D). In this experiment, the injection site involved the medial interlaminar nucleus (MIN) where it curves laterally underneath the LGN (see Figure 3.2 d). This pattern was found at the most negative visual field elevations labeled in this experiment, which would be consistent with the retinotopy of this part of the MIN where it appears underneath the LGN (Sanderson, 1971a).

### **Tangential Organization of Geniculocortical Projections**

The relationship between the patches of geniculate labeling from the C-laminae and the CO blobs was examined in sections cut tangential to the cortical surface. Figures 3.10, 11, and 12 show labeling from the C-layers of the LGN in tangential sections. In each case, sections reacted for HRP to visualize thalamic afferents were aligned with sections reacted for CO to visualize the blobs, using the pattern of radially penetrating blood vessels. Figure 3.10A shows an example of labeling from the C layers of the LGN in layer 3 of area 17. The labeling is arranged in patches with a center-to-center spacing of slightly less than 1 mm. Often, the patches align to form rows, with bridges of labeling connecting patches in a row. A similar pattern of patches, or blobs, with connecting bridges is seen in the section stained for CO in Figure 3.10B. To facilitate comparison between the two patterns, each patch of anterograde labeling in Figure 3.10A has been marked with an asterisk, and these asterisks have been transferred to the CO stained section using the blood vessels as landmarks. Except for the top right part of Figure 3.10B, where the plane of section passes out of layer 4 into layer 5, there is good correspondence between the patches of anterograde labeling and the CO blobs.

Figure 3.11 shows, from a different experiment, another example of the relationship between labeling from the C layers of the LGN and CO blobs in area 17. In this case, the sections shown are not from layer 3, but from layer 4a. Note that the patches of anterograde labeling are more dense and have a slightly larger diameter than those in layer 3, but that they have a similar spacing. (The greater density of labeling in layer 4a versus layer 3 was also noted in the coronal sections, and is thought to reflect Y versus W inputs, respectively.) Likewise, the CO blobs in layer 4a are more robust than, but have a similar spacing to, those than in layer 3. As in layer 3, there is good correspondence between the patches of anterograde labeling and the CO blobs in layer 4.

Figure 3.12 shows that the relationship between patches of labeling from the C layers of the LGN and CO blobs is also present in area 18. The section in 12A is from layer 3, and the section in 12B grazes the layer 3/4 border. In area 18, the spacing of both the patches of anterograde labeling and the CO blobs was slightly larger than in area 17. The patches of anterograde labeling, and especially the CO blobs, were not as well defined as those in area 17. However, the correspondence between the anterograde labeling and the CO staining was still reasonably good.

## **Discussion**

The pattern of geniculocortical terminations in the cat's visual cortex was examined. It was desirable for this study to examine geniculocortical projections arising from particular classes of geniculate cells, in isolation from labeling of other cell classes. In the cat LGN, X, Y, and W cells are only partially segregated into different lamina. The two largest geniculate layers, layers A and A1, contain a mixture of X and Y cells. The C layers, ventral to the A layers, can be subdivided into an upper, magnocellular division (layer C) containing both Y and W cells, and a lower, parvocellular division (layers C1 and C2) containing mostly W cells. Knowing the

Figure 3.10 Comparison of cytochrome oxidase blobs and C-laminae labeling in layer 3 of area 17. **A** shows a tangential section through the lower part of layer 3 in area 17 containing peroxidase labeling arising from the lateral geniculate C-laminae. In this dark field photomicrograph, patches of anterograde labeling are numbered. **B** shows an adjacent section reacted for cytochrome oxidase, over which the numbers of **A** were superimposed, showing the alignment between the two patterns. Scale bar: 1 mm; applies to both **A** and **B**.

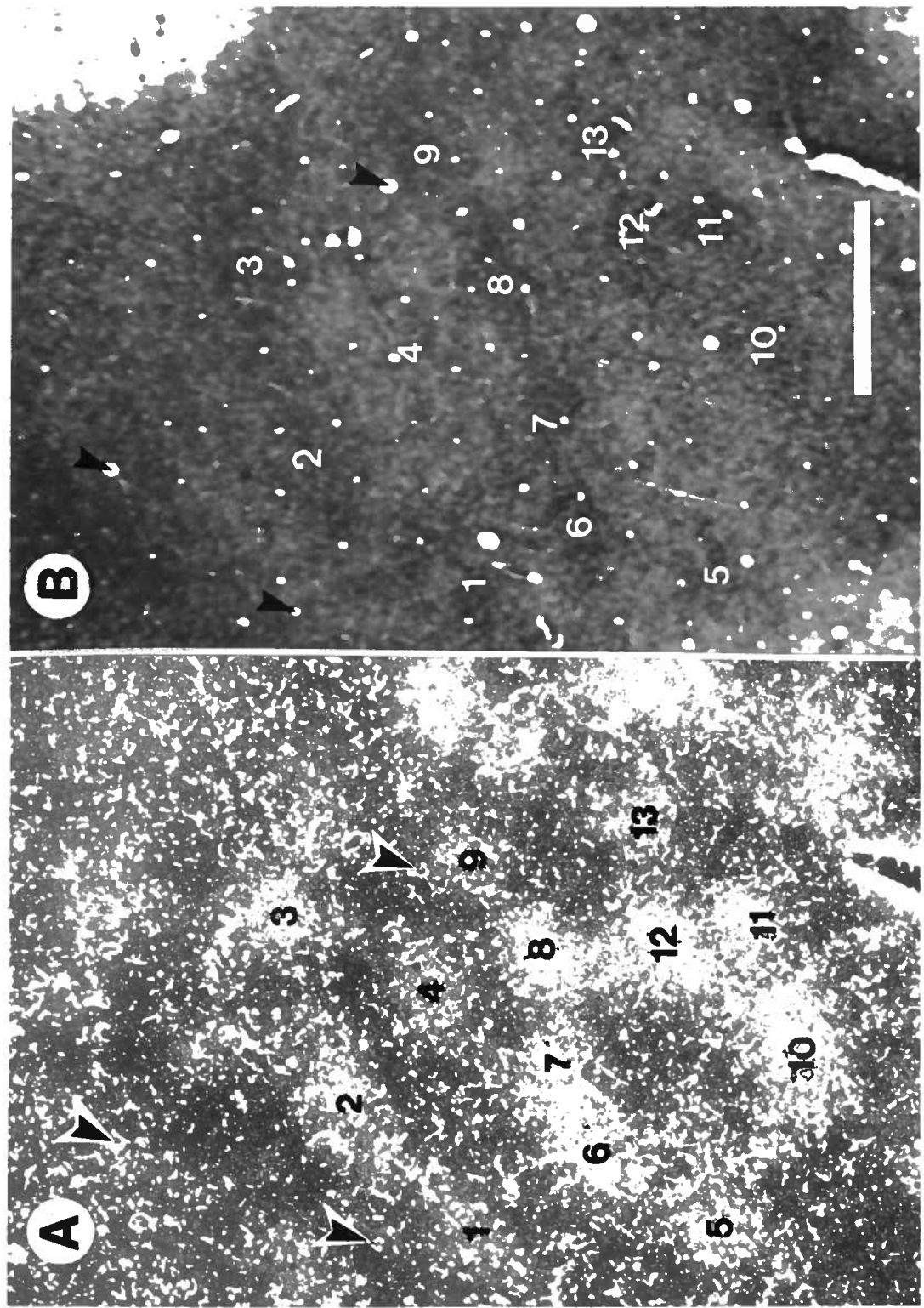


Figure 3.10

Figure 3.11 Comparison of cytochrome oxidase blobs and C-laminae labeling in layer 4a of area 17. **A** shows a tangential section through the layer 4a in area 17 reacted for peroxidase. **B** shows an adjacent section reacted for cytochrome oxidase. As in Figure 3.10, asterisks have been used to mark patches of anterograde labeling and then superimposed on the cytochrome oxidase pattern using blood vessels for alignment. Scale bar: 1 mm; applies to both **A** and **B**.

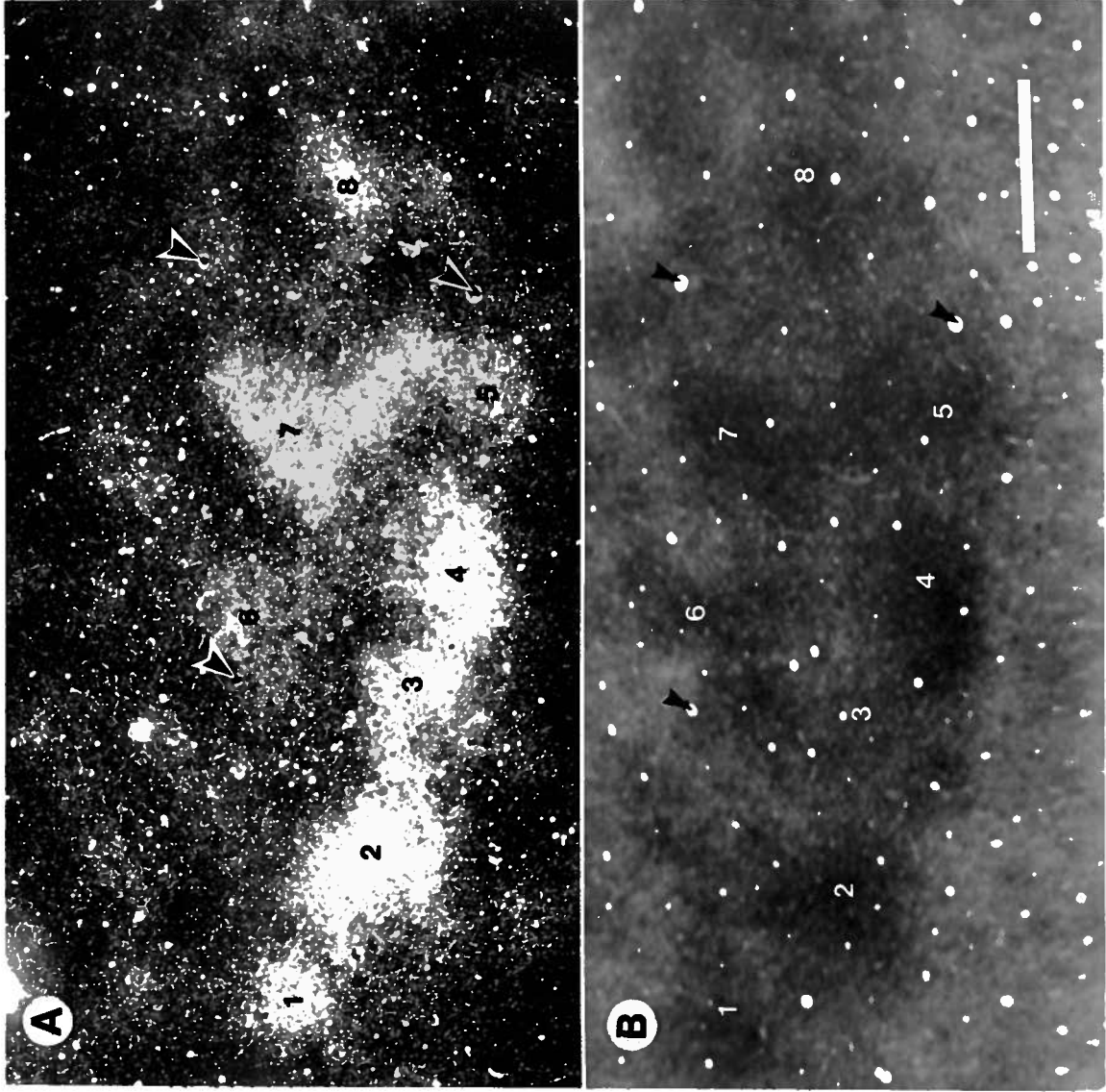


Figure 3.11

**Figure 3.12 Comparison of cytochrome oxidase blobs and C-laminae labeling in area 18. A** shows a tangential section through the lower part of layer 3 reacted for peroxidase. **B** shows a slightly deeper section reacted for cytochrome oxidase. Other conventions as in Figure 3.10. Scale bar: 1 mm; applies to both **A** and **B**.

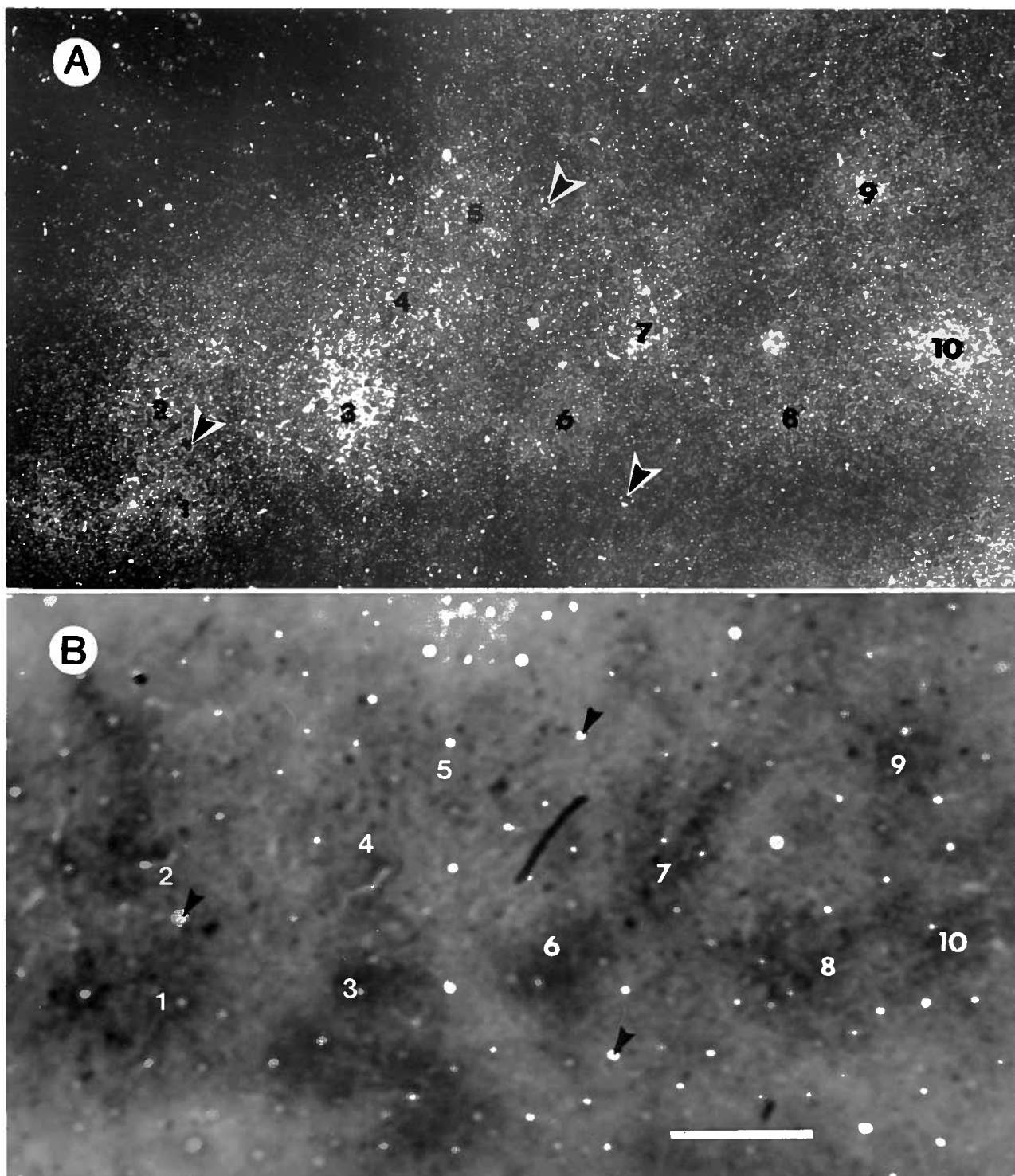


Figure 3.12



laminar distribution within the LGN of the various cell types, it is possible to analyze our results from bulk injections of tracers into particular lamina in terms of X, Y, and W projections.

### Laminar Pattern of Geniculocortical Terminations

The input from the A laminae, containing X and Y cells, was nearly completely confined to layers 4 and 6 in areas 17 and 18. Other studies have suggested that Y cell projections might extend several hundred microns into layer 3, especially in area 18 (Humphery *et al.*, 1985b). These discrepancies are probably due to the use of different laminar schemes and to the inconsistent usage of the same scheme between different studies. For instance, the small pyramidal cells of O'Leary's (1941) layer 5a have been considered both equivalent to (Garey, 1971), and excluded from (LeVay and Gilbert, 1976), layer 4c of Otsuka and Hassler's (1962) lamination scheme, according to different authors.

Regarding the Y cell projections in layer 3 of area 18 reported by Humphery *et al.* (1985), their layer 3/ 4 border appears to correspond to O'Leary's 4a/4b border, as the cells marked "border pyramids" in their Figure 7 are smaller than some pyramidal cells in the figure that are several hundred microns more superficial in the cortex. This scheme of area 18 lamination appears to be related to the fact that the cells in layer 4a of area 18 are larger than their counterparts in area 17, and were thus considered a sublayer of layer 3 (layer 3b) by Otsuka and Hassler (Otsuka and Hassler, 1962). Size aside, however, the cell types of this layer, including the star pyramids, are similar in areas 17 and 18, as noted in Golgi studies by Lorente de N6 (Lorente de N6, 1943). As previously mentioned, use of this scheme also appears to account for the claim that the band of dense CO staining spans the layer 3/4 border in area 18 (Price, 1984). Regardless of whether it should be termed layer 4a or layer 3b in area 18, this sublayer is marked by similar cytology, geniculate A laminae inputs, and dense CO staining in both area 17 and area 18.

The input from the C layers was segregated into an upper and a lower tier in the visual cortex, straddling the A laminae input in layer 4. Our findings concerning the lower tier of labeling contrast slightly with those of LeVay and Gilbert (LeVay and Gilbert, 1976), who concluded that this tier straddles the layer 4/5 border. This may have been due, in part, to the scheme of cortical lamination used (see above). Also, it can be difficult to determine this border in Nissl stained sections, although it was very clearly marked in the alternate sections stained for CO in this study. The lower tier of C laminae labeling appears to specifically target the small pyramidal cells of layer 5a. It would be interesting to examine closely the response properties of cells in layer 5a for physiological evidence of this W-cell projection.

We were also able to show that the upper tier of labeling, straddling the layer 3/4 border, is actually composed of two components, since labeling from the parvocellular C layers (C1 and C2) projected to layer 3 (and also layers 5a and 1), but not to layer 4. Therefore, the labeling in layer 4 appears to arise from the Y-cells in the magnocellular layer C, and the labeling in layer 3 from the W-cells in layers C1 and C2. If future experiments confirm this finding, then W cell input would be completely segregated from cortical cell layers receiving X-and Y-cell input.

### **Geniculate Inputs and Cytochrome Oxidase Staining**

The laminar pattern of geniculate terminations in visual cortex is thought to be related to that shown by histochemical staining for the metabolic enzyme cytochrome oxidase (CO). It has been repeatedly shown that termination sites of thalamic inputs often have high levels of CO staining, and that levels of CO staining are correlated with levels of neuronal activity (Wong-Riley, 1979; Wong-Riley and Riley, 1983; Wong-Riley et al., 1989). It is thought that the high activity level of geniculate terminals, in turn, creates higher activity levels in cortical cells monosynaptically activated from the LGN. The higher activity levels in geniculate recipient layers means these layers will have increased metabolic demand and, therefore, higher CO levels

relative to cortical layers not receiving direct input from the LGN (Kageyama and Wing-Riley, 1986). Also, W, X, and Y geniculate cells have different levels of CO staining, which appear to correlate well with reported differences in rates of maintained and visually evoked activity among these different populations.

At the level of the cortex, layer 4a, the main termination site of Y input in area 17, stains more densely for CO than layer 4b, which is thought to receive only X input. It has been suggested that different levels of activity and, hence, CO staining might be present in populations of cortical cells postsynaptic to different classes of geniculate inputs (Kageyama and Wong-Riley, 1985). Thus, density of CO staining in a cortical layer may be a marker for the number and type of geniculate afferents received. The close correspondences between the dense band of CO staining in layer 4 and the terminations of the more active X- and Y-cells from the LGN and between the lesser CO staining in layers 3 and 5a and the terminations of the less active W-cells are consistent with this. Our data appear to extend this relationship between CO staining and geniculate inputs to comparisons of different cortical columns, as well as layers. In particular, the CO blobs were shown to be specifically targeted by the projections from the C layers of the LGN. The differences in CO staining between blobs and interblobs could be seen in layer 3, where W-cell terminations are made, and also in layer 4a, where the Y-cells from magnocellular layer C terminated.

It is suggested that, in each layer, the difference in CO staining between blob and interblob is due to the presence of a geniculate input in the blobs that is not present in the interblobs. In layer 3, this is readily apparent, as there is no geniculate input to layer 3 in the interblobs. In layer 5a, there is a patchy geniculate input aligned with the blobs in the supragranular layers, but no CO staining. It is possible that the W-cell input to layer 5a arises from a different class of W-cells in the C-layers, which have lower levels of activity than those that project to the blobs in layer 3. It is known that W-cells in the parvocellular C laminae are

physiologically heterogeneous and that several morphologically identified subclasses (gamma, epsilon, g1, g2) of retinal "W-cells" project there (Leventhal, 1982).

In layer 4, although there is obviously geniculate input to and dense CO staining in both blobs and interblobs, this study showed that the Y-cells from the C layers terminate only in the blobs. As Y-cells in the LGN have greater spontaneous and evoked activity than X-cells, and also stain more darkly for CO than X-cells, it is suggested that Y-cell input is responsible for the more dense CO staining in layer 4a blobs versus interblobs. The less dense CO staining in the remainder of layer 4 would then be due to X-cell terminations. At present, it is not known if Y-cells in the A layers of the LGN also selectively target the CO blobs, as is the case for those from the C layers. This question was not possible to address with the bulk injections used in this study, as the A layers contain a mixed population of X-cells and Y-cells so it was not possible to selectively label either population alone. Experiments combining intracellular staining of identified Y-cells from the A laminae with CO histochemistry are needed to answer this question.

Although there is currently no data on the relationship of Y-cell projections from the geniculate A layers to the CO blobs, it is interesting to note that in many other respects A-layer projections show few differences from the Y-cells in the C layers of the LGN. Since single retinal Y-cell axons often send collaterals to lamina A, lamina C, and the MIN (Bowling and Michael, 1980; Sur et al., 1987), it is not surprising that Y-cells in all of these regions have similar physiological response properties (Dreher and Sefton, 1979). Also, the morphology of the geniculocortical arborizations of Y-cells from the various parts of the LGN appears similar (Humphery et al., 1985a; Humphery et al., 1985b). Intracellular injection of HRP has shown that geniculocortical arbors of Y-cells from the A layers, layer C, and the MIN (but not X-cells) possess a patchy distribution of terminals (Humphery et al., 1985a; Humphery et al., 1985b). While thought to be due to the spacing of ocular dominance columns, this patchiness might also be due to the spacing between CO blobs. One difference in connectivity of A and C layer Y-

cells is that a small percentage of presumed Y-cells (based on soma size) in layer C and the MIN project to extrastriate visual areas whereas essentially no cells in the A layers do (Tong et al., 1982). (Some A layer cells do project to extrastriate areas in the kitten, but these appear to be lost during development (Bruce and Stein, 1988; Tong, 1991) ). Thus, there is little reason to suspect that Y-cells in layers A and C should have different projection patterns in visual cortex. Concentration of Y-cell input in the blobs is also suggested by our recent results showing that clusters of cells projecting from area 17 to the posterior medial lateral suprasylvian area (Shipp and Grant, 1991) are concentrated in the CO blobs (chapter 4), and this area is thought to be dominated by Y-cell input (Berson, 1985; Rauschecker et al., 1987).

Because there is no segregated population of X-cells in the LGN, we were not able to examine X-cell terminations in isolation in this study. However, comparing the results of the C-laminae and A-laminae labeling (and assuming that the Y-cell terminations from layer C are representative of all geniculate Y-cell terminations), it appears that X-cell terminations must include both 4a and 4b in the interblobs and at least 4b underneath the blobs. It is not possible to tell, from the results of this study, whether intermingling of X-cell terminals and Y-cell terminations occurs in the layer 4a blobs, or whether X-cell terminations avoid the blobs altogether. A marker for X-cell terminals has recently been tentatively proposed, however (Dyck and Cynader, 1993a). Receptor autoradiography has shown that mesulergine (a selective ligand for the serotonin 1c receptor) binding in the visual cortex disappears after lesions of the LGN. This suggests that these receptors, like nicotinic acetylcholine receptors (Prusky et al., 1987), are located on LGN terminals. Unlike the nicotine receptors, which were present throughout the thickness of layer 4 in both areas 17 and 18, the serotonin 1c receptors were restricted to area 17, mirroring the distribution of X-cell terminations. Moreover, binding was different in the two sublayers of layer 4, forming a continuous band in layer 4b, with evenly spaced columns extending into layer 4a. Comparison with CO staining showed that these columns precisely interdigitated with the CO blobs (Dyck and Cynader, 1993b). If serotonin 1c receptors truly

mark X-cell terminals, it would suggest that X-, Y-, and W-cell terminations are largely segregated within the cat's visual cortex. A schematic diagram illustrating the laminar and columnar terminations of LGN X, Y, and W cells demonstrated in this study is shown in Figure 3.13.

### **Relationship of C-laminae patches to Ocular Dominance Columns**

LeVay and Gilbert (1976) were the first to note that the projection from the C-laminae to area 17 was patchy. They suggested that this patchiness was due to the fact that even though the C-laminae receive inputs from both eyes, the input to the C-laminae from the contralateral eye was greater than the input from the ipsilateral eye. It was thus suggested that the patches of C-laminae labeling represented the ocular dominance columns of the contralateral eye. In a similar vein, this chapter has argued that the input from the C-laminae to layer 4a is from Y-cells, and these Y-cells are thought to be confined to lamina C, which receives input from the contralateral eye only. However, evidence from CO staining suggests that the C-laminae patches are not aligned with contralateral OD columns. It was shown in the current study that the patches of labeling from the C-laminae align with the CO blobs, and the relationship of CO blobs and OD columns in the cat has been examined, albeit with slightly conflicting results (Murphy et al., 1991; Dyck and Cynader, 1993b). One study (Dyck and Cynader, 1993b) concluded that the OD and CO blob systems were independent, with CO blobs found roughly equally over both the centers and edges of OD columns, while the other study (Murphy et al., 1991) found that CO blobs tended to be associated with the centers of OD columns. Both of these studies, however, agreed that CO blobs in the cat were over both contralateral and ipsilateral eye dominance columns. Thus, it is not likely that the patchiness of the C-laminae projections was due to OD columns.

Figure 3.13 Diagram of the X, Y, and W pathways of the cat's visual system. The diagram shows the three different cell classes in the retina (bottom), and the lateral geniculate (middle). The top part of the diagram shows the termination in area 17 of W-, X-, and Y-geniculocortical fibers, shown by three different densities of shading, W being lightest and Y being darkest. It is assumed that the Y-cell terminations from layer C described in this study are representative of all geniculate Y-cell terminations. The crosshatched pattern in layer 6 and layer 4a shows mixing of X-cell and Y-cell inputs. The X-cell input to layer 4a of the cytochrome oxidase blobs is marked with question marks because it was not possible to tell from this study whether X-cell terminations are found in or avoid the 4a blobs.

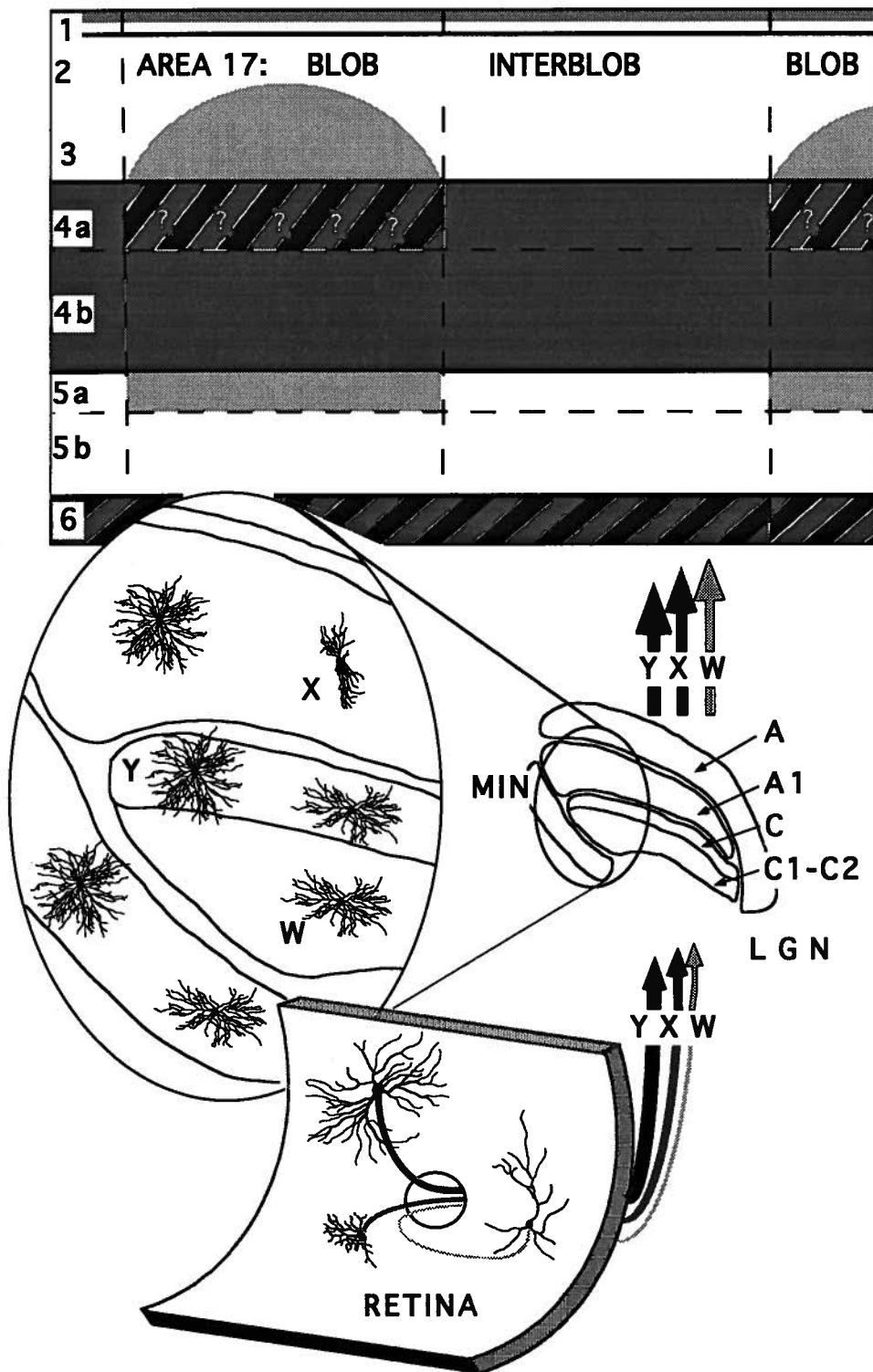


Figure 3.13



If CO blobs are associated with both ipsilateral and contralateral OD columns, however, how can every CO blob, some of which must be over ipsilateral OD columns, have a Y-cell projection to layer 4a that apparently comes from the magnocellular lamina C, a contralateral eye-dominated layer? There are several possible explanations. First, cat OD columns are not as well defined as in macaque monkeys, for instance, and it has been argued that inputs from the contralateral eye are more confluent than those from the ipsilateral eye, which are more obviously patchy (Shatz et al., 1977). However, at least one recent study has shown that the segregation of inputs from the two eyes in the cat's visual cortex is better than previously expected (Hata and Stryker, 1994). Therefore, overlap of contralateral and ipsilateral inputs probably does not account for the Y-cell input into CO blobs over ipsilateral OD columns. Is it possible that an ipsilateral Y-cell-containing counterpart to the contralateral Y-cell-containing layer C exists? It has been noted that a few ipsilateral retinal Y-cell axons terminating in lamina A1 also send a collateral to the C-laminae (Bowling and Michael, 1984). Another, more likely source of ipsilateral Y-cell input to visual cortex is the large cells that are found in the intralaminar space between layers A1 and C. Often, the density of cells in this space is nearly as great as the density of cells in lamina C itself, making the border between lamina A1 and C much less clear than the border between lamina A and A1. The large size of cells in the intralaminar space is suggestive of Y-cells, and the position of these cells next to lamina A1 suggests that they could possibly receive ipsilateral inputs. Unpublished observations from this laboratory show that abundant retinal projections are made to the intralaminar space between A1 and C, but not between A and A1.

### **Geniculocortical Projections in Area 18**

We also studied geniculocortical terminations in area 18. Previous studies have shown that X-cell input is lacking in area 18 (Tretter et al., 1975; Dreher et al., 1980; Harvey, 1980; Humphery

et al., 1985b). The W-cell input in area 18 appears to have the same laminar termination pattern and relationship with the CO blobs as seen in area 17. The Y-cell input, however, has a different laminar pattern of termination in area 18 than in area 17. In agreement with the study of LeVay and Gilbert (1976), we found that labeling in layer 4 from the C laminae, instead of being confined to layer 4a as in area 17, extended throughout layer 4. However, labeling in layer 4 was often slightly patchy, being densest in the CO blobs, although the gaps between the patches were never as free of labeling as was the case in area 17. Sometimes the patchiness in layer 4 disappeared, showing complete filling-in with terminal labeling, although the W-cell terminations in layers 3 and 5a were still patchy. However, a similar pattern of layer 4 showing complete filling-in with patches of labeling in layer 3 and 5a was sometimes seen in area 17 following very large injections which spread to involve all layers of the geniculate at particular isoelevation representations; a similar explanation for the lack of patchiness in area 18 in some sections cannot be ruled out. Therefore, it is likely that projections from the C laminae are somewhat patchy in layer 4 of area 18. Projections from the A layers, however, appeared to be continuous in layer 4 of area 17, raising the possibility that projections from the C layers of the geniculate to area 18 are organized differently than projections from the A layers. However, both the A layer and the layer C projection to area 18 is thought to arise from Y-cells and, as discussed above, Y cells in the various parts of the LGN have not been shown to differ significantly.

Another explanation of these results is that Y-cell input from the different parts of the LGN to area 18 is similarly organized, but that input is not homogeneously distributed, being stronger to the blobs in layer 4a than to other parts of layer 4. Reconstructions of individual intracellularly filled Y-cell axons, from both A and C layers in area 18, have shown that, although these axons have projections to both layers 4a and 4b, the projection to layer 4a is invariably stronger than that to layer 4b (Freund et al., 1985). The patchiness of Y-cell axons, which we have suggested might be partly due to their selective termination in blobs, appears to

be less distinct in area 18 than in area 17, with many more boutons distributed to the spaces between the patches (Humphery et al., 1985a; Humphery et al., 1985b). The single axon data are thus consistent with the hypothesis that the driving geniculate input that is responsible for the CO blobs of layer 4a of area 18 is the same, albeit more profuse, Y-cell input that is found in the other parts of layer 4. Presumably, when labeling of layer 4 in our experiments was relatively weak, the patchiness was visible; however, when the labeling was more robust, whether from A layers or C layers, the patchiness was no longer visible due to the high contrast in the WGA-HRP reaction procedure. It would then be expected that a more quantitative labeling procedure would show a difference in numbers of Y-cell geniculate terminations between blobs and interblobs in area 18. The increased CO activity in the layer 4a blobs of area 18 would thus be caused, not by the presence of a special class of inputs with higher activity than those that terminate elsewhere in layer 4, but by a higher concentration of the same inputs that terminate elsewhere in fewer numbers.

## 4 CORTICAL AFFERENTS TO A LATERAL SUPRASylvian AREA

The medial bank of the suprasylvian sulcus of the cat contains a visually responsive area which has the distinction of being one of the first areas outside of the striate cortex in any animal to be found to be visually responsive. This area was first mapped in detail by Tusa and colleagues (Palmer et al., 1978), who subdivided the area into several smaller areas. One of these areas, the posterior medial lateral suprasylvian area (PMLS) receives input from the striate cortex. The area defined by the presence of area 17 inputs does not exactly match the area defined as PMLS by Tusa et al., suggesting that their maps of the area need to be revised (Sherk, 1986). On these grounds it has been suggested that the terminology of Tusa et al. be dropped, replacing the term PMLS with the more generic lateral suprasylvian area (Sherk, 1986); the term, however, is maintained here (with full awareness that extent of the area differs from that originally proposed by Tusa et al.) because it is topographically descriptive, is compatible with the presence of other visual areas in the suprasylvian sulcus and, at any rate, has become entrenched in the literature.

An earlier study showed that many of the corticocortical connections of PMLS are patchy (Symonds and Rosenquist, 1984a). Perhaps more interestingly, two recent studies using relatively large injections have suggested that cells in area 17 projecting to PMLS have a truly discontinuous, hard patterned organization (Shipp and Grant, 1991; Ferrer et al., 1992). Because PMLS has a high percentage of neurons selective for direction of stimulus motion (Hubel and Wiesel, 1969b; Spear and Baumann, 1975; Camarda and Rizzolatti, 1976; von Grünau et al., 1987; Gizzi et al., 1990; Yin and Greenwood, 1992), the patchy pattern of connections with area 17 was argued to provide evidence for segregation of a motion pathway in area 17 (Shipp and

Grant, 1991). However, it was not completely clear that these studies used large enough injections to demonstrate a truly discontinuous distribution of PMLS-projecting cells.

The purpose of this study was to confirm these results by using large series of injections extensive enough to cover most of the lower visual field representation of PMLS. The second aim of the study was to compare the hard patterned labeling pattern of PMLS-projecting cells in area 17 to the blobs shown by CO staining. It was hypothesized that some regular relationship might exist between these two patterns. Very large injections of retrograde tracers were made in PMLS. Tangential sections through flattened visual cortex were used to better appreciate the variation in labeling density and in CO staining. The existence of a discontinuous organization of PMLS-projecting cells in area 17 was confirmed. In addition, this finding was extended to area 18. In both of these areas, the patches of PMLS-projecting cells were found to correspond to cytochrome oxidase blobs. These results show that a tangential organization marked by differences in CO staining and corticocortical connections is not restricted to visual areas of primates, but is also found in certain visual areas of the cat. Some of these results have been previously presented in abstract form (Boyd and Matsubara, 1992).

### **Methods and Materials:**

Data presented were obtained from eight experiments involving large injections of tracers into the PMLS of adult cats of both sexes. Five animals received injections of WGA-HRP. Three animals received injections of cholera toxin subunit B, either unconjugated (CTB) or conjugated to 7nm colloidal gold particles (CTB-Au).

The brain was exposed from stereotaxic coordinates AP -3 to +6 and ML 7-15 mm. Injections were made into the medial bank of the suprasylvian sulcus, beginning just anterior to the genu where it becomes the posterior suprasylvian sulcus, and continuing for 5 or more mm. Several laboratories have physiologically mapped this area, and it is known to contain the lower

visual field representation of PMLS/LS (Palmer et al., 1978; Grant and Shipp, 1991; Sherk and Mulligan, 1993). Pipettes with long, narrow tapers were tilted medially at 30° to 45° (depending on AP level) from vertical in order to follow the slope of the sulcus. Ten to fifteen 500-750  $\mu$ m spaced penetrations were made through the 4-5 mm depth of the sulcus, injecting tracer at 1 mm intervals along each penetration. About 10-12 ml of tracer was injected in total in each experiment. Survival times varied from 1-4 days.

## **Results**

### **Tangential organization of PMLS-projecting neurons**

In order to demonstrate that the distribution of PMLS projecting neurons was truly discontinuous, it was necessary to make the injection sites very large. It was also important that the injection site be of uniform density. Figure 4.1A is a low power photomicrograph of part of a tangential section illustrating one of the injection sites used in this study. The more than 15 small injections made side by side have fused into one continuous injection site, with no gaps or fluctuations in density between injections. Fluctuations of labeling density, then, were not likely due to differences in the uptake of tracer from different parts of the injection site. This is more easily appreciated in Figure 4.1B, which shows the same injection site at a slightly higher power. Here, many of the individual pipette tracks are visible. In addition to the even density of staining between pipette tracks, note that many of the pipette tracks can be followed for 2-3 mm before they pass out of the plane of section. Thus, the pipettes were angled correctly down the medial bank of the suprasylvian sulcus. The exact angle of the injection pipette was crucial, since the area of interest was located down the bank of the suprasylvian sulcus, and since an incorrect angle would lead to injection of tracer into the white matter. An injection site, similar to those used in the present study, but cut in the coronal plane, is shown in Figure 4.1C. The dense center

Figure 4.1. Examples of injection sites in PMLS typical of those used in this study. **A.** The dashed white line outlines the WGA-HRP injection site in this tangential section. Anterior is towards the top of the figure, and medial is towards the left. The boundary of areas 17 and 18, determined from an adjacent section stained for CO, is outlined by the dashed black line. The small right-pointing arrowheads show patchy labeling medial to area 17 in the splenial visual area. The small left-pointing arrowheads show patches of labeling in area 19. The large left-pointing arrowhead shows labeling in the posterior suprasylvian sulcus. Scale bar: 5mm. **B.** Same injection site shown in Figure 2A, at higher magnification. The white arrowheads show the close spacing of individual pipette tracks. Scale bar: 2mm. **C.** WGA-HRP injection site similar to the ones used in this study, but cut in the coronal plane. This figure shows the minimal involvement of the white matter in these injections, and the depth of the injections within the sulcus. Scale bar: 1mm.

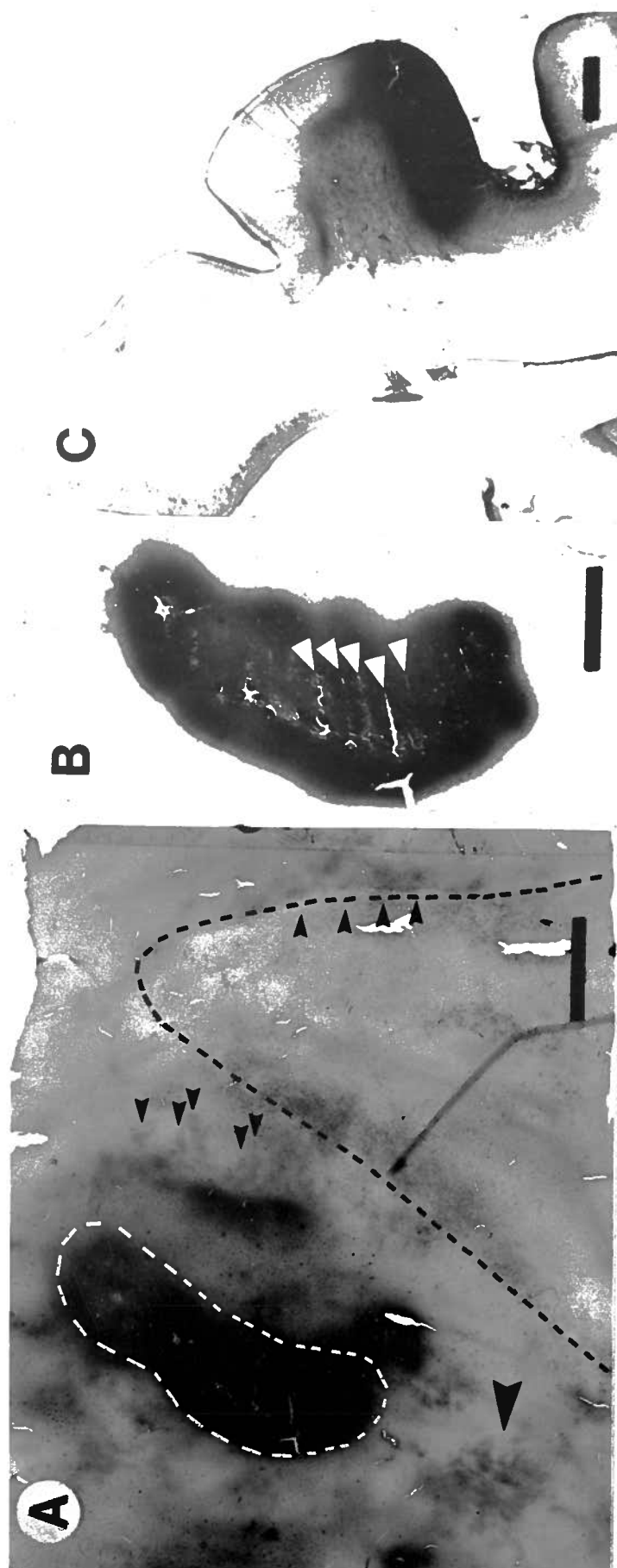


Figure 4.1



of the injection site is confined to the cortical gray matter. There is a slight spread of tracer into the underlying white matter. This was probably typical for the injection sites used in this study. As only damaged fibers in the white matter are thought to transport HRP effectively (Ferster and LeVay, 1978), the slight spread of tracer into the white matter was assumed not to have affected the results. This assumption is also supported by the fact that similar patterns of labeling were obtained from injections confined to gray matter using CTB-Au, a tracer which is not readily diffusable due to gold conjugation (Lewellyn-Smith et al., 1990). Additionally, patterns of thalamic connectivity arising from these injections were always in agreement with results from other studies of the PMLS (Grant and Shipp, 1991; Tong, 1991); as surrounding areas of cortex have different patterns of thalamic connectivity (Raczkowski and Rosenquist, 1983; Rosenquist, 1985), this again suggests that the injection sites were confined to the cortical gray matter of the PMLS.

The injection sites used in this study were purposefully larger than those used in previous studies (Shipp and Grant, 1991; Ferrer et al., 1992), attempting to show a hard patterned distribution of PMLS-projecting cells in area 17. The extent of labeling in area 17 from the injections in earlier studies only covered an extent of about 5mm and thus only 5-6 cycles of the pattern (Figure 5 of Shipp and Grant (1991), e.g.) and may not have been very much larger than the convergence of multiple patches of area 17 onto a single injection site. Would PMLS-projecting cells still be hard patterned with injections large enough to give labeling over a much larger extent of area 17? Figure 4.2 is a reverse-contrast "histograph", made by placing the section directly into the enlarger, showing cells in a tangential section of area 17 retrogradely labeled from a very large series of injections in PMLS. Retrogradely labeled cells formed an irregular lattice of dense clusters of labeling separated by spaces of less dense labeling. The spacing of these clusters ranged from 0.5 to 0.9 mm. Note that the patchy labeling shown in this figure has an extent of well over 10 mm. Thus, convergence from spatially separated columns in

Figure 4.2. A tangential section through area 17 showing cells retrogradely labeled from a large WGA-HRP injection in PMLS. This "histograph" was produced by placing the slide-mounted tissue directly into the photographic enlarger, so labeled cells appear bright on a dark background. The retrogradely labeled cells do not have a uniform distribution, but are clustered at intervals of slightly less than 1mm. Scale bar: 1mm

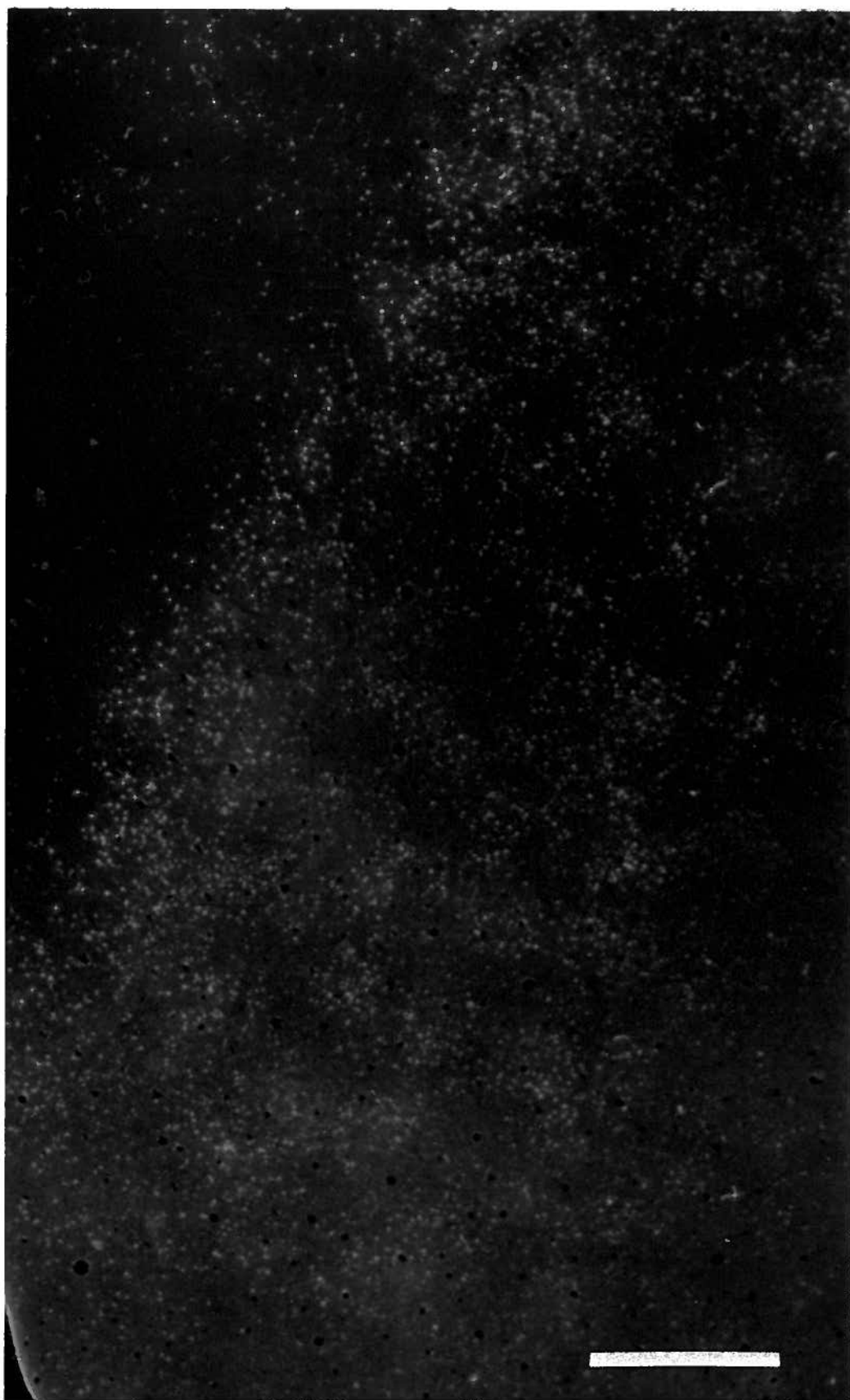


Figure 4.2

area 17 onto a single injection site in PMLS was effectively ruled out as a source of the patchiness, and a hard patterned projection from area 17 to PMLS was confirmed.

Figure 4.3A shows a reconstruction of labeling in areas 17 and 18 following a large injection in PMLS. In this experiment, only four tangential sections were used to show CO staining and the remainder were reacted for HRP to show PMLS-projecting cells. Labeling from all of the HRP-reacted sections is collapsed onto a single plane, wherein each dot represents a single retrogradely labeled cell body. In order to identify the position of the 17/18 border, which is difficult to determine in tangential sections, a small injection of CTB was made in area 17 near the 17/18 border, just anterior to the area shown in Figure 4.3. The patches of corticocortical labeling in area 18 (which could be distinguished from local, intrinsic labeling in area 17 by their larger spacing and different laminar distribution) arising from the injection of CTB in area 17 provided a guide to the placement of the 17/18 border in Figure 4.3A. The dashed line indicating the border was placed parallel to the lateral border of area 18 (visible in the CO stained sections) and midway between the lateral-most of the local patches in area 17, and the medial-most of the corticocortical patches in area 18. Although these groups of patches were only a few mm apart, they could be differentiated by the larger sizes of the patches in area 18. The patchy pattern of PMLS-projecting cells in both area 17 and area 18 is evident.

Figure 4.3B shows the same data expressed as the density of labeled cells under a 100  $\mu\text{m}$  grid. The largest number of PMLS-projecting cells under a single 100  $\mu\text{m}^2$  grid box was 36, corresponding to 3600 PMLS-projecting cells/ $\text{mm}^2$ . The average density of labeled cells within the dashed rectangle was 928 cells/ $\text{mm}^2$ . As can be seen from the transects shown in Figure 4.3D-E, the density of labeled cells appeared to be slightly greater in area 18 than in area 17, although an average density was not calculated for area 18 as the smaller area labeled made it more difficult to get a sample that was not biased towards either the patches of labeled cells or the spaces in between them.

The fluctuations in density of PMLS-projecting cells were especially apparent when the reconstructions of labeling patterns were blurred with spatial averaging or a Gaussian filter, as shown in Figure 4.3C. Patches of relatively greater density can clearly be seen in both area 17 and area 18. It is apparent that the patches are, on average, slightly larger and more widely spaced in area 18 than in area 17. In area 18, the largest spacing observed between patches was slightly larger than 1mm, while in area 17, the largest spacing observed was slightly less than 1mm. The differences in labeling in areas 17 and 18 are also shown in Figures 4.3D and 4.3E. These profile plots of transects through area 17 and 18 taken along the marked lines in Figure 4.3B show the differences in periodicity and labeling density between these two areas.

### **Correspondence of PMLS-Projecting Cells and CO Staining**

Direct comparison of CO blobs to patches of PMLS-projecting cells was obtained by reacting alternate sections for HRP and CO. Figure 4.4 is a low power photomicrograph showing the alignment of CO staining with PMLS-projecting cells in area 17. To make this figure, a section reacted for HRP was placed directly on top of an adjacent section stained for CO, and carefully aligned using blood vessels common to the two sections. Note that this direct comparison of alternate sections shows that the dense patches of PMLS-projecting cells align with the CO blobs.

The correspondence between CO blobs and PMLS-projecting cells in areas 17 and 18 was also evident after quantification of the labeling pattern. Another example of the correspondence of CO blobs with patches of PMLS-projecting cells is shown in Figure 4.5. In this figure, part of the computer reconstruction of PMLS-projecting cells shown in Figure 4.3 was graphically superimposed on a digitally captured image of CO staining from an adjacent section. Area 18 is to the right, while area 17 is to the left; the area 17/18 border runs

Figure 4.3. Computer-generated plot of PMLS-projecting cells in areas 17 and 18. A. WGA-HRP labeling from 15 tangential sections, aligned and collapsed onto a single plane to give a surface view of PMLS labeling. Each dot represents a single retrogradely labeled cell. The 17/18 border (dashed line) was determined from the pattern of labeling from an injection of CTB into area 17 near the 17/18 border. Scale bar applies to A-E B. the same data as in Figure 4.4A expressed as the density of labeled cells per unit area. The size of each grid square is 100  $\mu\text{m}$ . The dashed box outlines the area used to calculate the average density of PMLS-projecting cells (see text). The arrows show the lines sampled for the profile plots shown in D and E. Lines D-E illustrate transects through area 17 and 18, respectively. This data was then Gaussian filtered to produce C. Note the difference in spacing of the pattern in area 18 (E), which is slightly larger than in area 17 (D). D. Profile plot of transect through area 17 marked "D" in Figure 4.4B. The numbers to the left show the minimum and maximum number of cells encountered in the plot; the number underneath the plot corresponds to its length. Arrows mark peaks in the density of labeling. E. Profile plot of transect through area 18 marked "E" in Figure 4.4B. Other conventions as in 4.4D. F. Power spectra of spatial frequency for area 18 (thin line) and area 17 (thick line). Each line shows the averaged spectra of three (area 18) or five (area 17) separate transects. The left axis shows the Fourier energy at each frequency along the bottom axis. As would be expected from visual inspection, the major peak for area 18 occurs at slightly less than 1 mm/cycle, while that for area 17 occurs at just greater than 1mm/cycle.

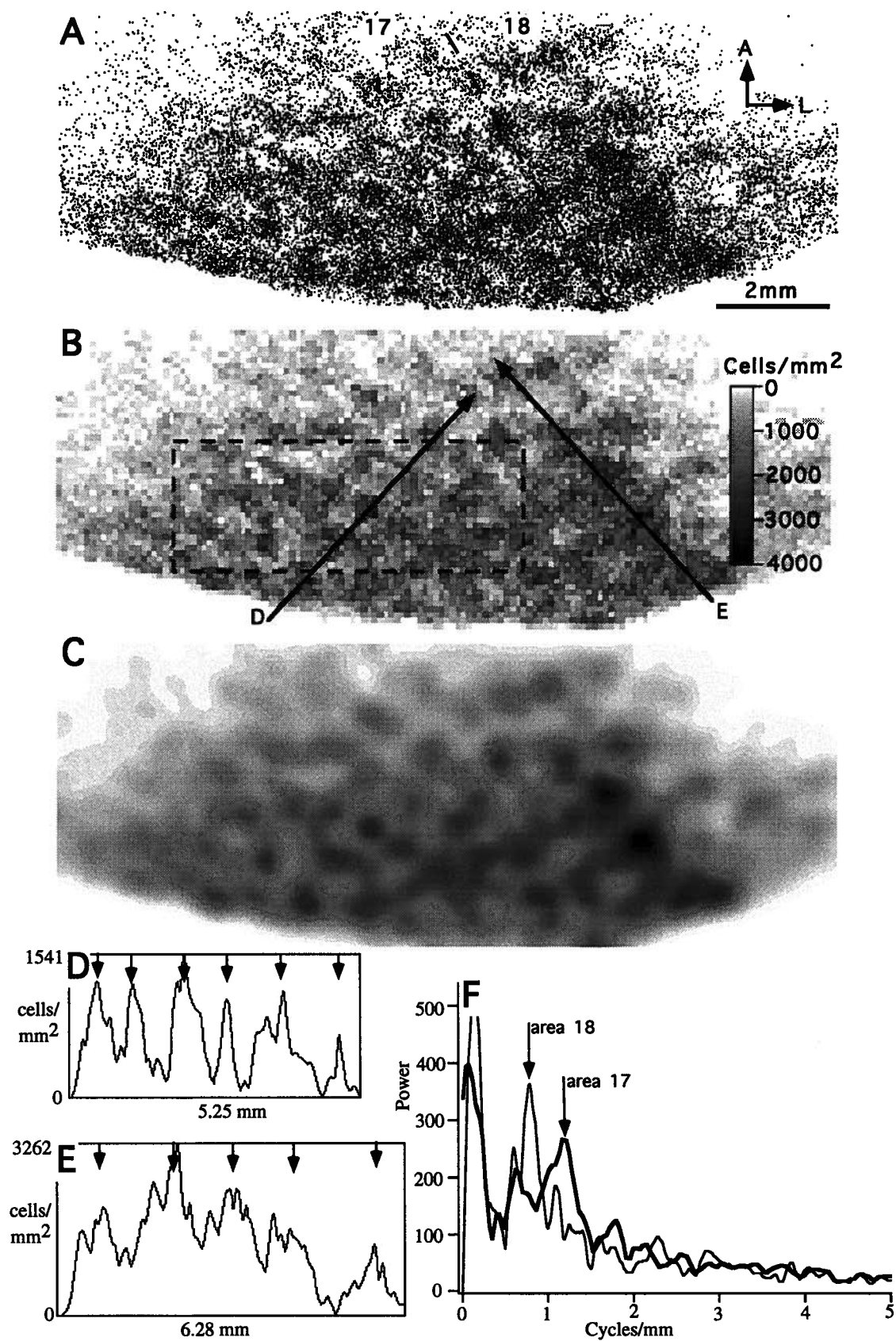


Figure 4.3

approximately through the middle of the figure. It can be seen that, as in area 17, patches of PMLS-projecting cells in area 18 tend to lie within the CO blobs.

### **Labeling in Other Cortical Areas**

Many other areas other than 17 and 18 also contained extensive labeling, as has been previously described in earlier studies (Symonds and Rosenquist, 1984a; Grant and Shipp, 1991). As the borders of many of these areas are difficult to determine, especially in flat sections, it is not easy to assign labeling to individual cortical areas. However, it is interesting to note that labeling in areas other than areas 17 and 18 were also patchy following the very large injections used in this study. In Figure 4.1A there is an area of patchy labeling posterior to the injection site in the posterior suprasylvian sulcus which may correspond to area VLS (large arrow-head), and irregular clumps of labeling medial to area 17 (small right-pointing arrow-heads), in what has been called the splenial visual area (SVA) (Kalia and Whitteridge, 1973). Note also in Figure 4.6 the patchy labeling anterior and slightly medial to the injection site, on the crest of the suprasylvian gyrus. This is the first demonstration that, in addition to area 17, extrastriate areas can also demonstrate hard patterning of corticocortical connections arising from PMLS injections. In all labeled areas, with one exception, the patches of labeling had a spacing of roughly 1mm.

In area 19, however, a completely different, and quite unexpected, pattern of PMLS-projecting cells was found. The patches of PMLS-projecting cells in area 19 had a larger spacing than in any other area, several times greater than the spacing of patches of labeling in area 17 and 18. Patches of labeling were often elongated at right angles to the long axis of area 19. An example of these patches is visible in Figure 4.1A (small left-pointing arrow-heads). Another example of these large patches in area 19 is shown in Figure 4.6 (arrows). The labeling shown in Figure 4.6 is shown again in Figure 4.7A, but displayed as a density map.. A photomicrograph,



Figure 4.4 Photograph of two superimposed serial tangential sections through area 17, one reacted for CO to show the blobs and one reacted for WGA-HRP to show the patches of PMLS-projecting cells. The two sections were aligned using blood vessels as landmarks. Many of these paired blood vessels are visible in the photomicrograph (arrowheads). As the focal plane is at the level of the WGA-HRP-reacted section, the blood vessels in the CO-reacted section appear slightly out of focus. The patches of PMLS-projecting cells align with the CO blobs in area 17. Scale bar: 2mm.

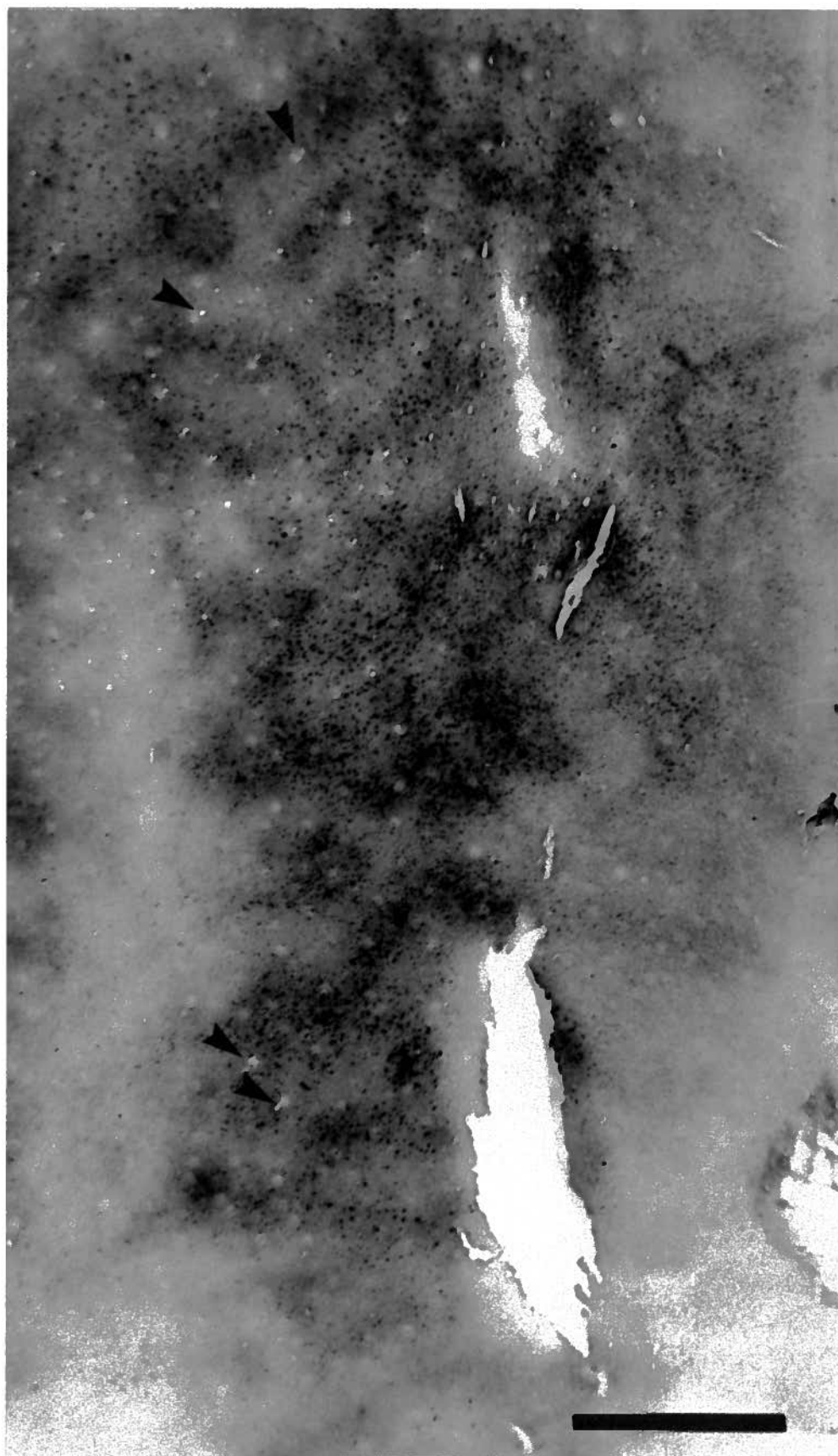


Figure 4.4

Figure 4.5. Computer-generated plot of PMLS-projecting cells in areas 17 and 18 superimposed onto a digitally captured image of CO staining. This figure shows the same PMLS-projecting cells shown in Figure 4.3. As in Figure 4.4, the pattern of blood vessels was used for alignment. The patches of PMLS-projecting cells align with the CO blobs in area 18 as well as in area 17. The CO blobs and patches of PMLS-projecting cells tend to be slightly larger in area 18 than in area 17.

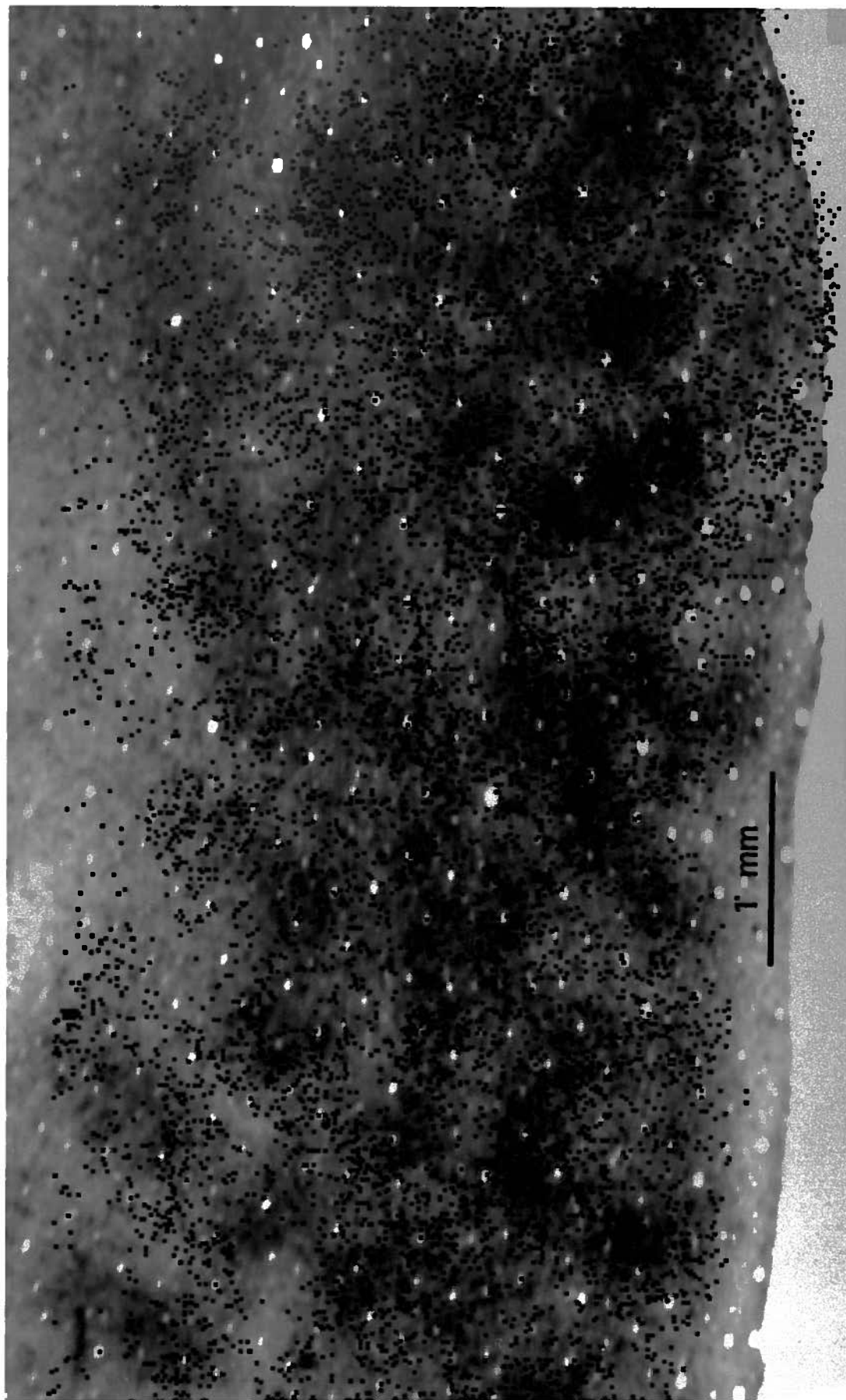


Figure 4.5

Figure 4.7B, shows how clearly these patches are visible, even in a single section. PMLS-projecting cells in area 19 were extensive throughout nearly the entire series of tangential sections, in contrast to areas 17 and 18 where retrograde labeling was quite sparse in the deeper sections. Terminal labeling was also differently organized among these areas. In areas 17 and 18, terminal labeling was found to be confined to layers 1 and 6, distinctly separate from the labeled cells in layers 3 and 4, and was not patchy; in area 19, terminals were found in the same layers and in the same patches as the labeled cells (Fig. 4.7C).

## **Discussion**

By making significantly larger injections in PMLS than were used in previous studies (Shipp and Grant, 1991; Ferrer et al., 1992), the experiments reported in this chapter have confirmed previous suggestions that cells in area 17 projecting to PMLS have a truly discontinuous organization; i.e., they show hard patterning. Additionally, hard patterning of PMLS-projecting cells in areas 18 and 19 has been found. Moreover, in areas 17 and 18, a matching pattern of CO staining was observed. What do these results tell us about the tangential organization of PMLS-projecting areas?

### **Role of Y-cells in Tangential Organization of CO Blobs**

Shipp and Grant have previously discussed the discontinuous organization of PMLS-projecting cells and the possible implications for columnar organization in area 17 arising from this (Shipp and Grant, 1991). The Y-cell pathway dominates the inputs to PMLS, as measured physiologically by differences in latency to stimulation along different parts of the visual pathway. The absolute latency suggests a polysynaptic and most likely corticocortical origin of at least some of these inputs (Berson, 1985; Rauschecker et al., 1987). Thus, it was speculated

Figure 4.6. A computer generated plot of PMLS-projecting cells labeled with CTB-Au in four alternate tangential sections. Each dot represents a single labeled cell. The edge of the tissue is shown in solid black lines, and the fundi and lips of the lateral (Lat) and suprasylvian (SS) sulci are indicated by finely dashed lines. The outline of areas 17 and 18 is indicated by a coarsely dashed line. The arrows indicate patches of labeling in area 19. The outline of the injection site (Inj) is shown. Medial (M) and anterior (A) cortical axes are indicated by the arrows. The cortical areas that some of the foci of dense labeling correspond to are indicated based on gyral and sulcal patterns. Note the patchiness of the labeling, and the large size of the patches of labeling in area 19. SVA, splenial visual area; VLS, ventral lateral suprasylvian area.

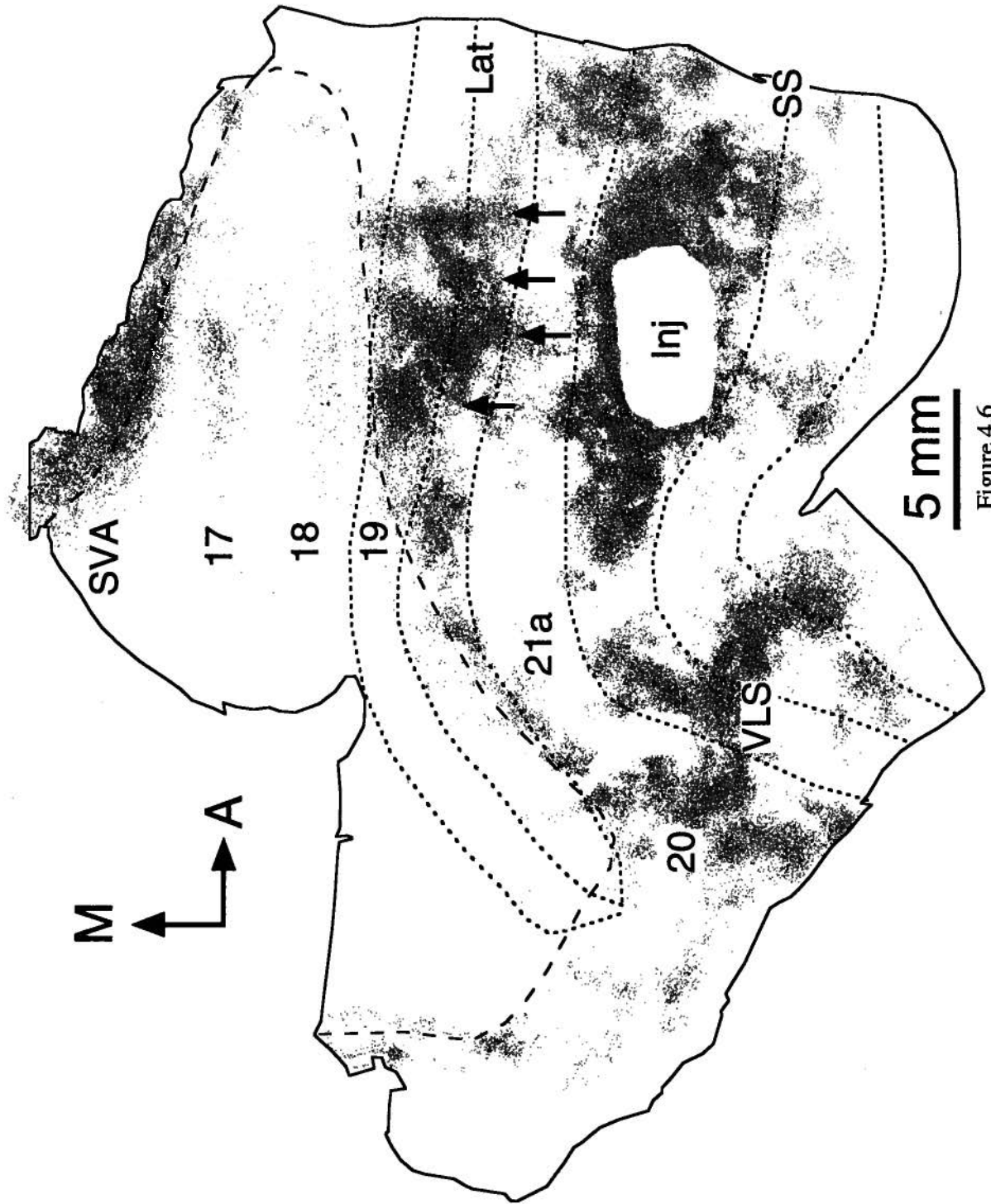


Figure 4.6

Figure 4.7. The pattern of PMLS-projecting cells in area 19. **A.** Density chart of labeled cells in area 19 retrogradely labeled from a CTB-Au injection in PMLS (data from figure 3). Note the dense patches of PMLS-projecting cells with a spacing of approximately 2 mm. Often, the patches are elongated into stripes that run across the width of area 19. **B.** A photomicrograph of a section through area 19 from the same experiment illustrated in **A**, showing the same clusters of CTB-Au labeled cells in a single section. **C.** A photomicrograph of a section through area 19 from a different experiment in which WGA-HRP was injected in PMLS. Anterograde as well as retrograde labeling is clustered into elongated patches. In **A**, **B**, and **C**, medial is towards the left, and anterior is towards the top. Scale bars in **B** and **C**: 1mm.



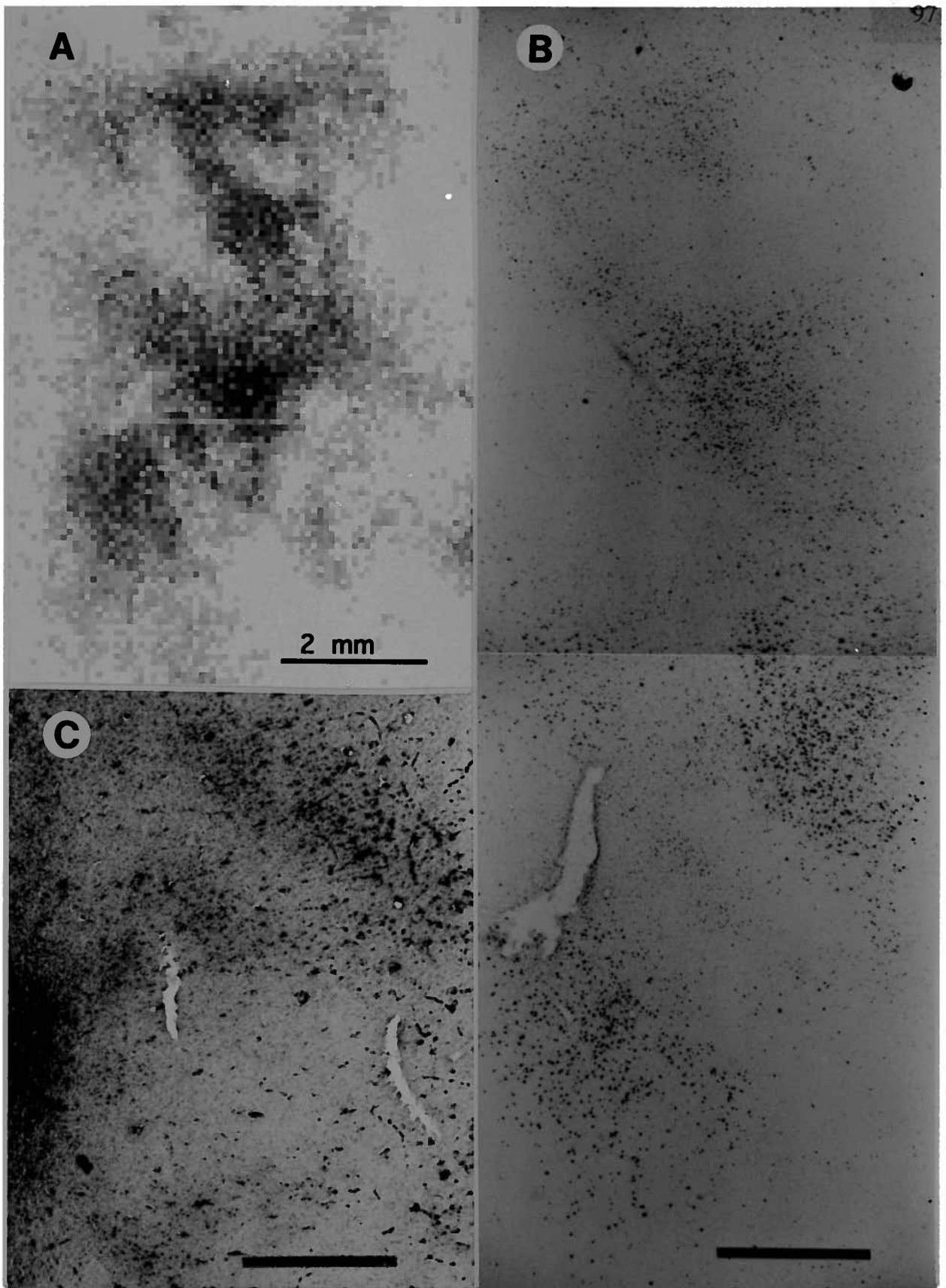


Figure 4.7

that the PMLS-projection bands might correspond to a (hypothetical) tangential segregation of the Y-cell pathway through area 17. In support of this suggestion, they cited evidence for a columnar organization of spatial frequency selectivity in area 17 (Tootell et al., 1981; Berardi et al., 1982) which might be expected if Y-cells, possessing larger receptive fields were segregated from X-cells with smaller receptive fields. It has recently been shown that the C-laminae of the lateral geniculate nucleus (LGN), which contain Y- and W-cells (Sherman, 1985; Spear et al., 1989; Casagrande and Norton, 1991), project selectively to the CO blobs (Chapter 3; Boyd and Matsubara, 1993). As the clusters of PMLS-projecting cells are also within the CO blobs, there is now some evidence for a segregated pathway driven by Y- and W-cells extending from the retina, through the LGN and area 17, and into extrastriate cortex.

### **Tangential Organization of Area 18**

It is thus perhaps rather odd that in area 18, an area that appears to be dominated by Y-input and does not appear to receive X-input (Tretter et al., 1975; Humphery et al., 1985b), we have found a similar segregation of inputs from the LGN C-laminae and outputs to PMLS into CO blobs. The CO blobs in area 18, if not marking a segregation of Y- and W-cell input from X-cell input, may be showing sites of increased density of LGN inputs, or they may be marking a segregation between different sub-classes of Y-cell input. Alternatively, there may be differences in projections from area 17, or some other cortical area, to interblobs and blobs in area 18. Any of these possibilities could explain the CO blob-related corticocortical connectivity of area 18. Future experiments will hopefully address these possibilities.

**LS-projecting Cells in Area 19**

The distribution of PMLS-projecting cells in areas other than areas 17 and 18 was also hard patterned. Interestingly, the patches of LS-projecting cells and their spacing in area 19 was much larger than in areas 17 and 18, or any of the other labeled areas in this study. The significance of this is not known, but it points towards area 19 having a columnar organization as does areas 17 and 18, but with a periodicity about double that of these areas.

There is little physiological evidence for columnar organization in area 19. It was noted by Hubel and Wiesel that cells with similar orientation specificity were grouped together in area 19, but the organization of orientation specificity across the surface of the cortex was not studied (Hubel and Wiesel, 1965). Ocular dominance columns, on the other hand, have been shown not to be present in area 19 (Hubel and Wiesel, 1965; Tieman and Tumosa, 1983). It has been noted, however, that the retinogeniculocortical inputs to area 19 have a patchy organization, with a spacing that is at least as large as the spacing shown here (Anderson et al., 1988).

In conclusion, the discontinuous organization of CO staining and corticocortical connectivity demonstrated in this study suggests the presence of novel forms of columnar organization in multiple visual areas of the cat. This columnar organization may be related to the segregation of different processing streams, one of which passes through PMLS.

## 5 ORGANIZATION OF CORTICAL AFFERENTS FROM AREAS 17 AND 18 TO AREA 19

Area 17 of the cat has projections to multiple target areas. These include area 18, area 19, and areas of the lateral suprasylvian gyrus. Cells in area 17 projecting to each of these areas have a patchy distribution (Ferrer et al., 1988; Ferrer et al., 1992). This raises the interesting question of how all of these different patchy patterns are related. One study has concluded that there is a "...complex relationship between the sets of association cells projecting to different extrastriate regions: they do not completely overlap, only partially, and share some cortical zones but not others" (Ferrer et al., 1992). As it has been shown in this thesis that at least one population of cells projecting from area 17 (those projecting to PMLS) are concentrated within the CO blobs (Chapter 4), one way of determining the spatial relationship of the various corticocortical labeling patterns would be to compare them all to patterns of CO staining.

In this chapter, the tangential distribution of cells projecting to area 19 were examined. Area 19 has been variously thought of as being a specialized extrastriate area (Hubel and Wiesel, 1965) or as forming, with areas 17 and 18, three "parallel primary visual cortical areas" (Spear, 1991). Although there is direct geniculate input to area 19, it is derived only from the W-cells of the LGN (Dreher et al., 1980), and is distributed in a patchy fashion, such that parts of area 19 receive no LGN input at all (Anderson et al., 1988). A substantial portion of the input to area 19, then, may be from intercortical sources.

Cells in area 17 projecting to area 19 have been reported to have a patchy distribution (Gilbert and Kelly, 1975; Gilbert and Wiesel, 1981; Bullier et al., 1984; Bullier and Kennedy, 1987). A previous study has provided evidence that the projection from area 17 to area 19 is hard patterned (Ferrer et al., 1992). The purpose of this study was to confirm these results by

using a series of large injections, extensive enough to cover a substantial visual field representation of area 19. The second aim of the study was to compare the labeling patterns in area 17 to the blobs shown by CO staining.

A third aim of the study was to examine local connectivity within area 19. This was of special interest because studies of projections to the PMLS (Chapter 4) show that PMLS-projecting cells in area 19 are organized in larger, more widely spaced patches than are found in areas 17 and 18. It was thus of interest to see if this same scale of patchiness would be reflected in local connectivity.

Large injections of retrograde tracers were made in area 19, and alternate tangential sections were stained for CO or to visualize the tracer. Unlike PMLS projecting-cells, cells projecting to area 19 were found in both blobs and interblobs of area 17 and 18, though perhaps not with equal density. Small injections gave patchy labeling in areas 17 and 18 that either aligned with the blobs or with the interblobs. These results show that, although both blob and interblob compartments of area 17 and 18 project to area 19, their terminations are kept segregated into different compartments of area 19. Some of these results have been previously presented in abstract form (Boyd and Matsubara, 1992; Boyd and Matsubara, 1994).

## **Methods and Materials**

Data presented were obtained from ten experiments involving injections of tracers into area 19. Two animals received a large series of injections of CTB-Au. The remaining animals received small, focal injections of CTB-Au or unconjugated CTB. In some cases, one injection of each tracer was made side by side in area 19.

Two different approaches were used in making the large injections. In one case, injections were made at levels AP 0 to +6, where area 19 is located on the medial bank of the lateral gyrus. As for injections into the PMLS, pipettes with long, narrow tapers were tilted

medially at 30° from vertical in order to follow the slope of the sulcus. Seven 500  $\mu$ m spaced penetrations were made through the 4-5 mm depth of the sulcus, injecting tracer at 1 mm intervals along each penetration. About 10  $\mu$ l of tracer was injected in total. In the other approach, injections were made farther forward in the brain where area 19 is exposed on the surface of the lateral gyrus, from AP +9 to +13. A series of 24 injections in a 4 by 6 matrix, with a spacing of approximately 750  $\mu$ m between each injection, was made starting at AP +10 and working forward. Approximately 10-12  $\mu$ l of tracer was delivered in total.

Small, focal injections of CTB-Au and CTB were made where area 19 is on the surface of the lateral gyrus, at approximately AP +12. In these cases, 0.2  $\mu$ l of tracer was injected. Paired injections of the two tracers were placed 1-2 mm apart. In all cases, survival times varied from 1-4 days.

## **Results**

### **Both Blobs and Interblobs Project to Area 19**

As was done for the PMLS, large series of injections were made in order to determine if the area 19-projecting cells were truly hard patterned, as has been claimed (Ferrer et al., 1992). Figures 5.1 and 5.2 show the results from one of these injections. As can be seen, connections from areas 17 and 18 to area 19 are not concentrated within CO blobs as are the projections to area PMLS. Although both blobs and interblobs project to area 19, there still appears to be some fluctuation in labeling density suggesting that one of the compartments, either the blobs or the interblobs, projects more strongly than the other to area 19.

Another example is shown in Figures 5.3 and 5.4. In this experiment, the injection was made farther anterior, where area 19 is on the lateral gyrus. Also, note that the posterior part of the injection in this case encroached on area 18. This results in a different pattern of labeling in

the posterior part of the labeled zone. Here, the labeling is distinctly patchy, whereas further anterior the labeling is less patchy. Note that the change from patchy to more continuous labeling occurs at the A-P level where labeling in the splenial visual area (SVA) commences. As SVA projects to area 19, but not to area 18, this shows the approximate level where the labeling shifts from area 18-projecting more posteriorly to area 19-projecting more anteriorly. This change in labeling pattern from a single series of injections that crosses areal borders demonstrates the different patterns of connectivity that area 17 has with areas 18 and 19. As was done for PMLS-projecting cells in areas 17 and 18, plots of labeling density were computer-generated and then filtered with a Gaussian filter. Labeling in areas 17 and 18 from the same experiment shown in Figure 5.1 is shown enlarged in Figure 5.5A, and expressed as a density plot in Figure 5.5B. The same data are shown after Gaussian filtering in Figure 5.5C. The average density of labeled cells within the boxed area in Figure 5.5B is 1959 cells/mm<sup>2</sup>. This density value is uncorrected for the fact that half the sections were not used to visualize the retrograde labeling, but instead, were processed for CO. A density plot from the same experiment shown in Figure 5.6A is shown in Figure 5.5D. In this experiment, a single, small injection was made in area 19. Again, half of the sections were processed for CO, so the values of labeling density would be correspondingly higher. The arrows in Figures 5.5B and 5.5D show the transects used to generate the profile plots in Figures 5.5E-G. The density plots show that the fluctuations in labeling density are not as great after area 19 injections as they are after PMLS injections. The density of labeled cells along the transects does not drop to the near 0 values seen following the PMLS injections. It can also be seen that the density of area 19-projecting neurons in areas 17 and 18 is about the same.

### **Segregation of Projections to Area 19**

Although the large injections in area 19 gave rise to fairly uniform labeling in areas 17 and 18, small injections in area 19 often, although not always, gave rise to very distinct patches.

Figure 5.1. Labeling in areas 17 and 18 from a large injection in area 19. **A.** A dark field photomicrograph of a tangential section through visual cortex showing cells in areas 17 and 18 retrogradely labeled from a large series of injections of CTB-Au in area 19. The injection site is visible towards the bottom of the figure. **B.** A section from the same experiment, stained for CO. The dashed line shows the lateral border of area 18, determined from CO staining in the full series of sections. The arrowheads mark corresponding blood vessels in **A.** and **B.** Scale bar: 2mm



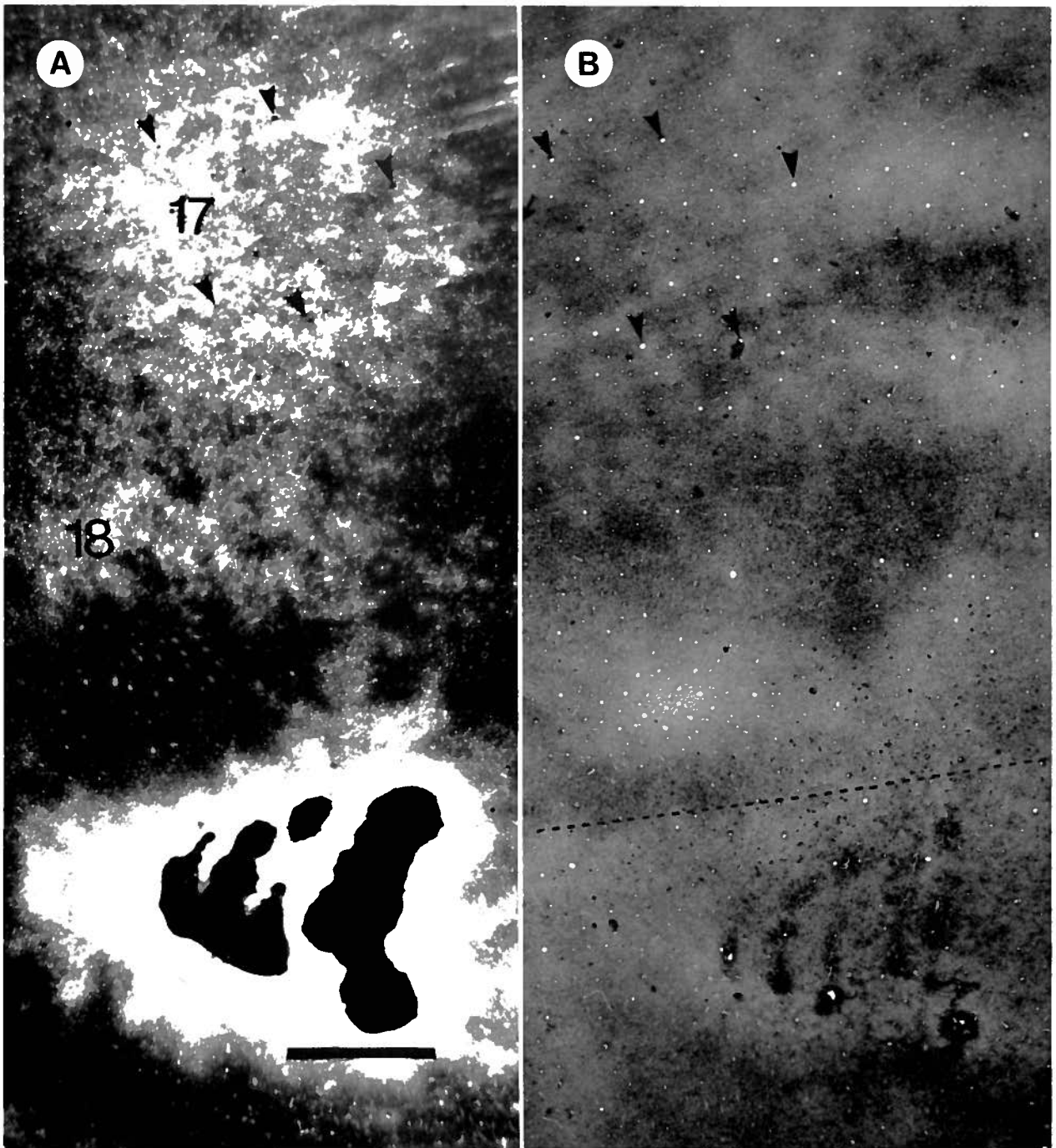


Figure 5.1

Figure 5.2. A computer generated plot of area 19-projecting cells labeled with CTB-Au in the full one-in-two series of sections from the same experiment shown in Figure 5.1. Each dot represents a single labeled cell. The edge of the tissue is shown in solid black lines, and the fundi and lips of the lateral (Lat) and suprasylvian (SS) sulci are indicated by finely dashed lines. The outline of areas 17 and 18 is indicated by a coarsely dashed line. The outline of the injection site (Inj) is shown. Medial (M) and anterior (A) cortical axes are indicated by the arrows. Some of the labeled cortical areas are indicated based on gyral and sulcal patterns. SVA, splenial visual area; PMLS, posteromedial lateral suprasylvian area; VLS, Ventral lateral suprasylvian area.

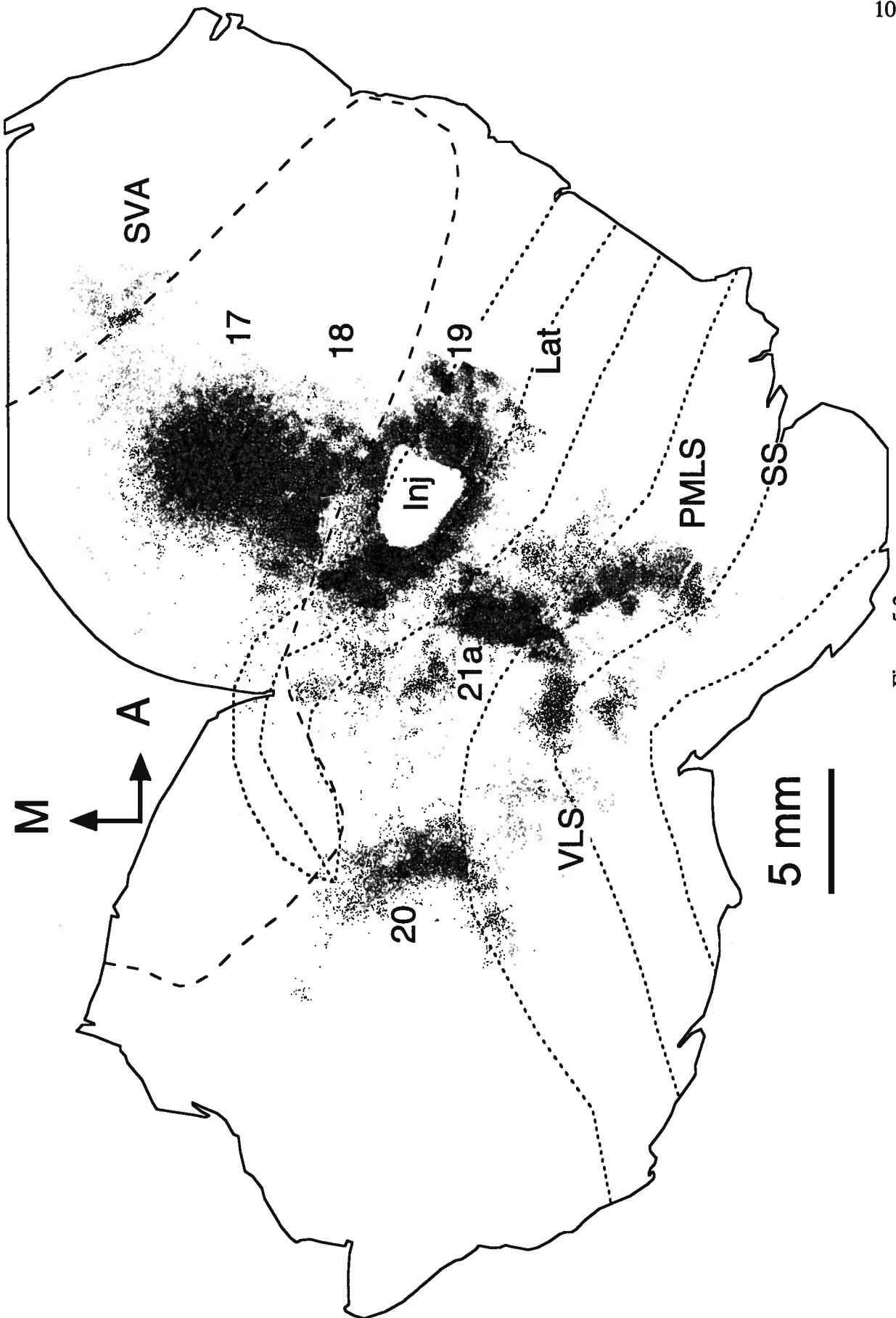


Figure 5.2

Figure 5.3. Another example of labeling in areas 17 and 18 from a large injection in area 19. This dark field photomicrograph shows a tangential section through visual cortex following a large series of injections of CTB-Au that was in area 19 for the anterior portion (rightward in the figure) but was in area 18 in the posterior portion (leftward in the figure). The injection site is visible towards the bottom of the figure. The visuotopic organization of areas 17, 18, and 19 allows cells in area 17 labeled from that part of the injection in area 18 to be distinguished from those labeled from that part of the injection in area 19. The bulk of the labeling in area 17 arises from the area 19 injection. The beginning of the labeling in the splenial visual area (SVA), marks the transition from area 18-projecting cells more posteriorly to area 19-projecting more anteriorly. Scale bar: 2 mm. A section from the same experiment, stained for CO, is shown in the inset. The arrowheads mark rows of injections that are partly within the oval shaped region of dense CO staining that contains areas 17 and 18. Scale bar: 5 mm.



Figure 5.3

Figure 5.4. A computer generated plot of area 19-projecting cells labeled with CTB-Au from the same experiment shown in Figure 5.3. In this composite figure, all cells labeled in the one-in-two series of section reacted for CTB-AU were charted and displayed. Labeling conventions as in Figure 5.2.

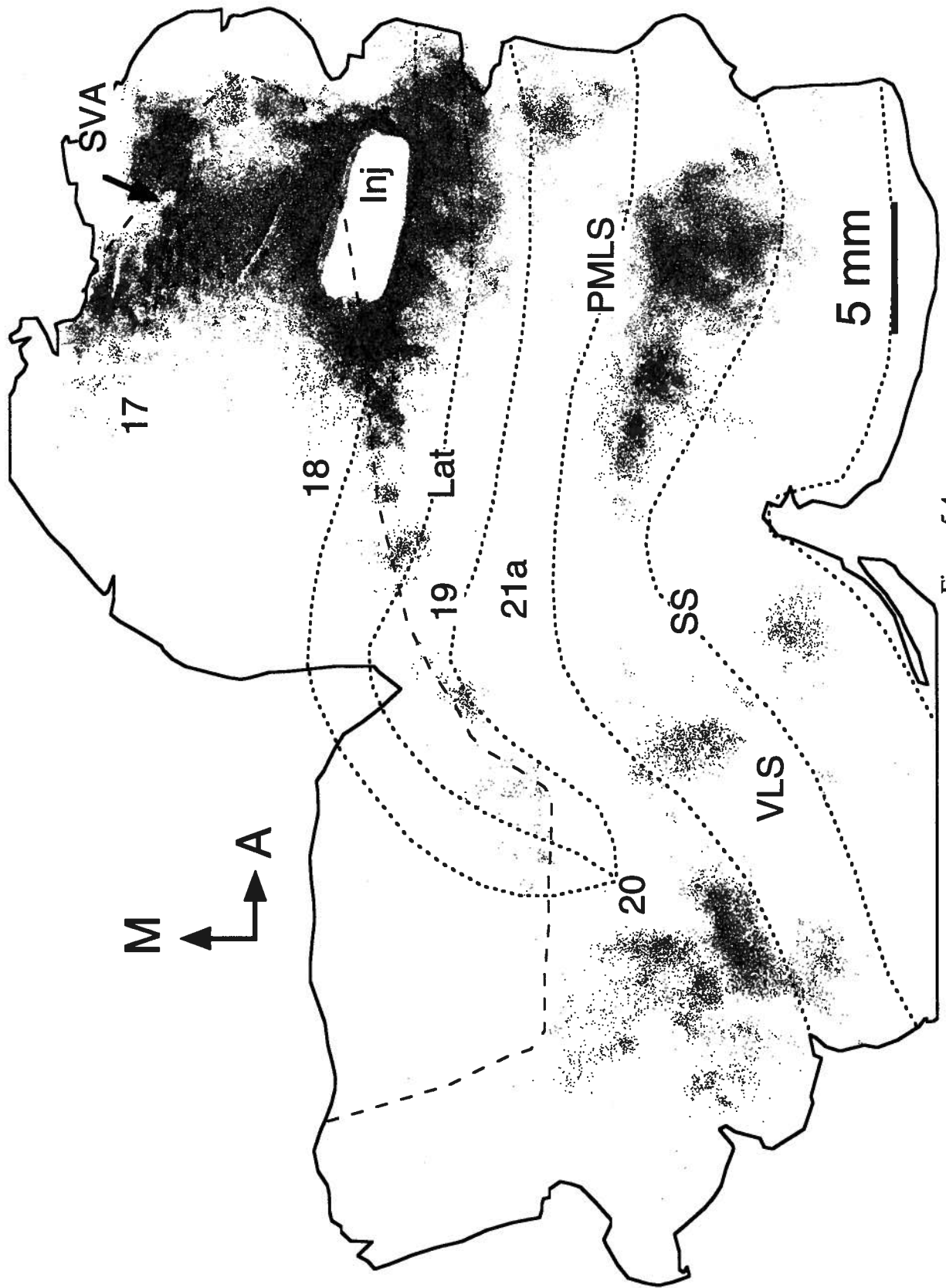


Figure 5.4

Figure 5.5. Computer-generated plots of area 19-projecting cells in areas 17 and 18. **A.** Enlargement of labeling in areas 17 and 18 from Figure 5.2. Scale bar applies to A-G. **B.** The same data as in Figure 5.5A expressed as the density of labeled cells per unit area. The size of each grid square is 100  $\mu\text{m}$ . This data was then Gaussian filtered to produce **C.** The arrows show the lines sampled for the profile plots shown in **D** and **E.** The fluctuations in labeling density are much less evident than for injections in PMLS (compare to Figure 4.4). **D-E.** Profile plots of lines marked "D-E" in Figures 5.5B. The numbers to the left show the minimum and maximum values encountered in the plot. The number on the bottom shows the length of the transects. **F.** A density plot of labeling in areas 17 and 18 from the small injection shown in Figure 5.6A. Same conventions and scale as for **B.** The arrow shows the line sampled for the profile plot shown in **G.** Note that labeling in areas 17 and 18 was not patchy from this small injection, which was not always the case (see Figures 5.6-7). **G.** the profile plot shown in **F.** Conventions as in **D.** **H.** Power spectra of spatial frequency for transects shown in **D** (thick line) and **G** (thin line). The left axis shows the Fourier energy at each frequency along the bottom axis. Although there is a slight peak in the power spectra near 1 cycle/mm, note that this peak has relatively little energy compared to the power spectra shown in Figure 4.4. Only results from single transects, instead of averages, are shown because averaging results from single transects broadened the peaks until they were indistinguishable.



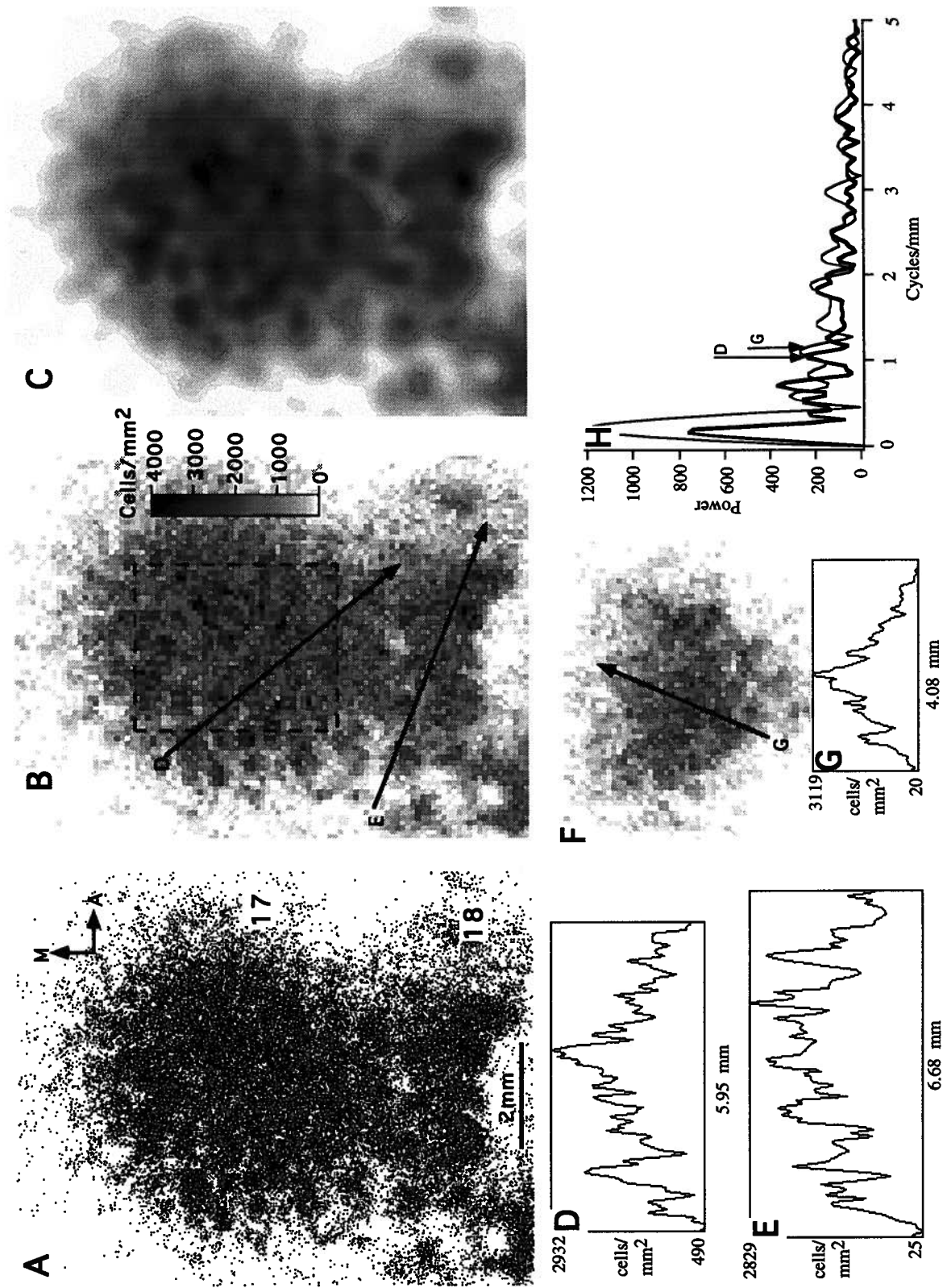


Figure 5.5

Examples of injections which gave rise to non-patchy and patchy labeling, respectively, are shown in Figures 5.6A and B. Charts of these experiments are shown in Figure 5.7. Note that the sizes of these two injections are very similar, yet one produced distinct patches in areas 17 and 18 (5.7B), and the other produced continuous labeling, with almost no hint of periodicity (5.5 D, G, 5.7A).

In order to further examine the mechanism by which patchy labeling might be obtained with small injections but not large injections, paired injections of two different, distinguishable tracers (CTB and CTB-Au) were made side by side in area 19. In some cases, patches of labeling from the two tracers overlapped, and in some cases they interdigitated. In other cases, one tracer gave patchy labeling and the other tracer gave more continuous labeling. An example where the two tracers interdigitated is shown in Figure 5.8. An example of a case where labeling from the two tracers was in the same patches is shown in Figure 5.9. In both cases, the injections are of similar size and spacing.

### **Relationship to Cytochrome Oxidase Blobs**

In some experiments, adjacent sections were reacted for CO in order to visualize the CO blobs in areas 17 and 18. Patterns of labeling from area 19 were aligned with the CO stained sections using radially-penetrating blood vessels as landmarks. An example of this alignment is shown in Figure 5.10. In Figure 5.10A, two sections, one reacted for CO and the other to silver-intensified for CTB-Au, were directly superimposed on the microscope stage and photographed. Figure 5.10 shows the same experiment, but here the retrogradely labeled cells were first charted, and then graphically superimposed on a computer-captured image of the CO stained section. The graphic superimposition has the advantages that many more of the labeled cells, not just those that are visible in a single section, can be shown at one time, and that small differences in shrinkage of the sections during processing can be easily compensated for by using computer

scaling commands. By both methods, it can be seen that there is quite good correspondence between CO blobs and the patches of cells projecting to area 19.

Figure 5.11 shows three further examples of alignment between CO staining and area 19 projecting cells. Figures 5.11A and 5.11B are from area 17 and area 18, respectively, of the experiment shown in Figure 5.6B. Again, there is good correspondence between the blobs and the patches of cells projecting to area 19. Figure 5.11C shows the CTB labeled cells in area 17 from the experiment shown in Figure 5.7. The CO staining pattern in this case is not as clear, due to unevenness in the plane of section. Nevertheless, it is apparent that the patches of retrogradely labeled cells are not aligned with CO blobs, but are found mostly in the interblobs. The CTB-Au labeled cells from this case, which interdigitated with those labeled by CTB, were aligned with the CO blobs. Thus, the CO blobs in areas 17 and 18 appear to be important in ordering the patchy connections terminating in area 19.

### **Intrinsic Connectivity in Area 19**

While the main focus of this study was the connectivity of area 19 with areas 17 and 18, data was also obtained on the local connectivity within area 19 itself. Local connections in area 19 can be seen in Figures 5.6 to 5.9. The patches of labeling in area 19 were of a larger size and spacing than patches arising in area 17 or 18 from the same injections. Sometimes, these patches were noticeably elongated, as seen in Figure 5.6. The difference in size of intrinsic patches in area 19 and area 17 from two separate injections in the same hemisphere is reinforced by Figure 5.12. These injections were separated in the anterior-posterior dimension by about 7 mm, so intracortical labeling was not confused with intercortical labeling. Local connections of area 17 (Fig. 5.12B) had, as previously reported (Gilbert and Wiesel, 1983; LeVay, 1988; Gilbert and Wiesel, 1989), a spacing of about 1mm. Local connections of area 19 (Fig. 5.12A), with a spacing of about 2 mm, were organized with a periodicity larger than that of local connections within area 17. This suggests that the internal organization of areas 17 and 19 may be substantially different.

Figure 5.6. Dark field photomicrographs of two different patterns of labeling in visual cortex following similarly-sized small, focal injections of CTB-Au in area 19. **A.** In this case, also shown in Figure 5.5D, labeling in 17 and 18 was not patchy. **B.** In this case, labeling was patchy in areas 17 and 18. Also, note the patches of intrinsic labeling in area 19 itself, which have a larger spacing than labeling in areas 17 and 18, and are often elongated. SVA, splenial visual area. Scale bar: 2 mm.

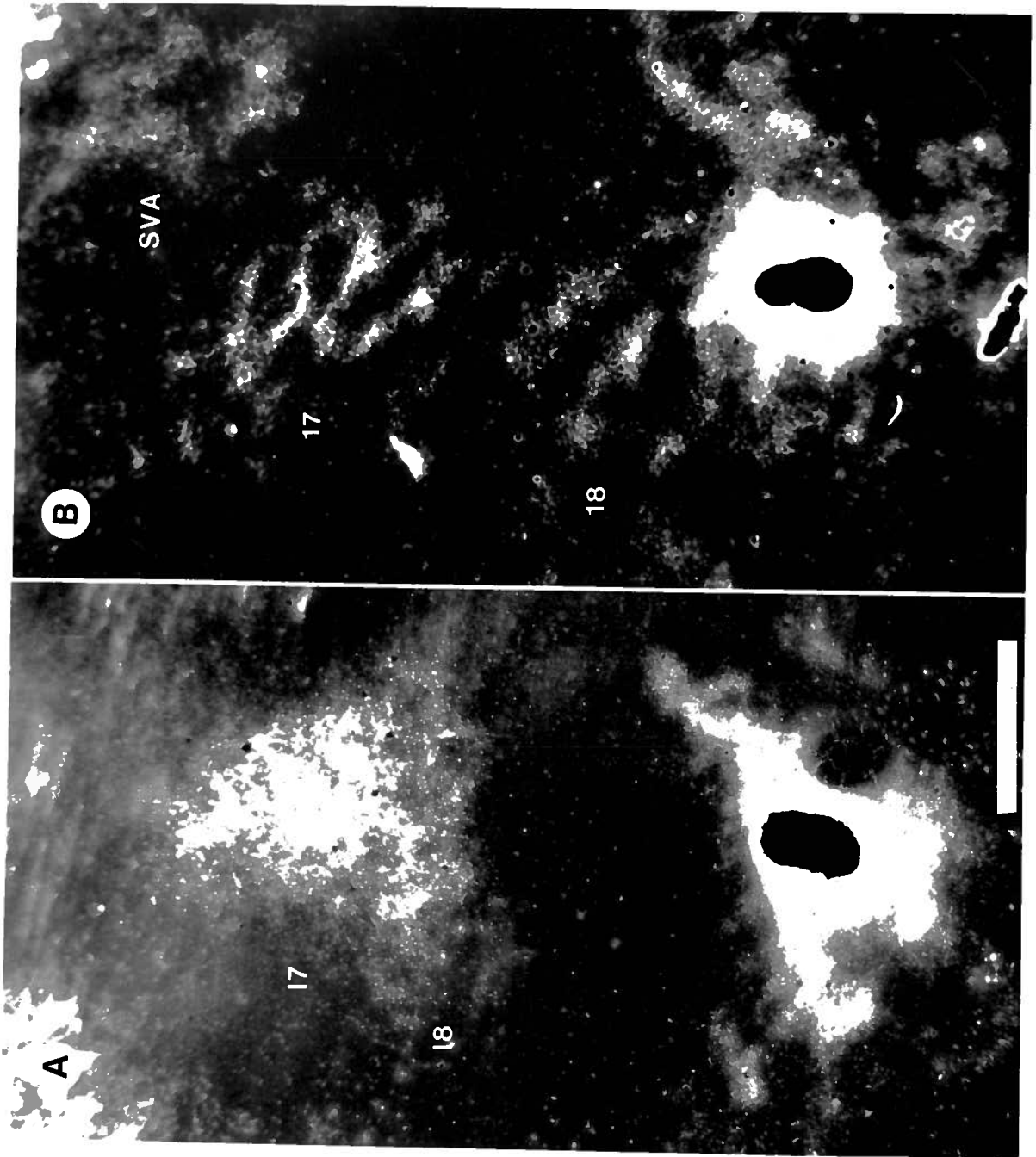


Figure 5.6

Figure 5.7. A computer generated plot of area 19-projecting cells labeled with CTB-Au in the full one-in-two series of sections from the same experiments shown in Figure 5.6. Each dot represents a single labeled cell. The difference in the patchy pattern of 5.5B and the non-patchy pattern of Figure 5.5A is just as obvious when all of the cells, not just those in a single section, are shown. The injection site (Inj) is shown in white. The lateral border of area 18, as determined from the adjacent sections stained for CO, is shown as a solid black line. Note that labeling in areas 17 and 18 is separated by a gap in B, but not in A. This is likely due to the fact that the visuotopic organization of azimuth in areas 17 and 18 is mirror symmetric around their border, which represents the vertical meridian, and that the two injections were at different azimuths. Thus, A illustrates an injection near the vertical meridian in area 19, labeling the vertical meridian representation that forms the 17/18 border, while B illustrates an injection at some point more peripheral in area 19, such that the gap between the patches of labeling in areas 17 and 18 represents the vertical meridian at the 17/18 border.

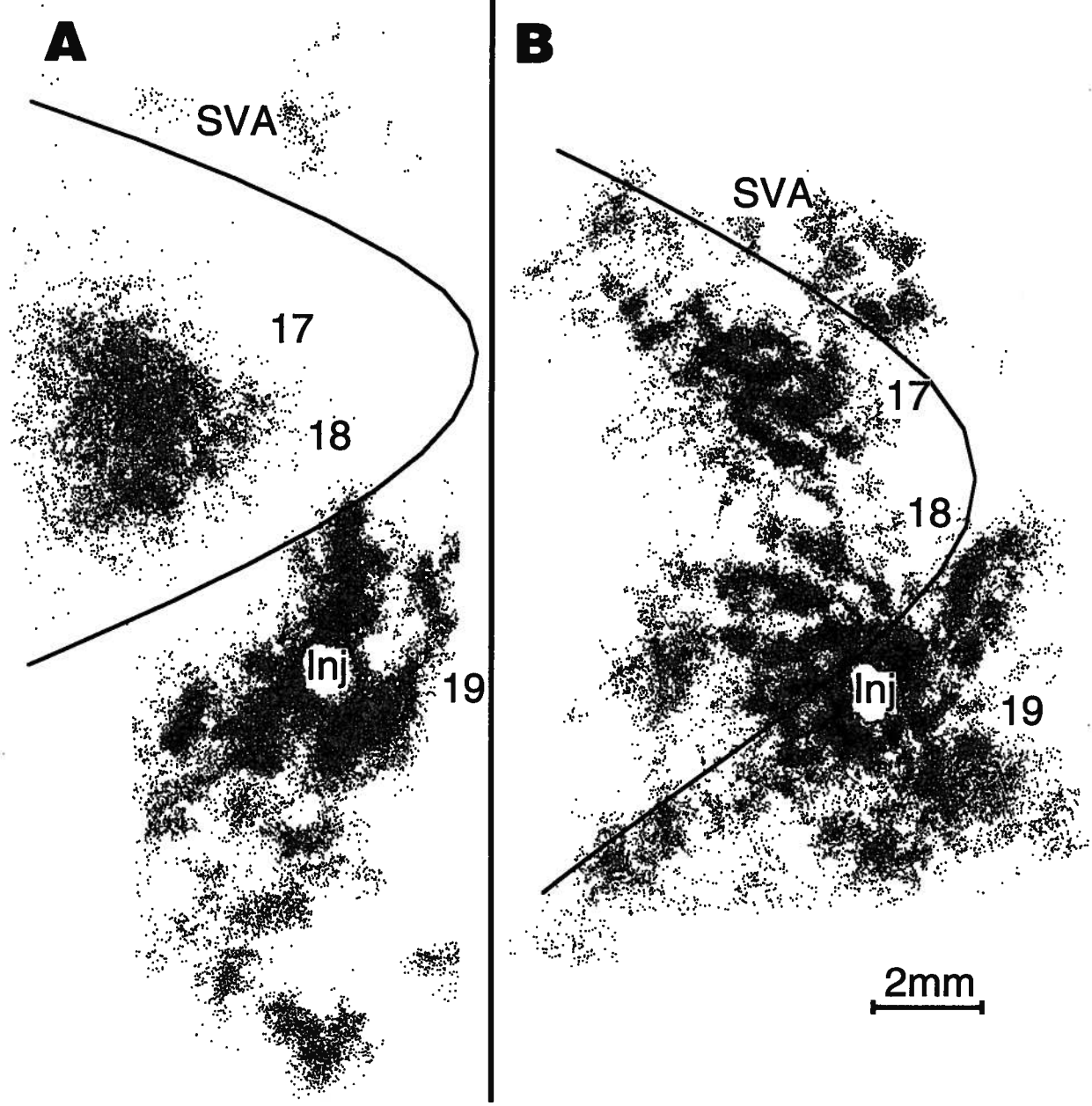


Figure 5.7

Figure 5.8. A computer generated plot showing the results of paired injections of unconjugated CTB and CTB-Au in area 19. A one-in-two series of sections was charted and each dot represents a single labeled cell. White cells contained CTB-Au, which were retrogradely labeled from the larger injection to the right of the figure. Black cells contained unconjugated CTB, labeled from the smaller injection site. The extent of areas 17 and 18, determined from CO staining, is shown by a solid black line. In this case, labeling in areas 17 and 18 from the two injections formed an interdigitating pattern. Again, note the large, sometimes elongated patches of local connectivity within area 19.



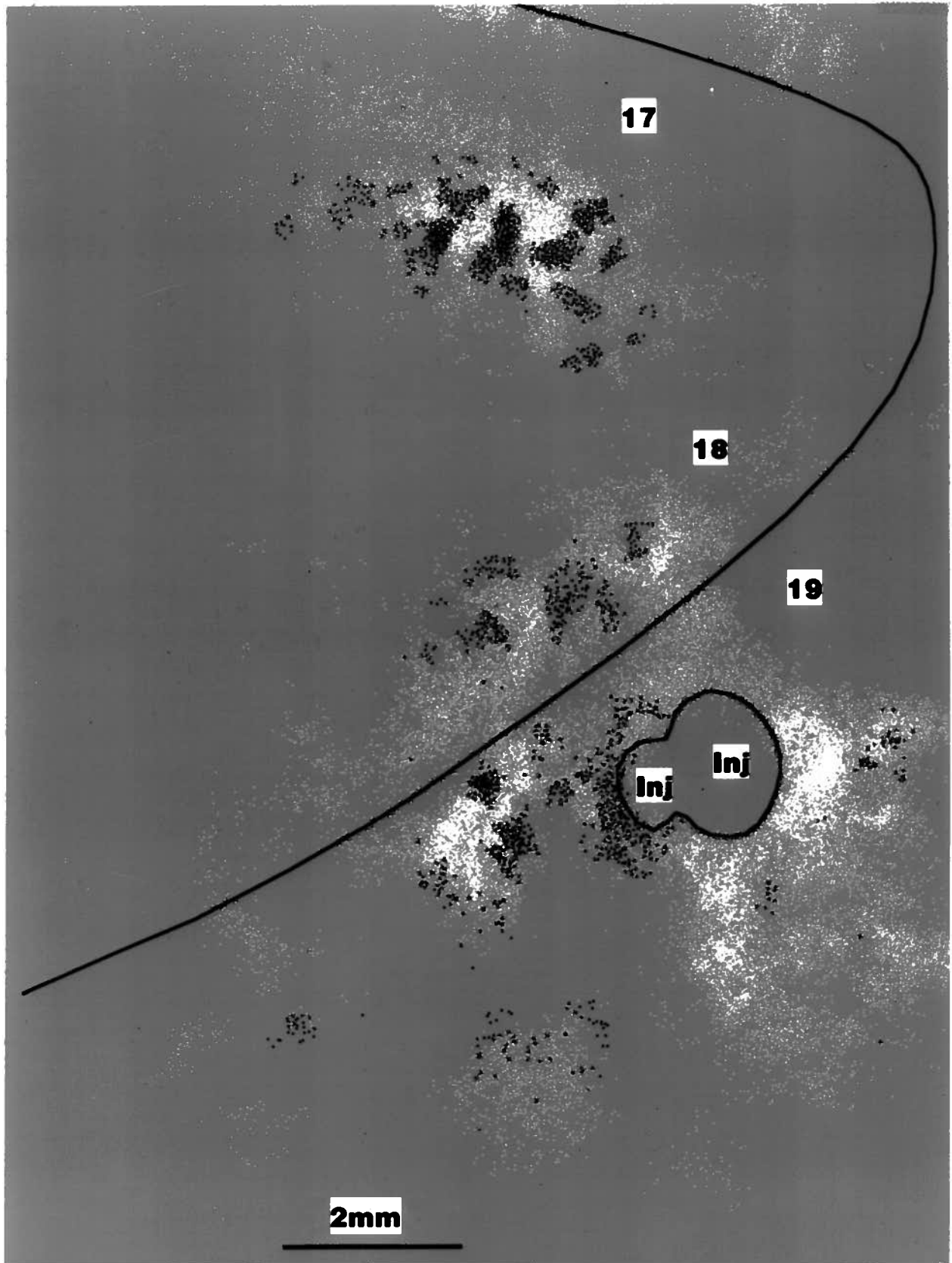


Figure 5.8

Figure 5.9. A computer generated plot showing the results of another example of paired injections of unconjugated CTB and CTB-Au in area 19. Labeling conventions as in Figure 5.8. In this case, labeling in areas 17 and 18 from the two injections overlapped in the same sets of patches.

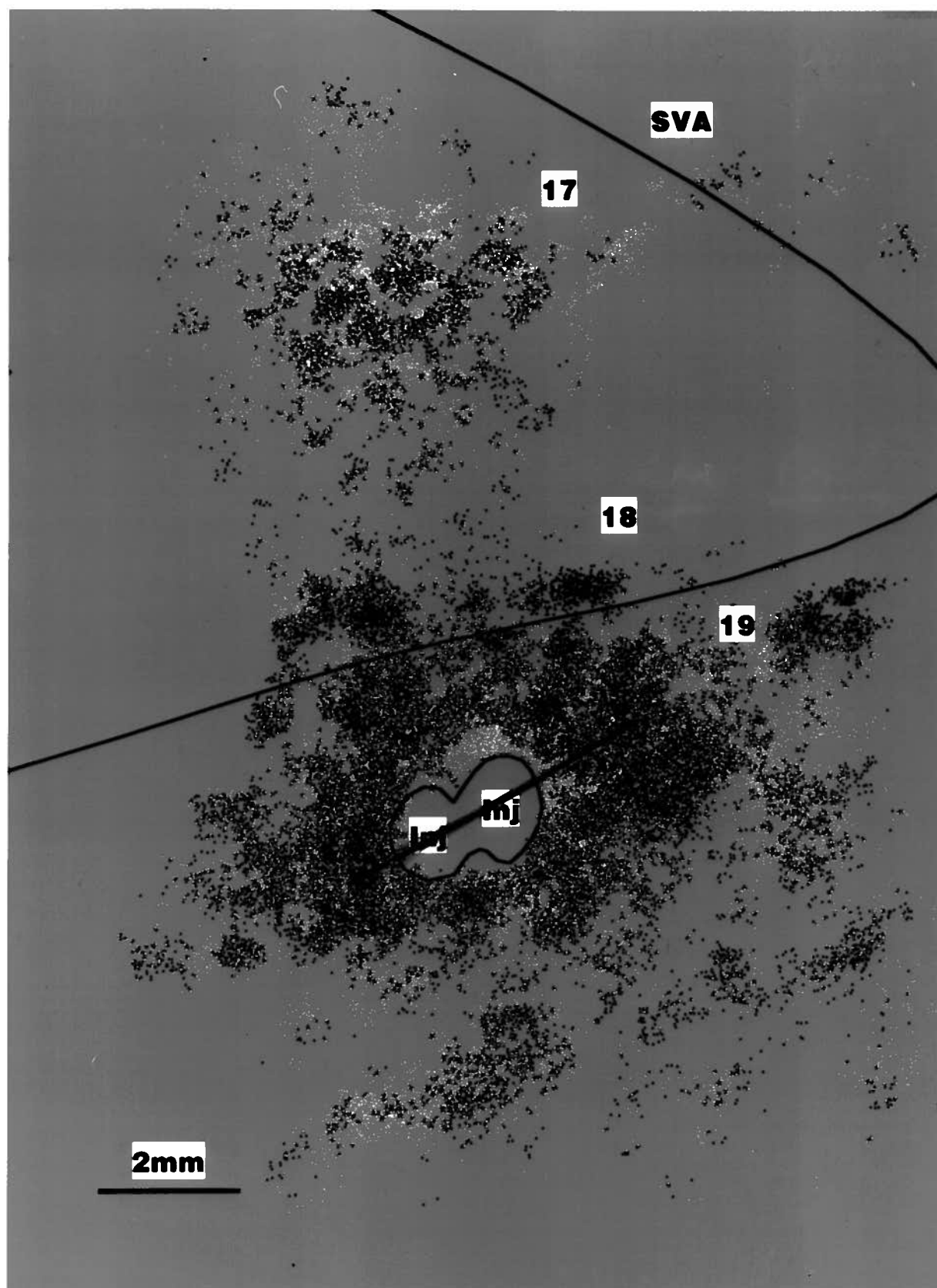


Figure 5.9

## **Discussion**

### **Are the Area 19 Connections Truly Soft Patterned?**

It was found in this study that the projections from areas 17 and 18 to area 19 arise from both the CO blobs and interblobs. Thus, after large injections (and sometimes even small injections) of tracers in area 19, labeling in areas 17 and 18 was continuous. This finding is at odds with a previous report that the projection from area 17 to area 19 is discontinuous (Ferrer et al., 1992). Figure 5 of Ferrer et al. shows large cell free gaps 1-2 mm wide separating patches of labeling in area 17 following a large series of injections in area 19. Also, nearly all of the labeled area in their figure has a density of less than 2000 cells/mm<sup>3</sup>. In order to compare this to the density of labeled cells obtained in this study, it is necessary to convert from density based on volume of labeled tissue to density based on surface area of cortex. The value of Ferrer et al. was calculated based on the total volume of layers 2/3 and upper layer 4; as the distance from the surface of the cortex to the middle of layer 4 is certainly less than 1 mm, the values for labeling density obtained in their study would be smaller if expressed as cells/mm<sup>2</sup>. Thus, the density of area 19-projecting cells reported by Ferrer et al. was much lower than was found in this study. The differences in labeling density may have been due to methodological differences between the two studies, as Ferrer et al. used the fluorescent tracers diamidino yellow and fast blue, while colloidal gold-conjugated cholera toxin was used in the present study. It is argued here that the lesser labeling density of the previous study might also have contributed to the finding of a discontinuous labeling pattern.

Although it might be argued that the continuous labeling pattern found in this study following large injections in area 19 might be artifactual due to involvement of white matter or other cortical areas, this is unlikely. First, patterns of labeling in the LGN never contained labeled cells in the A-layers, which would be expected if the white matter or area 18 had been

Figure 5.10 Relationship of patches of area 19-projecting cells and CO blobs in area 17. **A.** Photograph of two serial tangential sections through area 17, directly superimposed. The bottom section was reacted for CO to show the blobs and the top section was reacted for CTB-Au to show the patches of area 19-projecting cells. The two sections were aligned using blood vessels as landmarks. Many of these paired blood vessels are visible in the photomicrograph (arrowheads). As the focal plane is at the level of the HRP-reacted section, the blood vessels in the CO-reacted section appear slightly out of focus. As there is unequal shrinkage in the two histochemical procedures, it is not possible to align the two sections perfectly. Nevertheless, the correspondence between area-19 projecting cells and CO blobs is evident. **B.** Computer-generated plot of the same patches of area 19-projecting cells shown in A, superimposed onto a digitally captured image of CO staining from an adjacent section. As in A, the pattern of blood vessels (black circles) was used for alignment. However, differences in shrinkage could be corrected by scaling the computer-generated plot. Also, cells from the entire one-in-two series of sections can be shown in the computer reconstruction. As in A, the patches of area 19-projecting cells can be seen to align with the CO blobs. Scale bar: 2mm.

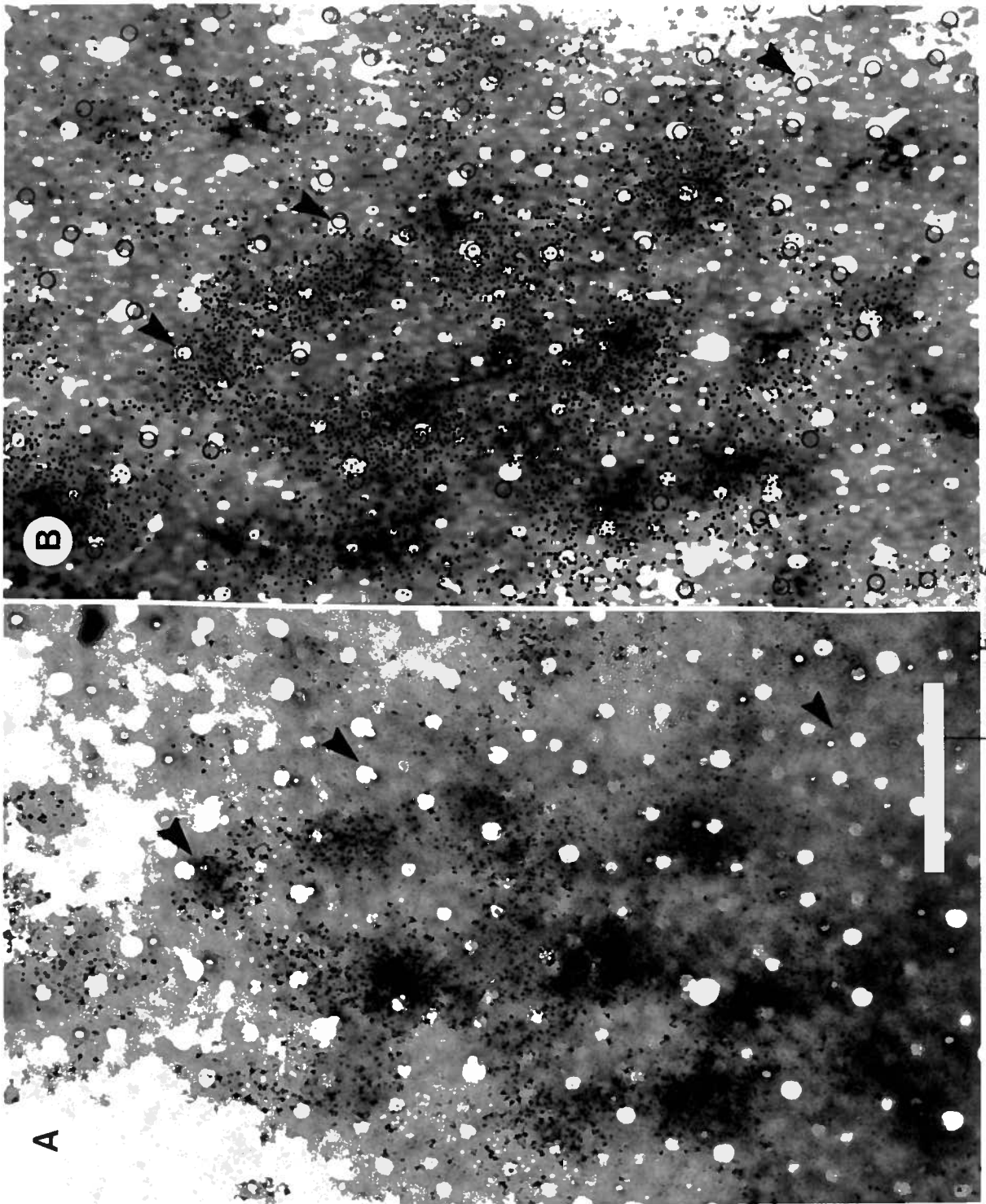


Figure 5 10

Figure 5.11 Relationship of patches of area 19-projecting cells and CO blobs in areas 17 and 18.

**A.** Computer-generated plot of the same patches of area 19-projecting cells in area 17 shown in Figure 5.7A, superimposed onto a digitally captured image of CO staining. As in Figure 5.10, the pattern of blood vessels was used for alignment. In this case as well, the patches of area 19-projecting cells can be seen to align with the CO blobs. **B.** Computer-generated plot of patches of area 19-projecting cells in area 18 from the same experiment shown in Figure 5.7A, superimposed onto a digitally captured image of CO staining. Note that the patches of area 19-projecting cells and associated CO blobs are slightly larger in area 18 than in area 17. **C.** Computer-generated plot of the patches of CTB-labeled cells in area 17 shown in Figure 5.8, superimposed onto a digitally captured image of CO staining. The light oval area in the center of the figure corresponds to the area of the suprasplenic sulcus. The sulcus was not optimally flattened in this experiment, and the plane of section in the area of the sulcus passes through the upper part of layer 3, where CO staining is very light. Nevertheless, it is possible to determine that, in this case, patches of labeling interdigitate with the interblobs. Scale bar: 2mm, applies to A,B, and C.

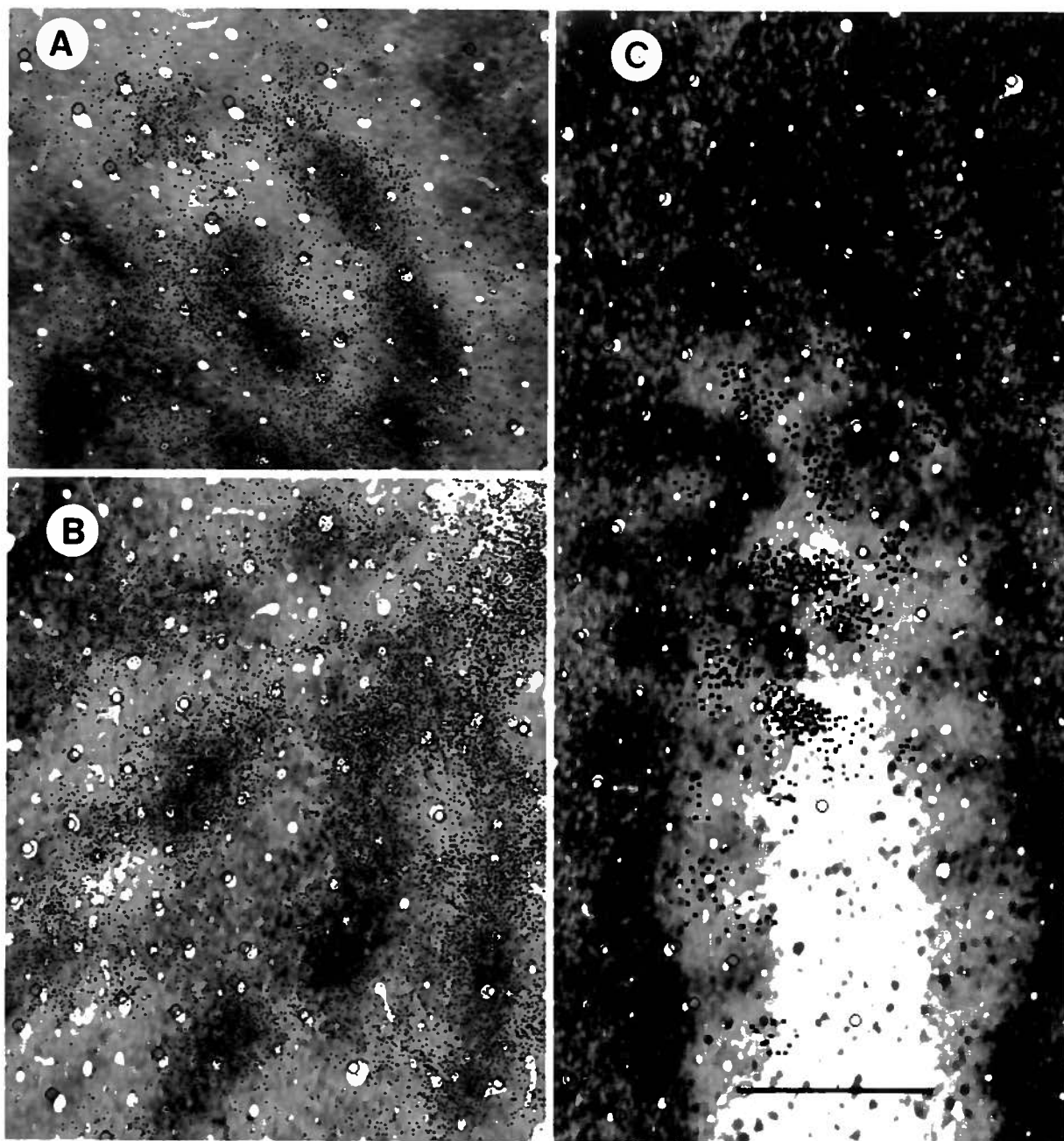


Figure 5.11



contaminated. Second, of the areas abutting area 19, area 18 receives inputs from a discontinuous pattern of cells in area 17 (Figure 5.3), and the cortex directly lateral to area 19 does not appear to receive projections from area 17 (Symonds and Rosenquist, 1984a). That the distribution of cells in areas 17 and 18 projecting to area 19 is truly continuous, i.e., soft patterned, was also indicated by the fact that even small injections in area 19 could sometimes give rise to continuous patterns of labeling in areas 17 and 18 (Figure 5.6).

Although labeling in areas 17 and 18 was continuous after a large injection, slight fluctuations in labeling density were visible. These may have been real, indicating that either blobs or interblobs project slightly more heavily to area 19. Alternatively, these relatively slight fluctuations in labeling density might have resulted from the injections being more heavily concentrated in one particular compartment of area 19 than the other. This is not as implausible as it may initially seem, as the columnar organization of area 19 appears to be of a larger scale than in areas 17 or 18 (see below). Thus, even injections spanning 5mm might be weighted to favor one compartment or the other in area 19.

### **Segregated Processing Streams through Area 19?**

Small injections of tracers in area 19 often, but not always, gave rise to segregated patches of labeling in areas 17 and 18. This suggested that some parameter in area 17 with a columnar organization was correlated with the organization of this projection. In experiments where alternate sections were reacted for CO, it was possible to show that either blobs or interblobs selectively projected to a single locus in area 19. This shows that area 19 continues the segregation of blob and interblob information began in areas 17 and 18. At least two types of columns can be demarcated in area 19, one that receives inputs from blobs, and one that receives inputs from interblobs. Thus, large injections would have included both columns of area 19 receiving inputs from blobs, and columns receiving inputs from interblobs, while small injections would have a greater chance of targeting a single type of column. Small injections that labeled

Figure 5.12 Patchy intrinsic labeling in areas 17 and 19. These two photomicrographs, printed at the same scale, show the difference in the size of intrinsic labeling in these two areas. **A.** Intrinsic labeling in a tangential section through area 19. The edge of the injection site is visible in the top right. Elongated patches of labeled cells, with a characteristic spacing of about 2 mm, are marked by arrowheads. Scale bar: 1mm, applies to **A** and **B**. **B.** Intrinsic labeling in a tangential section through area 17. This injection was made in the same hemisphere of the same animal shown in **A**. However, it was made slightly posterior to the injection in area 19, so corticocortical labeling from the two injections was separated by about 10mm, and was not confused. The edge of the injection site is visible in the top right. Patches of labeled cells, with a characteristic spacing of about 1 mm, half of that shown for labeling in **A**, are marked by arrowheads.

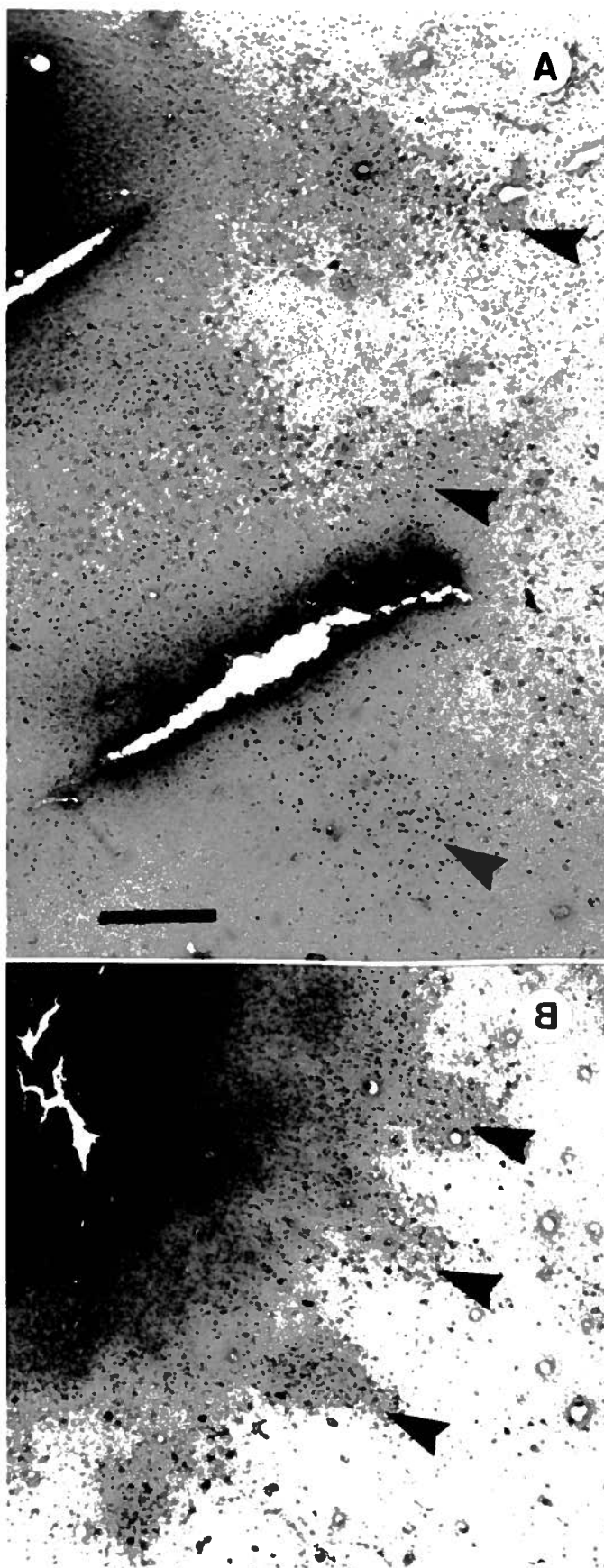


Figure 5.12

cells in both blobs and interblobs could be explained by the injection straddling the borders of two such columns. (A less parsimonious, but possible, explanation would be the existence of a third type of column in area 19, one that receives input from both blobs and interblobs of areas 17 and 18.)

It is interesting to note that outputs from area 19 to PMLS were also arranged in a discontinuous fashion (Chapter 4). It is not yet known if a relationship exists between the columns containing PMLS-projecting cells and the columns receiving either blob or interblob input from areas 17 and 18. As PMLS receives inputs only from the blobs of areas 17 and 18, it is suggested that it may, analogously, receive input only from the columns of area 19 that also receive inputs from the blobs.

It should be mentioned that it is possible that, in addition to CO blobs, another columnar system, such as orientation or ocular dominance is also involved in the organization of the projections from areas 17 and 18 to area 19. Clustering of orientation selectivity has been noted in area 19 (Hubel and Wiesel, 1965), but no evidence for ocular dominance columns has been found. Thus, columns of like orientation could be connected, as in the projection from area 17 to area 18 (Gilbert and Wiesel, 1989).

### **Columnar Organization of Area 19**

These data also shed some light on the relative scale of the columnar organization in area 19 versus areas 17 and 18. By three separate connectional organizations: inputs from the C layers of the LGN (Anderson et al., 1988); columns of cortex projecting to the PMLS (Chapter 4); and local connections (Figure 5.5, e.g.), area 19 has a larger spatial scale to its columnar organization than does areas 17 or 18. Anderson et al. (1988) showed that projections from the LGN to area 19 following transneuronal transport from interocular WGA-HRP injections formed large patches with a spacing of 2-3 mm. Although only one eye was injected, these patches do not appear to be related to ocular dominance because this property is not organized in a columnar

fashion in area 19 (Tieman and Tumosa, 1983). Similar results were also seen following the LGN injections reported in Chapter 3. A spacing of about 2 mm was also seen for the patches of PMLS-projecting cells in area 19, and for the patches of intrinsic labeling. In addition, a lower limit on the size of the columns of terminations from area 17 and 18 can be inferred from Figure 5.9. Here, two injections with a combined extent of about 2mm both gave patchy labeling of blobs in area 17. Thus, projections from blobs and interblobs must segregate, in area 19, into columns that are at least 2 mm wide. Thus, the input-defined columns and the output-defined columns likely have a similar spacing, which is consistent with the suggestion that they are related.

This larger scale of cortical organization in area 19 is apparently unique among cortical areas in the cat. Patches of labeling in other cortical areas from axonal transport studies, including areas 17, 18, and PMLS, all appear to have a spacing of about 1mm (Chapter 4; LeVay and Nelson, 1991; Symonds and Rosenquist, 1984a). Why area 19 should be so different from other cortical areas in this respect is not yet clear.

In summary, it has been shown that projections from blobs and interblobs of area 19 are segregated within different columns of area 19. Thus, a single column in area 19 receives input from blobs or interblobs, but not both. It is suggested that a relationship may exist between the various input- and output-defined columns in area 19, and that these columns mark a segregation of different processing streams from areas 17 and 18 through area 19 and into other extrastriate areas such as the PMLS.

## 6 TANGENTIAL ORGANIZATION OF CALLOSAL CONNECTIVITY

Among the most studied of corticocortical pathways in the visual system is the callosal system connecting the two hemispheres (Innocenti, 1986). The opportunities to examine visual responses after cutting the corpus callosum (Leporé et al., 1986; Engel et al., 1991), to record directly from callosal fibers (Hubel and Wiesel, 1967), and to record callosal and thalamocortical responses in the same cell using the split optic chiasm preparation (Berlucchi and Rizzolatti, 1969; Leporé and Guillemot, 1982), have no parallel in the study of other corticocortical connections. Because physiological correlates of this pathway can thus be obtained, the callosal system has been particularly useful for studies of corticocortical connectivity.

In some primates, callosal connection to areas V1 and V2 are patchy and are made most densely to the CO blobs (Cusick and Lund, 1981; Cusick et al., 1984; Cusick et al., 1985; Kennedy et al., 1986). It has been speculated that the differences in the physiological properties of blob and interblob cells are responsible for their differing callosal connectivity. Thus, it seemed interesting to ask whether the callosal pathway connecting the 17/18 border regions of the cat's visual cortex is patchy, and whether it is correlated with the blobs marked by CO staining.

Previous studies have reached different conclusions regarding a patchy organization of the visual callosal pathway in the cat. Most have found callosal cells and terminals in areas 17 and 18 to have a continuous distribution (Innocenti and Fiore, 1976; Innocenti, 1980; Segraves and Rosenquist, 1982; Innocenti and Clarke, 1984; Segraves and Innocenti, 1985), although some studies have suggested that the callosal pathway in the cat's visual cortex might be arranged in a discontinuous, patchy fashion (Berman and Payne, 1983; Voigt et al., 1988; Payne and Siwek, 1991). All of these studies used sections of tissue cut in the coronal plane, which is not the optimal plane of section for showing variation in labeling density in the direction tangential

to the cortical surface. In this study, sections cut tangentially through flattened cortex were used; this avoids the problems associated with the reconstruction of surface views from serial coronal sections. One previous study has examined the pattern of callosal labeling in cat visual cortex in the tangential plane (Olavarria and Montero, 1983), but this study was concerned mostly with extrastriate areas, and did not comment on the uniformity of labeling along the 17/18 border. This study is thus the first to examine in the tangential plane the modular organization of the visual callosal pathway in the cat.

Very large injections of retrograde and anterograde tracers were made centered on the 17/18 border in order to show the complete distribution of homotopic callosal cells and terminals in areas 17 and 18. Labeling was examined in tangential sections through flattened visual cortex. Callosal labeling was not completely uniform even along the 17/18 border, and connections medially in area 17, and laterally in area 18 displayed periodic fluctuations in density with a spacing of about 1mm and slightly greater than 1mm, respectively. Large, irregularly spaced bands of callosal connections swept from the lateral part of area 18 across area 19 and into more lateral areas. Cytochrome oxidase blobs in areas 17 and 18 were found to align with the callosal labeling.

## **Methods and Materials**

Six adult cats of both sexes were used to study the callosal pathways originating and terminating in the 17/18 border region. Four animals received injections of WGA-HRP and two animal received injections of BDA.

For two animals receiving WGA-HRP injections (cases 1 and 2) and for the two animals receiving BDA injections (cases 3 and 4), injections were made between stereotaxic coordinates A-P= -1 to +6, ML 0 to 3. This level corresponds to part of the visual meridian representation along the area 17/18 border (Tusa et al., 1978; Tusa et al., 1979). For the other two animals receiving WGA-HRP injections (cases 5 and 6), the craniotomy and durotomy were extended to

uncover nearly the whole anterior to posterior extent of the lower visual field vertical meridian representation.

In the first four animals, a series of 18 injections in a 3 by 6 matrix with 500 -750 mm spacing between each injection were made delivering a total of 10-12  $\mu$ l of tracer. In the last two animals, a larger series of injections delivering correspondingly more WGA-HRP (up to 40  $\mu$ l) was made. Survival periods were 48 hours for experiments with WGA-HRP and two weeks for the experiment with BDA

## **Results**

### **The callosal pathway is patchy**

Figure 6.1A shows a low power photomicrograph, taken through crossed polarizing filters, of callosal labeling in areas 17 and 18 of case 1. At this magnification, the terminal labeling is more evident than cellular labeling. In the center of the photomicrograph, there is a dense zone of callosal cells and terminals with less dense labeling extending medially and laterally. Based on evidence from previous studies in the coronal plane, it has been assumed that the 17/18 border is coincident with the densest zone of callosal labeling. (The 17/18 border is impossible to locate histologically in the tangential plane, although the border of areas 18 and 19 can be identified with myelin or CO stains). It is apparent that callosal labeling is not uniform, and that several different periodicities are present in the fluctuations of labeling density in different zones. Medially in area 17, and laterally in area 18, definite patches of dense callosal labeling are separated by less dense labeling. This can be seen more clearly in Figure 6.1B, which shows, from the same experiment but at higher magnification, patches of labeling 2-4 mm away from the border in area 17. Both retrogradely labeled cells and dust-like terminal labeling



Figure 6.1. Callosal labeling in a tangential section through the 17/18 border region of case 1. **A.** Low power photomicrograph. Medial is to the left, anterior is to the top. The dense callosal labeling along the presumed 17/18 border is marked by large patches of increased WGA-HRP labeling density. The arrows mark smaller patches of labeling that extend away from the border into area 17 (left) and area 18 (right). The patches in area 17 are smaller and more closely spaced than the patches in area 18. Mostly terminal labeling is visible at this magnification. Scale bar: 1mm. **B.** High power photomicrograph of callosal labeling from same experiment. Both cell and terminal labeling is found in the same clusters, which are separated by areas of less dense labeling. Scale bar: 0.5 mm

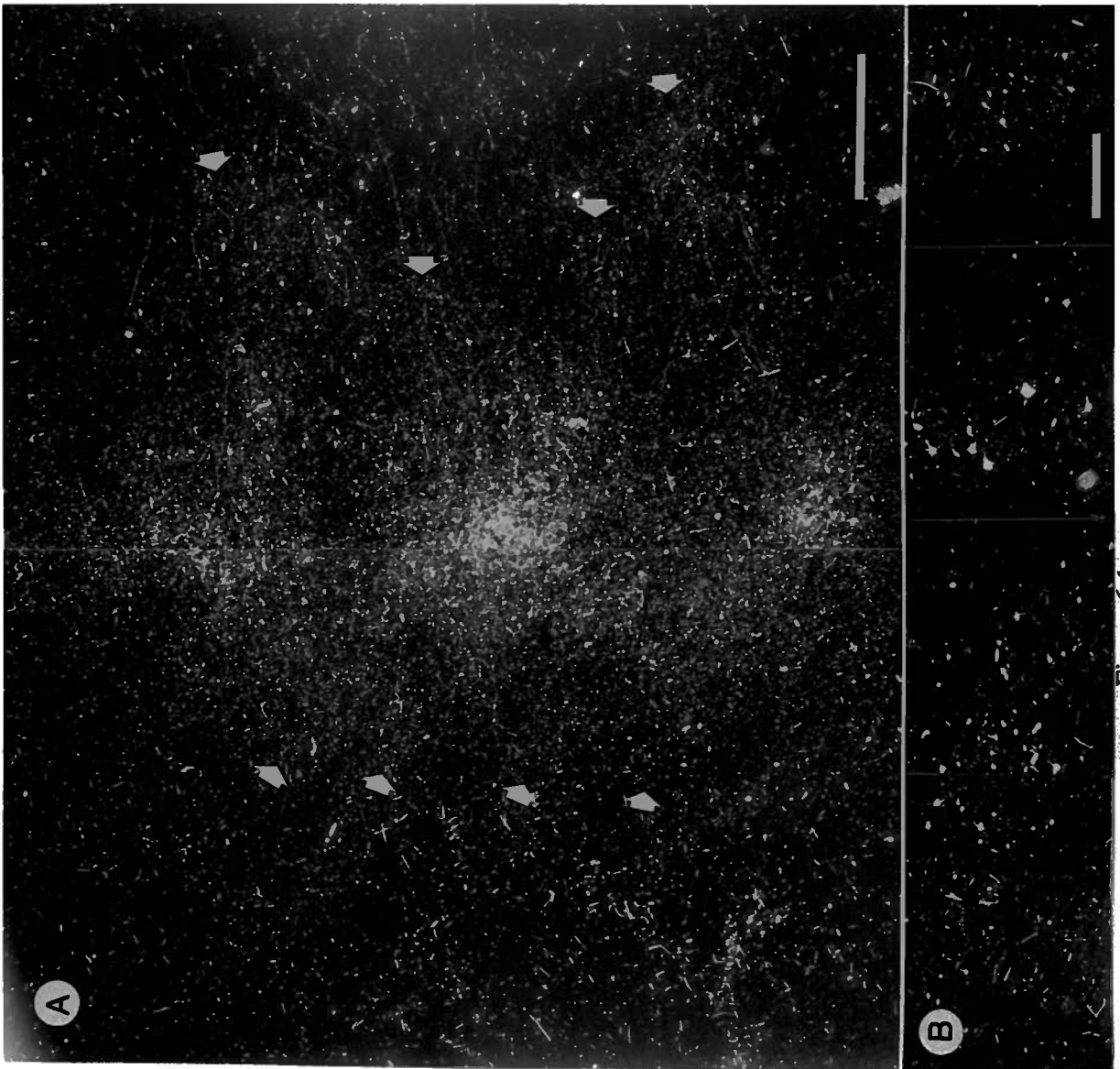


Figure 6.1

are found in the same clusters of callosal labeling, which have a spacing of about 1mm in area 17. In area 18, the patches of callosal labeling often had a slightly larger spacing than in 17. Even in the zone of densest labeling, along the presumed 17/18 border, the labeling was not continuous. In this zone, patches of increased labeling density often appeared larger and more widely spaced (about 2mm) than patches in areas 17 or 18, but there was also evidence of fluctuations in labeling density with a smaller periodicity (about 1mm) as well. The patchiness along the 17/18 border was most pronounced in case 1. In other cases, patchiness, especially the large periodicity patchiness, was less pronounced along the 17/18 border, although callosal labeling further away from the border retained its characteristic patchiness.

#### **Uniformity and size of the zone of effective tracer uptake**

The observed fluctuations in callosal labeling density were not likely due to the fact that more than one injection of WGA-HRP was made, as the injections coalesced to form a single, continuous zone of dense reaction product in the injected area. In order to determine if uptake of tracer from the injection site was uniform, the pattern of labeling in the lateral geniculate nucleus (LGN) was examined. The labeling in the LGN was always continuous, with no gaps that might suggest that uptake from the injection site was discontinuous. Lateral geniculate labeling from case 2 is shown in Figure 6.2. Although these photomicrographs were taken with crossed polarizing filters (Illing and Wässle, 1979), which increases contrast, the labeling also appeared dense and continuous with conventional brightfield optics.

Labeling in the LGN was also examined to determine the effective size of the injection site. In the four animals with restricted injections, it is probable that little callosal labeling resulted from uptake of tracer from areas other than 17 and 18, in spite of the fact that the halo of the cortical injection site extended laterally past the area 18/19 border. This is because labeling did not extend to the lateral part of the LGN, where the periphery of the visual field is represented (Sanderson, 1971a). As the three sections in Figure 6.2 are from levels along the

Figure 6.2. Labeling in the LGN at three different A-P levels following injection of WGA-HRP at the 17/18 border (case 2). Low power photomicrographs were taken with crossed polarizing filters, so labeling appears light on a dark background. The figures were printed at high contrast to show the maximum extent of labeling in the LGN. Outline of the LGN in each section is shown with dashed white lines. Approximate A-P levels for each section are: 7.5 mm anterior for A; 6 mm anterior for B; and 4.5 mm anterior for C. Medial is to the left, dorsal to the top. Arrows in B mark intralaminar spaces between laminae A and A1 (top arrow) and between laminae A1 and C (bottom arrow). Scale bar: 1mm.

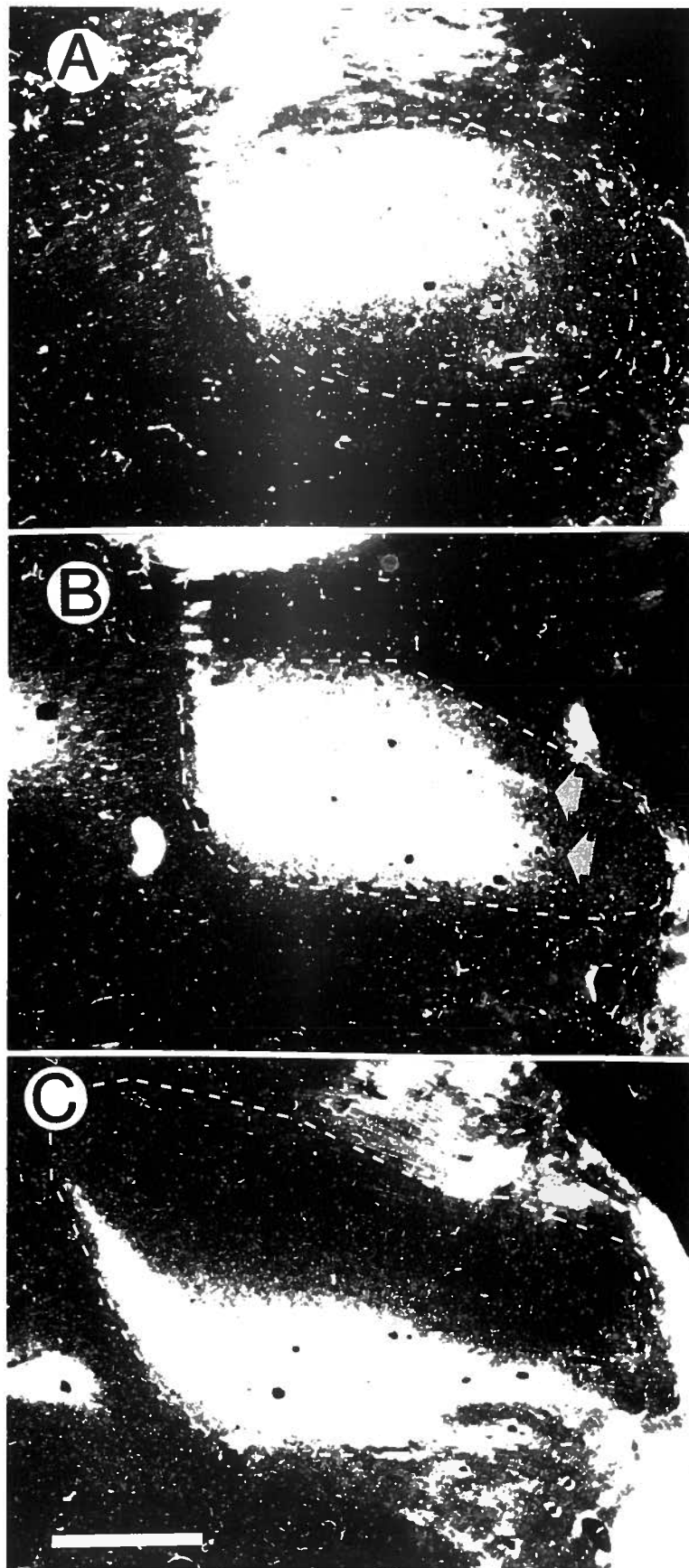


Figure 6.2

anterior-posterior axis separated by several millimeters, they also give some indication of the extent of the range of visual field elevation represented within the injection site. Labeling is concentrated in laminae A and A1 in anterior parts of the nucleus (Fig. 2A), and in the C laminae in posterior parts of the nucleus (Fig. 2C) because, due to the curved shape of the cat's LGN, lines of isoelevation do not run parallel to the coronal plane throughout the nucleus (Sanderson, 1971b). The finger-like projections of labeling seen in Figure 6.2b are in the intralaminar spaces and might represent greater divergence of corticogeniculate projections to the intralaminar spaces of the LGN, compared to corticogeniculate projections to the A and C laminae. In the last two animals, in which the series of injections were more extensive, the whole medio-lateral extent of the LGN was labeled at some A-P levels; in these two animals the possibility that some callosal labeling was from area 19 cannot be excluded, although these two experiments did produce callosal labeling patterns comparable to our other experiments. The labeling in the LGN was also much more extensive in its A-P extent in these animals. The LGN labeling thus showed that all the injections produced uniform uptake of tracer from a large area of visual field representation in the cortex.

### **Computer reconstructions of callosally labeled cells**

The patchy organization of callosal connections was evident not only in single sections, such as shown in Figure 6.1, but also, after appropriate averaging, in the reconstructions of retrograde labeling from serial sections through the entire thickness of the cortex. Figure 6.3A shows the reconstruction of retrograde labeling from case 2. Each dot represents a single retrogradely labeled cell body, and labeling from the entire set of tangential sections is collapsed onto a single plane. The pattern of labeling looks quite continuous, except possibly at the medial and lateral edges. The fluctuations in density of labeled cells are easier to appreciate in Figure 6.3B, which shows the same data expressed as the density of labeled cells under a 100  $\mu\text{m}$  grid. As described above, The zone of densest callosal labeling was used to estimate the 17/18 border.

The average change in labeling density progressing from medial to lateral was calculated, as shown in the graph in figure 6.3B. A one mm wide strip centered on the peak of a Gaussian function fit to the data was designated as the 17/18 border. Although the largest number of callosal cells under a single  $100\ \mu\text{m}^2$  grid box was 20, corresponding to 2000 callosal cells/ $\text{mm}^2$ , the average density along the border, obtained from the peak of the curve in figure 6.3b was about 800 cells/ $\text{mm}^2$ . Given that  $1\ \text{mm}^2$  of area 17 contains 61,900 neurons (Beaulieu and Colonnier, 1983), approximately 1.3 % of neurons in the vicinity of the 17/18 border project to the contralateral 17/18 border; this should be considered a minimum estimate, as the methods used may not have visualized all of the projecting cells.

The fluctuations in density of callosally projecting cells were even more apparent when spatial averaging and contrast enhancement were applied to the density data for case 2, as shown in Figure 6.3C. Patches of relatively greater density can clearly be seen in area 17, area 18, and even along the presumed border of these two areas. Again, the patches are sometimes slightly larger and more widely spaced in area 18 than in area 17 (Fig. 3, asterisks). Unlike case 1, the 17/18 border shows only fluctuations in labeling density with a 1mm periodicity; the 2 mm spacing was not observed in this case. The same process of averaging and contrast enhancement was applied to the data from case 1 to produce Figure 6.4. The reconstruction of retrograde labeling before averaging is overlaid on top of the figure in order to show the relationship between the raw data and the image generated from it. Although it is much easier to appreciate the patches in the processed image, they can be seen in the raw data, especially medially in area 17, using the superimposed image for comparison. As the labeling in area 17 extended farther from the 17/18 border than in any of the other cases, the details of the labeling pattern can be best appreciated in this case. The patches were aligned in irregular rows to form a complex lattice-like structure. This level of organization was only hinted at when examining the labeling from a single section, thus demonstrating the usefulness of our method of charting labeling in all serial sections.

Figure 6.3. Three different representations of the same data (case 2), same scale and vertically aligned. **A.** Each dot represents a single cell labeled with WGA-HRP, and data from all serial tangential sections was collapsed onto a single plane. "A" and "L" show anterior and lateral, respectively. Numbers show location of visual areas. **B.** The data in **A** replotted to show the density of labeled cells. Each pixel is 100  $\mu\text{m}$  square. The graph underneath shows the average density of pixels across the M-L extent of the labeling. The "0" in the x-axis of the graph shows the location of the peak of labeling density, as determined by a fitted Gaussian function. A 1 mm zone centered on the peak of labeling density is shown by dotted lines which are extended into **A** and **C**. **C.** The density data in **B** after the smoothing procedure described in the text. The same patches of callosal labeling are marked with asterisks in **B** and **C**.



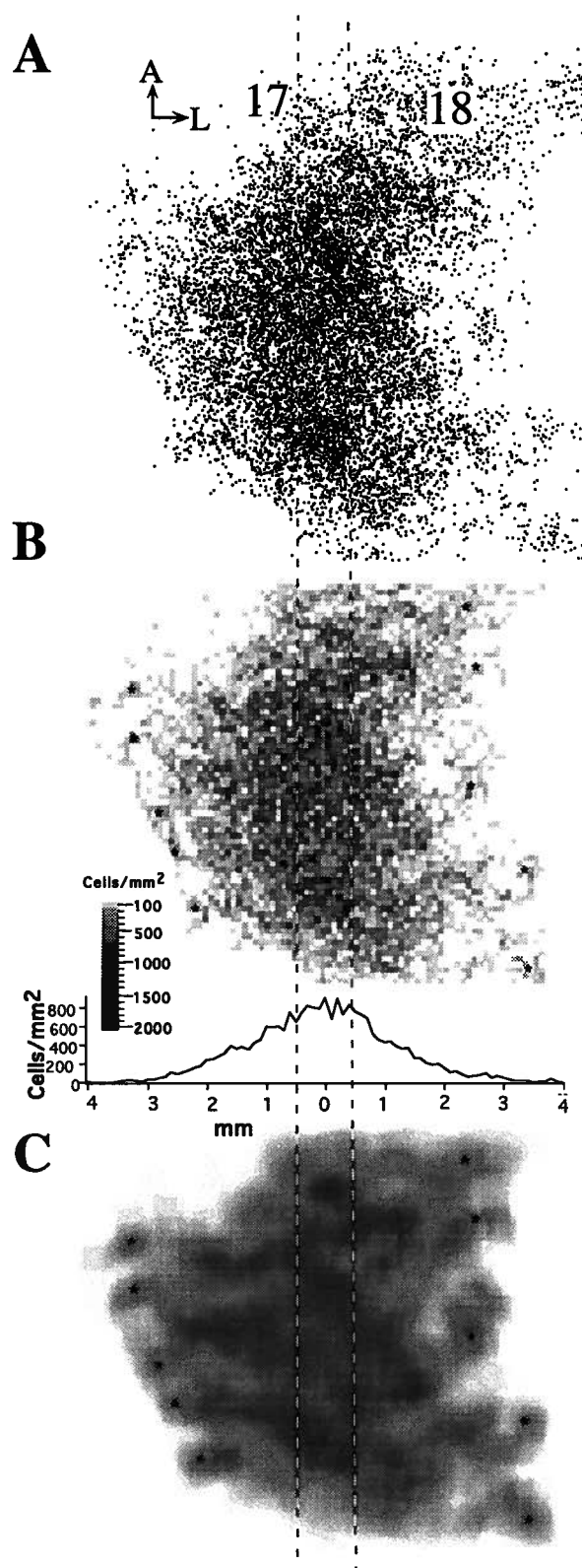


Figure 6.3

Figure 6.4. The complete pattern of callosal labeling from case 1. The positions of all the callosally labeled cells are shown superimposed onto the smoothed image obtained from the same data. The dashed lines mark a 1mm zone centered on the peak labeling density. The patches of labeling within the box are the same patches shown in Figure 6.1B, a photomicrograph of a single section.

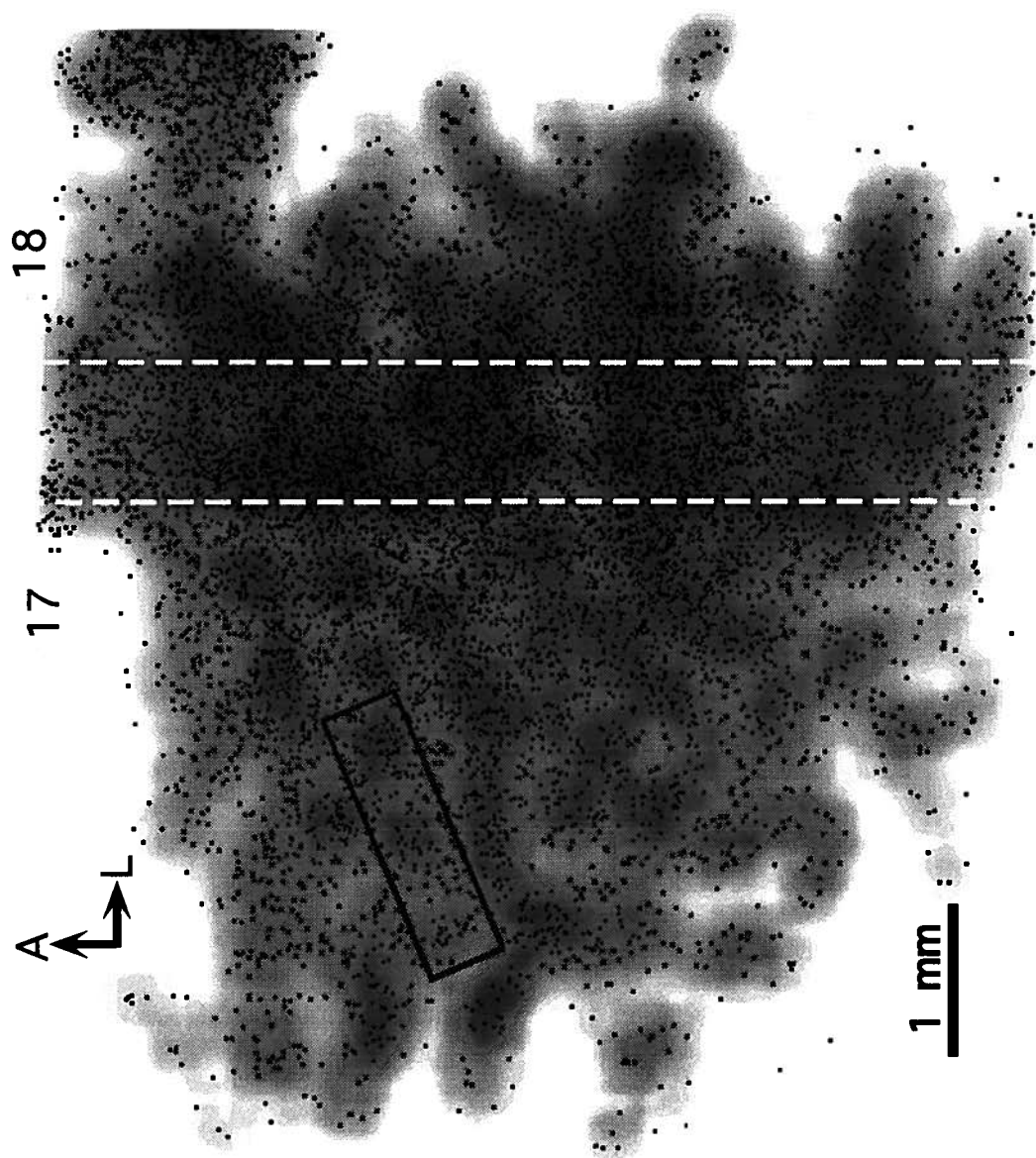


Figure 6.4

### **Distribution of callosal terminals**

The anterograde tracer BDA was used to demonstrate the terminations of callosal axons. Although terminal labeling was present from the WGA-HRP experiments, BDA has several advantages over WGA-HRP for anterograde labeling. One advantage is that, unlike WGA-HRP, BDA is transported rather poorly in the retrograde direction (Brandt and Apkarian, 1992; Veenman et al., 1992). Therefore, labeled terminals can more definitively be assumed to have arisen from cell bodies in the area injected, and not to have arisen from the collaterals of retrogradely labeled cells. This collateral labeling has conclusively been shown to occur following large WGA-HRP injections (Takeuchi et al., 1985; White and Keller, 1987). Also, BDA fills labeled axons completely, unlike WGA-HRP which gives a grainy, dust-like reaction product following anterograde transport.

As was accomplished for the WGA-HRP experiments, large, continuous injection sites were made by a series of closely spaced injections. Callosal labeling from a BDA injection is shown in Figure 6.5. The dense strip of fibers in Figure 6.5a along the 17/18 border shows the same patchy organization as seen with retrograde labeling. In this experiment, both larger (about 2mm spacing) and smaller scale (about 1mm spacing) patchiness can be seen along the border. Higher magnification photomicrographs of labeling medially in area 17 and laterally in area 18 are shown in Figures 5b and 5c, respectively. In both areas, a patchy distribution of fibers is present having the approximately 1mm spacing shown previously. Thus, the overall distribution of callosal terminals is similar to the distribution of callosal cells. In addition to anterograde labeling, some retrograde labeling was found from the BDA injections, raising the issue of collateral labeling. Retrogradely labeled cortical neurons were marked by perinuclear granular reaction product that extended only into proximal dendrites, making it unlikely that these cells had retrogradely transported enough tracer to fill their axon collaterals. It was concluded that the

Figure 6.5. Anterograde callosal labeling from a BDA injection. **A.** Labeling along the presumed 17/18 border zone. The labeling is patchy, with both the large and the small components described earlier being present. Medial is to the left and anterior is to the right. Scale bar: 1mm. **B.** Labeling 2-3 mm medially in area 17 from the same experiment. Patches of labeling are marked by arrow heads. A retrogradely labeled cell is marked by a small arrow. Scale bar: 500  $\mu$ m, and applies to both **B** and **C**. **C.** Labeling 2-3 mm laterally in area 18. Arrow heads mark patches of labeling. Patches are slightly larger and more widely spaced than in area 17.

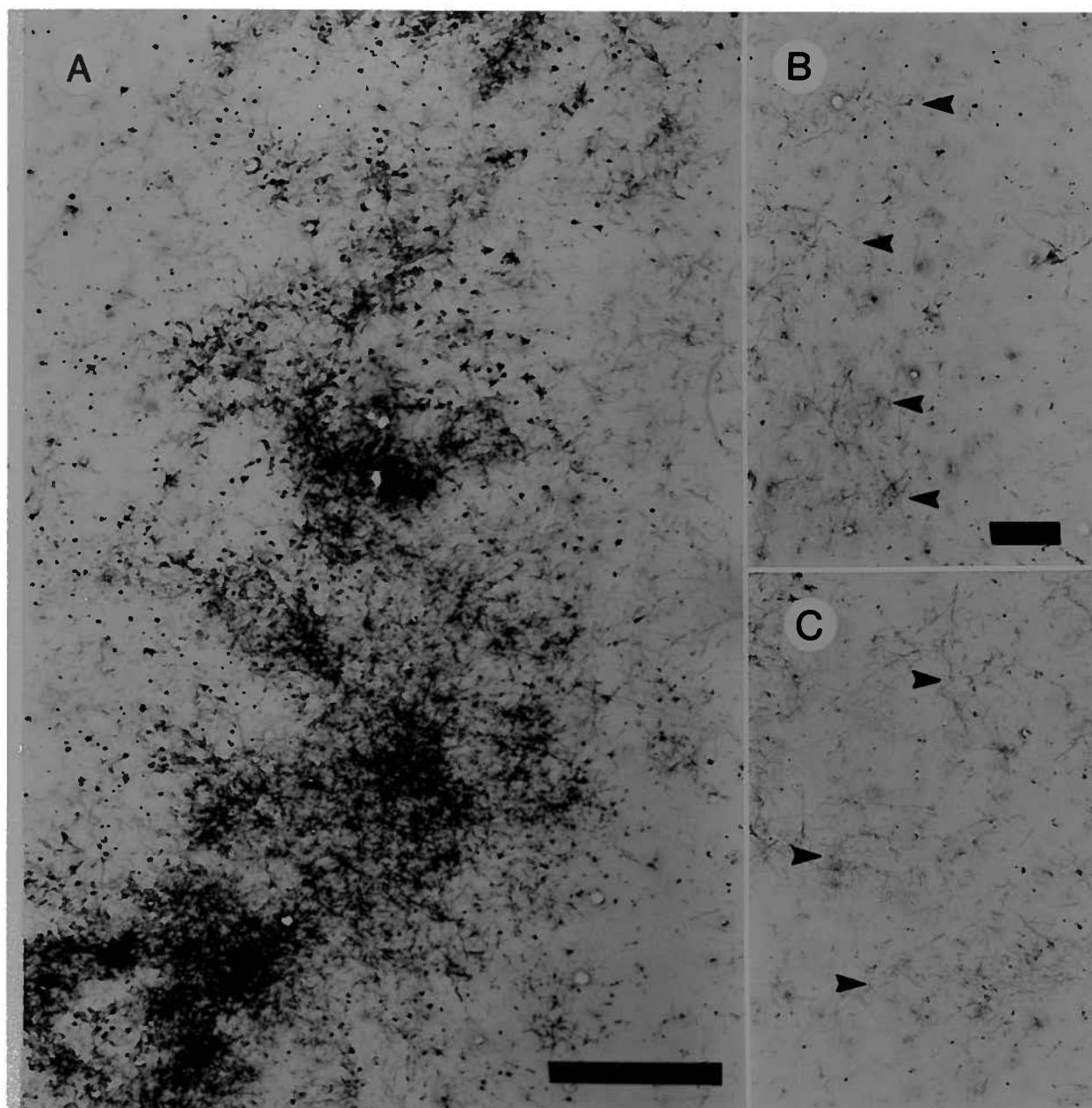


Figure 6.5

labeled fibers represented true anterograde transport from the injected hemisphere, not collateral labeling from retrogradely labeled cell bodies.

### **Callosal stripes in areas 18 and 19**

In cases 5 and 6, a more extensive series of injections was made and labeling patterns in area 19 were reconstructed, as well as 17 and 18. Figures 6.6a and 6.7 show the reconstruction of callosal labeling for cases 5 and 6, respectively. In addition to callosal labeling near the 17/18 border, there are multiple, irregularly spaced, 2-3 mm wide stripes of callosal labeling that begin in the lateral portion of area 18 and progress laterally across the surface of the cortex for many millimeters. Although present in the labeling from our earlier injections (see Fig. 4), it was only following more extensive injections that their organization and spacing could be appreciated. These stripes likely correspond to previous descriptions of isolated callosal projections laterally in area 18 which were termed callosal "islands" (Sanides and Albus, 1980). The reconstructions showed that callosal "islands" are actually medial-laterally elongated stripes of labeling that cross multiple visual areas.

### **Relationship of Callosal Labeling to CO Staining**

The patchy callosal labeling in areas 17 and 18 was compared to the pattern of CO staining in cases 5 and 6 by reacting alternate sections with CO histochemistry. Figure 6.6b shows an enlargement of the callosal labeling within the box in Figure 6.6a. As in previous cases, patches of labeling extend away from the 17/18 border into areas 17 and 18. In this case, labeling along the border itself was fairly continuous, but some fluctuations of labeling density can be seen there, especially in the upper part of Figure 6.6b. The CO pattern in the corresponding part of an alternate section is shown in 6c. In addition to finding CO blobs in area 17, as previously reported (Murphy et al., 1990), CO blobs in area 18 were also

Figure 6.6. Retrograde labeling and CO staining from case 5. A. Reconstruction of retrogradely labeled cells. Each dot marks the position of a single callosal cell retrogradely labeled with WGA-HRP. Two callosal stripes are marked by arrows. The boxed area is shown enlarged in B. B. Enlargement of callosal labeling from A. Some examples of clustered callosal labeling in areas 17 and 18 are shown with arrows. The small circles show some of the blood vessels used for alignment with the CO stained section. C. The pattern of CO staining in the same area. Note the blobs of increased staining. D. Superimposition of the callosal labeling pattern onto the image of the CO stained section. Alignment of the two was achieved by matching radially-penetrating blood vessels. The clusters of callosal labeling in areas 17 and 18 tend to align with the CO blobs.



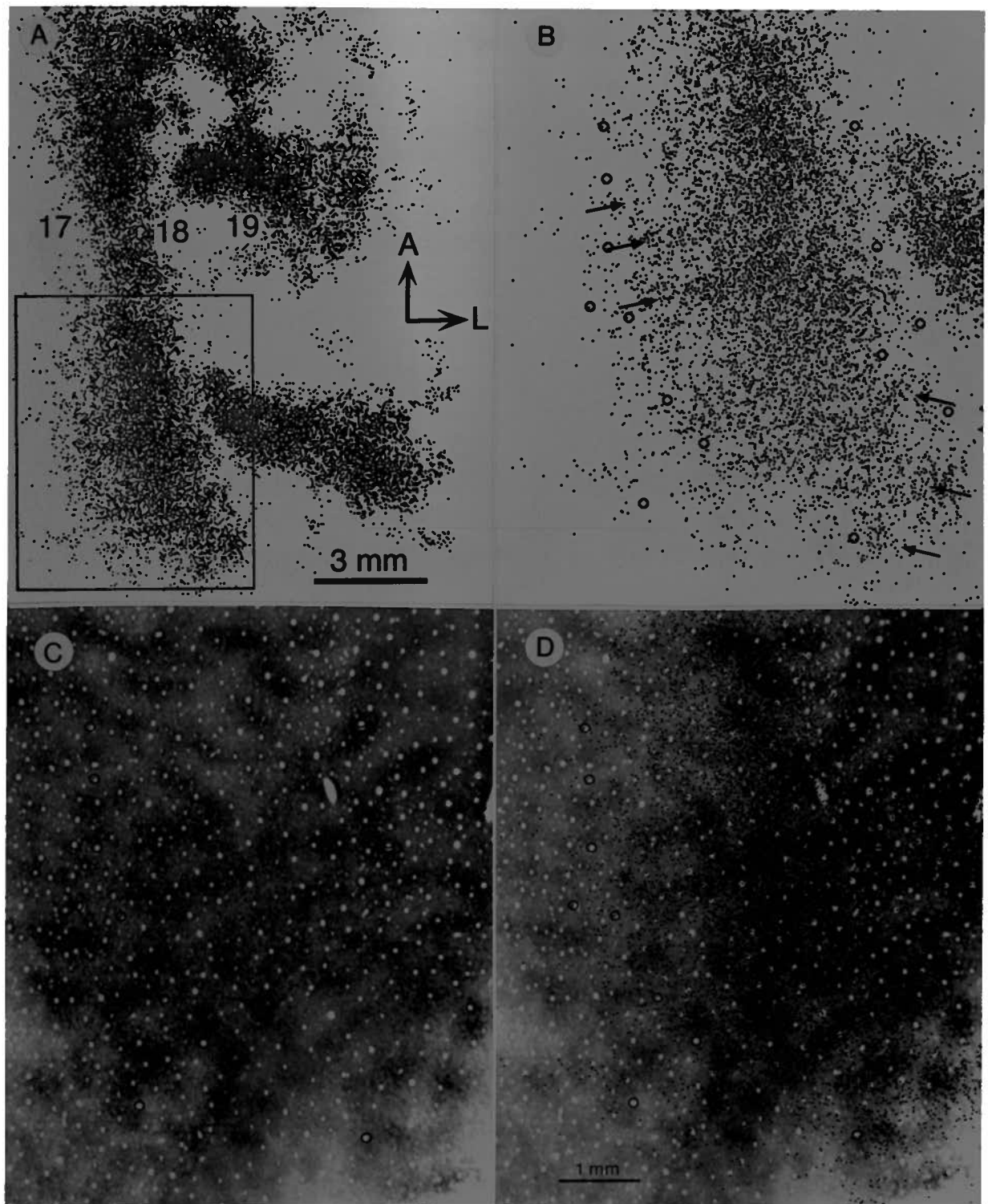


Figure 6.6

found which, although having a slightly larger spacing, resembled those in area 17. Matching blood vessels are shown for the two patterns. Figure 6.6d shows the callosal labeling superimposed onto the CO stained section. The patches of labeling extending medially into area 17 tend to overlie the CO blobs. In area 18 of this animal, the pattern of callosal labeling was less markedly patchy than in area 17, but here too, some correspondence between the CO blobs and the callosal labeling can be seen. The alignment of callosal labeling and CO staining is shown for another case in Figures 6.7 and 6.8. Figure 6.8 shows the callosal labeling from within the boxes in Figure 6.7 superimposed on the pattern of callosal labeling in the same manner as for case 5 in Figure 6.6. Again, the alignment of the patches of callosal labeling and the CO blobs is evident, especially in area 17. Two callosal stripes within area 18 are included in Figures 6.8 d-f, and it can be seen that there is no relationship between the CO staining pattern and the stripes of callosal labeling.

## **Discussion**

It is shown that the callosal pathway in the cat is organized in a truly discontinuous fashion. In fact, several distinct, differing forms of patchy organization are present in this pathway. At the border of areas 17 and 18, large patches of callosal labeling with a spacing of about 2 mm were often evident, although occasionally fluctuations in labeling density with spacing of about 1mm were also visible. Slightly lateral or medial to the border, where callosal labeling was less dense, smaller patches of callosal labeling could be seen. These had a spacing of approximately 1mm in area 17, slightly greater in area 18. These patches of callosal labeling, but not the larger patches along the border, were found to align with the CO blobs. Also present in area 18 were several large, irregularly spaced stripes of callosal labeling. These callosal stripes typically began about halfway across the mediolateral extent of area 18 and continued laterally through area 19 and as far as the suprasylvian sulcus; they had no apparent relationship with the CO blobs. Each of these forms of patchy organization will be discussed in turn.

Figure 6.7. Reconstruction of WGA-HRP retrograde labeling for case 6. The boxed areas are enlarged in figure 6.8. Arrows mark two callosal stripes. The dotted line marks the lateral border of area 18, as determined by CO staining.

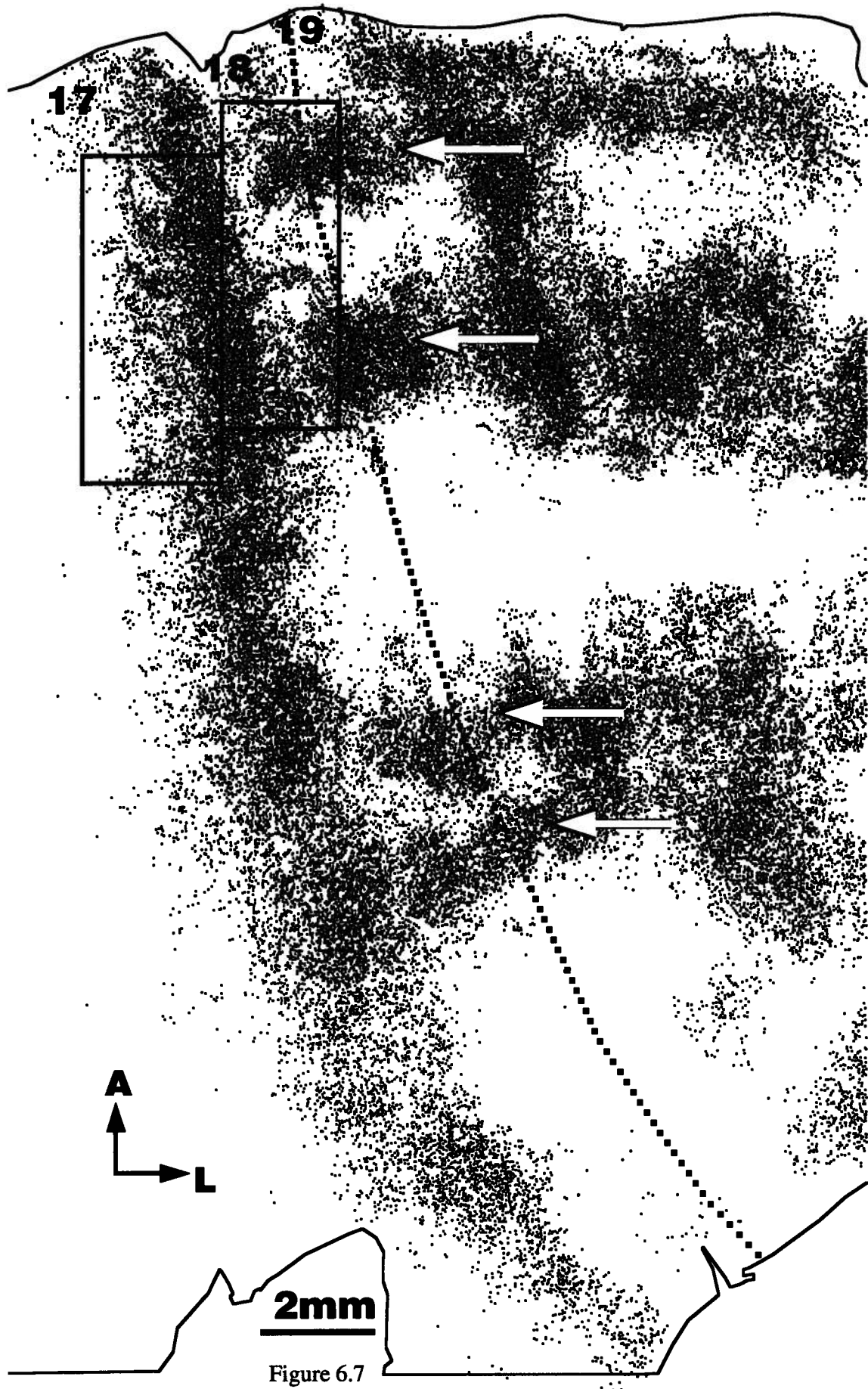


Figure 6.7

Figure 6.8. Alignment of WGA-HRP callosal labeling and CO staining for case 6. A.-C. show area 17 and D.-F. show area 18. A and D show the callosal labeling, B and E show the CO staining, and the C and F show the superimposition of the callosal labeling pattern onto the image of the CO staining. The two were aligned by matching radially-penetrating blood vessels, some of which are shown as small circles.

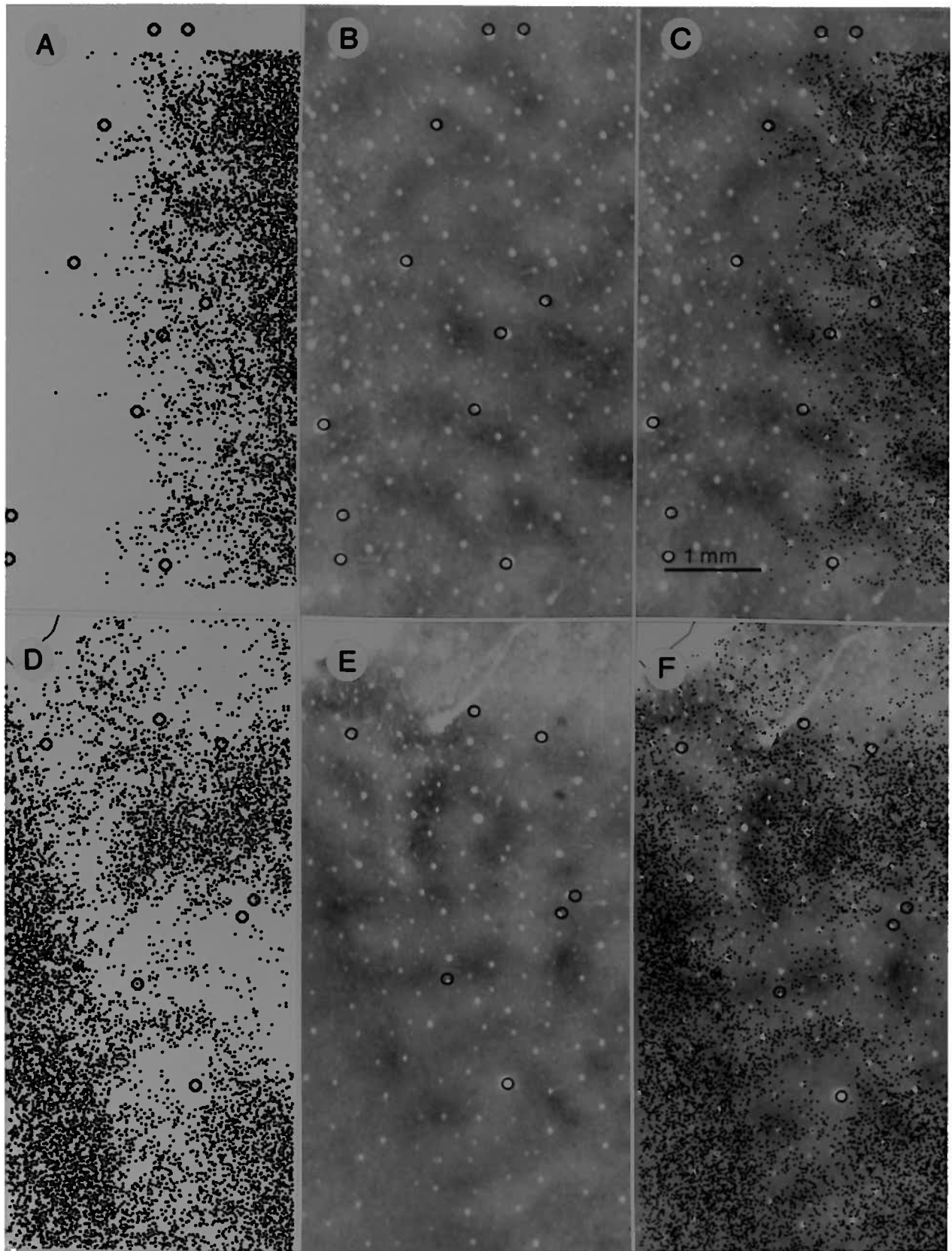


Figure 6.8

### **Patchy callosal labeling at the 17/18 border**

Irregular fluctuations in labeling density were often evident even in the area of densest callosal labeling, the presumed 17/18 border. These fluctuations appeared to have two components, one roughly the same size as the cytochrome blobs, and the other approximately twice as large. Presumably, the small scale fluctuations in callosal labeling density correspond to the CO blobs at the 17/18 border, as they do elsewhere. In Figure 6.6d, for instance, there are examples of small increases in labeling density along the border corresponding to CO blobs. However, because the fluctuations of labeling density along the border are often not very striking, especially for the retrograde labeling, it is more difficult to make these sorts of comparisons than it is for the more obvious patches of callosal labeling that occur slightly medial or lateral to the border. It would appear that both blobs and interblobs are callosally connected at the vertical meridian representation, but that sometimes the blobs have a greater density of callosal connections.

The presence of larger scale fluctuations in callosal labeling density at the 17/18 border is more difficult to interpret. However, our unpublished observations indicate that this large scale fluctuation in callosal labeling density along the 17/18 border is also present when the contralateral injection site is the lateral suprasylvian area. The large scale fluctuation is not present in the ipsilateral projection from the area 17/18 border to the lateral suprasylvian area suggesting that it is a unique feature of callosal pathways. Detailed electrophysiological mapping of neuronal receptive field locations in the 17/18 border region (Diao et al., 1990) has shown that cells with receptive fields located 1 to 7° into the ipsilateral hemifield are restricted to confined zones with a size and spacing similar to the larger scale fluctuations in callosal labeling along the 17/18 border. It is possible that the large scale fluctuations in density of callosal labeling along the 17/18 border might be the result of these zones of ipsilateral field representation making stronger callosal connections than surrounding areas of contralateral

representation. It is also interesting to note that the ipsilateral field zones were marked by the presence of larger receptive fields and broader orientation tuning than was found outside these zones (Diao et al., 1990). It has been suggested (Payne, 1990a; Payne, 1990b) that zones of ipsilateral field representation along the vertical meridian might be the main cortical target of layer 3 of the medial interlaminar nucleus, which is the only part of the LGN complex to contain any ipsilateral field representation (Lee et al., 1984). It would be interesting to see if the projections to visual cortex of this layer are organized into patches that match the large scale fluctuations of callosal labeling density and/or the patches of ipsilateral field representation.

### **Callosal connections and CO staining in areas 17 and 18**

Callosal connections within area 17, away from the vertical meridian representation, were found to be clustered, sometimes forming a complex lattice-like structure extending more than 5 mm from the 17/18 border. In cat area 17, the CO blobs form a lattice-like structure that matches the pattern of callosal labeling (fig. 4; fig. 8). The organization of callosal connections and CO staining in area 18 was similar, except that the blobs of CO staining and patches of callosal labeling were slightly larger than in area 17. This contrasts with the situation in the primate, where V1 is marked by blobs of CO staining similar to those in the cat (although having a smaller periodicity, and a more regular organization than in the cat) and V2 shows a series of CO-rich stripes oriented approximately at right angles to the V1/V2 border.

Often, the patchiness of callosal labeling was not as obvious in area 18 as in area 17. This might be related to the fact that, as area 18 is much narrower than area 17, less space in area 18 contained patchy callosal labeling. Also, the presence of the callosal islands in area 18 sometimes obscured the patchy labeling in the CO blobs. Therefore, it was more difficult to compare callosal labeling and CO patterns in area 18 than in area 17, although it appears that patches of callosal labeling in area 18 are in the CO blobs, as they are in area 17.



The organization of callosal connections in the cat is comparable to the organization described for various primate species. Callosal labeling within area 17 of the owl monkey was found to exhibit a periodic fluctuation in density with a spacing about 400mm (Cusick et al., 1984). In the galago, the same study showed an even greater extent of clustered labeling medially in area 17, and the clusters of labeling were coextensive with CO blobs. In the macaque monkey, callosal labeling in area 17, although more restricted in extent, is also patchy in a fashion that correlates with the CO blobs (Kennedy et al., 1986). In owl monkeys and macaques, the CO stripes of V2 are also preferentially connected callosally (Kennedy et al., 1986; Cusick and Kaas, 1988; Kennedy and Dehay, 1988; Olavarria and Lewis, 1992). Thus, the callosal connections of visual cortex in primates and cats appear to be organized similarly in that they are preferentially made to zones of high CO activity, regardless of the spatial organization of these zones, i.e., blobs versus stripes. Recently, blobs of dense staining of CO activity have been demonstrated in ferrets (Crescho et al., 1992). As of yet, the tangential organization of callosal connections in this species and its relationship to the CO blobs, has not been investigated.

### **The callosal stripes**

Although mainly concerned with the organization of areas 17 and 18, some observations were also made on callosal labeling in other visual areas. These areas were marked by stripes of callosal labeling extending from the lateral portion of area 18 to as far lateral as the fundus of the lateral suprasylvian sulcus. Within area 18, these stripes have been shown to correspond to anomalous representations of the vertical meridian in the lateral part of area 18 (Sanides and Albus, 1980), and there are also discontinuities in the visual field map of area 19 (Hubel and Wiesel, 1965; Donaldson and Whitteridge, 1977; Tusa et al., 1979) which may be associated with the stripes. It should be mentioned that visual cortex in the lateral suprasylvian sulcus contains duplicated representations of the vertical meridian (Sherk and Mulligan, 1993) which

might be expected to correspond to the course of the callosal stripes through that area as well. No changes were found in the pattern of CO staining in the vicinity of the callosal stripes, which included both blobs and interblobs in their territory. If the callosal stripes are truly associated with anomalous representations of central visual field, then the inclusion of both blobs and interblobs within them would not conflict with the observation that callosal connections in the rest of areas 17 and 18 become more and more confined to blobs with increasing distance from the vertical meridian. It is also possible that blobs may be slightly more heavily labeled than interblobs within the callosal stripes, as was sometimes seen at the 17/18 border.

## 7 GENERAL DISCUSSION

The studies described in the preceding chapters have provided important new information regarding the organization of corticocortical and intrinsic pathways in the visual cortex of the cat. Specifically, these studies have shown:

1. The finding of a patchy pattern of CO staining in area 17 of the cat (Murphy et al., 19888) was confirmed, and extended to area 18.
2. Projections from W-cells of the LGN were confined to the CO blobs, and were segregated into cortical layers (11, 13, and 5a) while the projections from the X-cells and Y-cells were confined to layer 4)
3. Projections from the large Y-cells in the magnocellular portion of layer C were confined to layer 4a of the CO blobs in area 17.
4. The finding that cells projecting from area 17 to visual area PMLS were hard patterned(Shipp and Grant, 1991) was confirmed and extended to area 18.
5. Patches of PMLS-projecting cells in areas 17 and 18 were concentrated in the CO blobs.
6. Cells projecting from area 19 to PMLS were also hard patterned, but with a larger spatial scale than patches in area 17 or 18.
7. Cells projecting from areas 17 and 18 to area 19 were found to be soft patterned; .e., both blobs and interblobs of area 17 and 18 projected to area 19.
8. The projections of blobs and interblobs were segregated into different columns in area 19. These columns were at least 2 mm wide.
9. Local connections in area 19 had a larger size and spacing than local connections in areas 17 or 18.

10. Callosal connections of areas 17 and 18 were patchy, with several different scales of patchiness present.
11. Callosal connections tended to be heavier to the CO blobs in areas 17 and 18, and this was especially true of callosal connections farther from the border of these two areas.

These data are consistent with the existence of segregated, parallel input and output processing streams throughout the visual cortex of the cat. In particular, the blobs of areas 17 and 18 receive classes of inputs from the LGN that the interblobs do not receive, and project, in turn, to a visual area that the interblobs do not project to. Many of the implications of these findings, with respect to the organization of pathways in the visual cortex of the cat, are discussed extensively within the individual chapters. Here, only aspects related to the hypothesis of segregated parallel pathways will be discussed, with an emphasis on comparison of these data to the system of parallel visual pathways in primates that has been so exhaustively demonstrated (Van Essen et al., 1992; Van Essen and Gallant, 1994)

### **Segregation of Pathways in Area 17: A Comparison with Primates**

It appears that CO blobs in the cat, like those in primates, are associated with the segregation of different processing streams. The similarity between pathways in cats and primates is most striking for the comparison between the W-cell pathway of the cat and the so-called "koniocellular" pathway in primates. At the level of the LGN, both the K layers of primates and the parvocellular C layers of cats receive input from the superior colliculus, while the rest of the LGN does not (Harting et al., 1991). Also, the parvocellular C laminae resemble the K layers of primate LGN in that they stain densely for one calcium binding protein (calbindin) and weakly for another (parvalbumin), while the opposite pattern is found in the main layers of the LGN in

both species (Stitchel et al., 1987; Casagrande, 1994). The neurochemical distinctness of the K pathway was strengthened by a recent study showing that K relay cells in the macaque are the only LGN cells that stain densely for calcium/calmodulin dependant protein kinase II (Hendry and Yoshioka, 1994); the staining pattern for this enzyme in the cat LGN is not yet known. Physiologically, the K layers contain cells with W-type properties (Irvin et al., 1986), at least in galagos, the only primate species in which the K layers have been studied physiologically. Like the parvocellular C-layers of the cat, the koniocellular layers terminate in layer 3 selectively within the CO blobs (Fitzpatrick et al., 1983; Weber et al., 1983; Livingstone and Hubel, 1987c; Lachica and Casagrande, 1992). It is interesting to note that in tree shrews, the small-cell layers of the LGN also receive projections from the superior colliculus (Fitzpatrick et al., 1980), stain densely for calbindin (Diamond et al., 1993)), and terminate specifically in patches in layer 3 (Fitzpatrick and Raczkowski, 1990). CO blobs have yet to be observed in this species. One intriguing difference in the projections of the parvocellular C layers of the cat LGN and the small-cell layers in other species is the projection to layer 5a, which has only been described in the cat. Whether this pathway has analogs in other species is unknown.

Another question concerning the similarity of geniculocortical organization in cats and primates is whether CO blobs in the cat are aligned with ocular dominance columns, as they are in most primates (Horton, 1984). At present, there are conflicting reports concerning this question, with one study finding that CO blobs are centered over OD columns, (Murphy et al., 1991), and another study concluding that these two columnar systems are relatively independent in the cat (Dyck and Cynader, 1993b). Certainly, the relationship between these two columnar systems cannot be as precise as it is in the macaque, for instance. This is because the spacing between CO blobs in the cat is too large to provide for blobs centered over the ocular dominance columns of each eye (compare Figs. 3.6A and 3.7A). In addition, ocular dominance columns in the cat have an irregular, highly branched pattern, and there is a greater degree of overlap of inputs from the two eyes in the cat (Anderson et al., 1988). The relationship between CO blobs

and ocular dominance does not hold for all primates, as evidenced by the squirrel monkey, in which inputs from the two eyes are nearly completely mixed, while CO blobs are very distinct (Weber et al., 1983; Horton, 1984). It has been speculated that OD columns arose independently in several different lines of mammalian descent, (Florence et al., 1986). This could explain why CO blobs are related to OD columns in some species, but not others. At any rate, it appears that the variation in geniculocortical organization between primates and cats is not that much greater than the variation among different primate species.

It is suggested that Y-cell input in area 17, at least the Y-cell input from layer C, in addition to W-cell input might also be confined to the CO blobs, thus accounting for the fact that the blobs are visible in layer 4a, but not in layer 4b. Although not a matter of universal agreement (Shapley and Perry, 1986), the Y-cell pathway in the cat has traditionally been, on the basis of similarities in relative cell size, and physiological properties, likened to the magnocellular pathway in primates (Casagrande and Norton, 1991). The suggestion that the blobs in the cat are part of a Y-cell driven, motion-densitive processing stream is at odds with findings in the macaque and squirrel monkey that the blobs are dominated by parvicellular instead of magnocellular inputs and do not contain direction selective cells (Livingstone and Hubel, 19874). However, it has been suggested that blobs or interblobs may be dominated by either magno- or parvo- streams in different primate species, possibly depending on specialization for nocturnal versus diurnal niches (Casagrande and Norton, 1991).

It is interesting to note that, in one report, the magnocellular inputs to V1 of the nocturnal new world owl monkey are confined to the CO blobs in layer 4a (Horton, 1984), just as it has been suggested here that the Y-cell inputs from the C-laminae are confined to the CO blobs in layer 4a in the cat. In the owl monkey, (Horton, 1984), and in the prosimian galago (Condo and Casagrande, 1990), CO blobs are visible in the top part of layer 4, where the magnocellular LGN afferents terminate, similar to the arrangement of CO blobs in the cat. (This does not appear to be the case in other, diurnal new world primates such as the squirrel monkey, or in any old world

primates examined (Horton, 1984). It is suggested that, in both cats and some nocturnal primates, the dense CO staining in blobs in layer 4a is a reflection of the concentration of Y-cell or magnocellular terminations. Also, an area that receives projections from the CO blobs in owl monkeys, the dorsomedial visual area, has a large percentage of direction selective neurons (Krubitzer and Kaas, 1989; Krubitzer and Kaas, 1993), as does PMLS in the cat. Thus, there is reason to believe that in some primate species, at least, a large celled, motion sensitive pathway through the blobs and into an extrastriate area may exist, as has been shown here for the cat.

Another piece of evidence that would suggest a specific magnocellular input to the CO blobs in primates is the staining pattern for the Cat-301 antibody (Hockfield et al., 1983). This antibody stains a cell-surface molecule on select populations of cells in the brain. In the LGN of macaque monkeys, this marker stains the magnocellular layers most densely (Hockfield et al., 1983; Hendry et al., 1988), while in the visual cortex, Cat-301 stains patches in layer 4C $\alpha$  and the bottom part of layer 4B (Hendry et al., 1988; DeYoe et al., 1990). These patches align with the CO blobs in layer 3 (Hendry et al., 1988). The presence of Cat-301 in layers of the LGN and cortex known to receive magnocellular input, as well as in extrastriate areas such as V3 and MT thought to be dominated by magnocellular inputs (DeYoe et al., 1990), suggest that the abundance of Cat-301 in the CO blobs versus the interblobs reflects some differential magnocellular input. Unfortunately, there are no published reports of Cat-301 staining in new world monkeys, and the antibody appears to label only faint, scattered cells in prosimian LGN and cortex (Hendry et al., 1988; Jain et al., 1994).

In the visual thalamus of the cat, Cat-301 recognizes Y-cells, but not X- or W-cells, in the A and C laminae of the LGN, and in the MIN (Sur et al., 1988). Interestingly, a recent report has shown that Cat-301 stained cells in the cortex are patchy (Chehil et al., 1992). Unpublished experiments from this laboratory have shown that the patches of Cat-301 labeling are in the CO blobs in the cat, just as they are in the primate. Again, these data are consistent with the idea that the blobs in the cat preferentially receive Y-cell input.

Thus, CO blobs in cats and primates appear to be manifestations of similar principles of visual cortical organization. It is suggested that further study will show that other differences between blobs and interblobs in primates, such as intrinsic interlaminar connectivity (Lachica et al., 1992; Lachica et al., 1993), dendritic field organization (Hübener and Bolz, 1992), and physiological response properties (Livingstone and Hubel, 1984; Tootell et al., 1988; Ts'o and Gilbert, 1988), will also be found between blobs and interblobs in the cat.

### Comparison of Area 18 and Area 17

One striking finding that has emerged from these studies is that columnar organization of CO staining, LGN inputs, and corticocortical connections of area 18 is very similar to that of area 17. Because of its strong input from the main layers of the LGN, area 18 has previously been considered to be a primary visual area (Tretter et al., 1975) and "a unique magnocellular area in the cat" (Henry, 1988). In other carnivores, such as ferrets, there is also strong input from the LGN to area 18 (Law et al., 1988), suggesting that this condition may be a feature common to all members of this order. It is speculated that area 18 in carnivores is not homologous to the second visual area V2 of other mammalian orders, for in primates (Bullier and Kennedy, 1983), rodents (Ribak and Peters, 1975), tree shrews (Conley et al., 1984), and even the marsupial opossum (Coleman and Clerici, 1981), the main projection from the LGN is restricted to area 17. It would be of interest to determine in which other mammalian groups the second visual area receives geniculate input, as in the cat, or lacks such input, as in primates.

It is suggested that area 18 may have arisen by duplication or splitting of area 17 (Kaas, 1989) subsequent to the divergence of the carnivore and primate lines. Interestingly, recent evidence suggests that *Cheirogaleus medius*, a prosimian primate, possesses a region of cortex inside architectonically defined V1 that contains a non-mirror image (V2-like) representation of the visual field (Paolini et al., 1994). This representation may be an independent example of a



partial duplication of primary visual cortex. An alternative suggestion is that the second visual areas of the different mammalian groups are homologous, and that LGN inputs to the second visual area were either selectively lost in some groups, or selectively gained in other groups.

### **Continuation of Segregated Streams Through Area 19**

Area 19 was found to receive inputs from both blobs and interblobs, and to keep these inputs segregated into different columns; these columns were of a larger size than blobs and interblobs in areas 17 and 18. It was also found that cells projecting from area 19 to PMLS were arranged in similarly large clusters, and it was hypothesized that a relationship between these two types of patches might exist. Thus, if the same columns of area 19 that received projections from the blobs in areas 17 and 18 projected to PMLS, then a segregated pathway of W/Y-cell projections could be traced through area 19. The projections from areas 17 and 18 to PMLS directly would then be an example of connections that skip a stage in the processing hierarchy (Felleman and VanEssen, 1991). It is interesting to note that projections from the C-layers of the LGN also terminate in large spaced patches in area 19 (Anderson et al., 1988), and it is suggested that these projections may also correlate with the input-and/or output-defined columns in area 19. In primates, projections from the thalamus have been shown to terminate in stripes of dense CO staining in area 18 (Curcio and Harting, 1978; Horton, 1984; Livingstone and Hubel, 1987c). As the CO stripes in primate area also V2 segregate inputs from blobs and interblobs of area V1, and segregate outputs to different extrastriate areas, there is a precedent for such intricate interrelationships of connections with different levels of the visual system.

Because it receives both blob and interblob information, area 19 must have a different function in the processing of visual information than area PMLS, for instance, which receives inputs mostly from the blobs in areas 17 and 18. Zeki and Shipp (1988) suggested that primate areas V1 and V2 act as segregators to funnel different visual information into different

extrastriate areas, such as MT and V4, which are specialized for particular visual functions. These results would suggest that area 19 in the cat should be considered a segregator of visual information, like V1 and V2, and not a specialized visual area, like primate area V3, as has been suggested (Payne, 1993).

If area 19 is truly acting as a segregator, then projections to different visual areas should be segregated within area 19. That is, there should be projections to other areas "slotting in" between the patches of cells projecting to PMLS, as for instance, patches of cells projecting to MT and V4 are interdigitated in area V2 of the primate visual cortex (DeYoe and VanEssen 1985). As area 19 has several robust outputs to areas other than PMLS (Symonds and Rosenquist, 1984; Figure 5.2), this is certainly a possibility. Unpublished experiments from this laboratory have, in fact, showed that when area PMLS and another extrastriate visual area that receives projections from area 19 (area 21a) were injected with two different tracers, the patches of labeling from the two tracers formed an interdigitated pattern in area 19. It is interesting to note that 21a and PMLS have been described as having rather different physiological properties (Toyama et al., 1994). This is consistent with the hypothesis of segregated processing streams in area 19.

### **The Organization of Inputs to PMLS**

Many studies of the physiological properties of PMLS have shown that this area contains neurons selective for the direction of stimulus motion (Spear, 1991). The segregation of inputs to this area suggests the existence of processing stream through areas 17-19 and into PMLS concerned with analyzing stimulus motion. In the visual cortex of primates, a similar organization exists in that area MT is also concerned with analysis of stimulus motion, and receives segregated inputs from V1 and V2 (Van Essen and Gallant, 1994). As the similarities between these two areas have led others (Zeki, 1974; Lund et al., 1979; Payne, 1993) to suggest

that they may be homologous, it is interesting to compare the organization of their respective connections from primary visual cortex.

The input from primary visual cortex to MT, originates mostly from a layer of large cells at the base of layer 4B, (Lund et al., 1975; Shipp and Zeki, 1989).and not from layer 3, as in the cat (Lund et al., 1979; Shipp and Grant, 1991). This comparison is not entirely valid, though, as the cat does not have a layer corresponding to primate 4B. However, Lund et al. (1979) have argued that the large pyramidal cells at the layer 3/4 border in the cat may be analogues of the large cells in layer 4B of the primate that project to MT; these border pyramids make up a sizable percentage of the cells that project to PMLS (Shipp and Grant, 1991). Moreover, a review of the cytology of V1 in different primates shows that layer 4B is only poorly differentiated in the prosimian galago (Casagrande and Kaas, 1994), and cells projecting to MT in galagos are more widely distributed in the upper parts of layer 3 (Diamond et al., 1985). It is possible that the confinement of cells projecting to MT and the creation of a special sublayer containing these cells is a refinement that reaches its full development only in simian, particularly old world, primates(Lund et al., 1979); Casagrande, 1994 #2145. Another possibility is that non-primates such as the cat, which do not have a homologue to primate layer 4B also do not have a homologue to primate area MT, and that this specialized sublayer of primary visual cortex developed in parallel with its target area.

### **Do Functional Correlates Exist?**

This study has shown an impressive degree of segregation of connectivity within different areas of the visual cortex of the cat. This raises the interesting question of whether there are any functional correlates of this segregation, as has been documented for similar patterns of segregation in primates. At present, there have been no studies examining differences in response properties inside and outside of CO blobs in the cat. The possibility that the CO

blobs in area 17 represent zones of Y-cell activity has been discussed above. As the physiological differences between X-cells and Y-cells in the LGN have been well characterized, physiological evidence for X-like and Y-like properties in blobs and interblobs of the cat could be sought. As previously mentioned, differences in preferred spatial frequency would be one such possibility, and a columnar organization of spatial frequency in the cat visual cortex has been previously described (Tootell and Silverman, 1981).

Differences in physiology of the CO blobs and interblobs in primates have been used to explain the result that the confinement of callosal connections to the CO blobs becomes more pronounced with distance from the vertical meridian representation in primates (Cusick et al., 1984); the difference in callosal connectivity between blobs and interblobs increases with increasing receptive field azimuth. As a similar organization of callosal connections was noted in cats (Chapter 6), differences in the function of blobs and interblobs in cats might also be inferred from their different callosal connectivity. One hypothesis is that receptive fields of cells in the CO blobs in primates are larger than those of cells in the interblobs (Livingstone and Hubel, 1984) and will therefore overlap with the vertical meridian at greater azimuths. If this mechanism were at work in the cat, it would be consistent with the notion that blobs in the cat are preferentially receiving Y-cell inputs, as these have larger receptive fields than X-cells (Casagrande and Norton, 1991).

Another possibility is that processing of information in the different CO compartments requires different callosal connectivity. For instance, the thick CO stripes in area V2 of the squirrel monkey contain a high proportion of cells responsive to binocular disparity (Hubel and Livingstone, 1987) which might be generated, in part, by their callosal connectivity. However, both the thin stripes as well as the thick ones are connected callosally (Olavarria and Lewis, 1992) and the thin stripes, at least in the squirrel monkey, possess unoriented cells which lack disparity tuning (Hubel and Livingstone, 1987).

A third hypothesis is that CO blobs have lower selectivity and more spontaneous activity than interblobs (Livingstone and Hubel, 1984). At that period in development when the original exuberance of callosal axons is "pruned back" (Innocenti, 1981; Innocenti and Clarke, 1984), the higher levels of activity may help to stabilize callosal axons in the blobs relative to the interblobs. In the cat, most callosal axons destined to be pruned are lost between the ages of two weeks and two months, with callosal axons continuing to be lost as late as three months of age (Elberger, 1993). Cytochrome blobs are present at least as early as 50 days of age in the kitten (Dyck and Cynader, 1993b) and these may be present at earlier ages, given that they develop prenatally in the macaque monkey (Horton, 1984). Therefore, CO blobs are present and can possibly affect callosal axon elimination for at least the latter part of the period during which this loss occurs. Whichever, if any, of these explanations is correct, it would appear to be difficult to account for the differential callosal connectivity of blobs and interblobs without the presence of some physiological differences between these two compartments.

As the segregation of connectivity seen in areas 17 and 18 is maintained in area 19, it is also suggested that segregation of physiological properties might exist in this area. Toyama et al. (Toyama et al., 1994) have recently compared the physiological properties of cells in area 19 to cells in PMLS and area 21a. They found that most cells in 21a had strong orientation tuning, but few were selective for direction of motion, and few cell were end-stopped, that is, they responded as well to very long bars as to bars that just filled the excitatory portion of the receptive field. Cells in PMLS, on the other hand, were selective for direction of stimulus motion, and were strongly end-stopped, but only weakly selective for orientation. Cells in Area 19 were either strongly endstoppped with moderate direction selectivity, or weakly end-stopped with strong orientation selectivity. Another study has shown that the two types of cells in area 19 with different end-stopping response properties are segregated into different columns . These results are consistent with the suggestion that area 19 acts as a segregator and different processing streams pass through it, while areas such as 21a and PMLS are more specialized, and receive

inputs from only a single processing stream. It is speculated that the different columns seen physiologically might correspond to the columns that provide output to the different extrastriate areas. Experiments combining electrophysical recordings with anatomical identification of the various processing streams would be necessary to answer these questions.

### Conclusions and Future Directions

It is concluded that segregated processing streams exist in the visual cortex of the cat, and that these are intimately associated with the CO blobs in areas 17 and 18, and with at least two different input- and output-defined columns in area 19. Still, many questions remain concerning the organization of parallel pathways through the visual cortex of the cat. At the level of the inputs to the visual cortex, the studies in Chapter 3 could not determine if Y-cells from the A-laminae terminate in the CO blobs, as do as those from the C-laminae, nor could they state with certainty the relationship of X-cell terminations to the CO blobs in layer 4a. These questions have important implications for the segregation of X- and Y-inputs, and for the homogeneity/heterogeneity of LGN Y-cells in the A and C laminae. These important questions can only be answered with techniques, such as intracellular filling, capable of resolving the trajectories of individual LGN axons.

In area 19, the relationships of the columns defined by inputs from areas 17 and 18, inputs from the LGN, and outputs to PMLS is completely unknown. Studies are required in which two of these pathways are labeled in the same experiment, such as combining large injections in the PMLS with small injections in area 19, hoping to hit either a PMLS-projecting column, or one of the intervening columns.

Secondly, area 19 also projects to areas other than PMLS (Symonds and Rosenquist, 1984a), and the organization of cells projecting to these areas needs to be examined and compared to those projecting to PMLS. As previously mentioned, unpublished data from this

laboratory suggests that cells projecting to area 21a are found in different columns than those projecting to PMLS, but the projections from area 19 to other areas, such as area 20, remain to be explored. For example, it is possible that more than two types of projection columns exist in area 19.

There is evidence that the connections of many different visual areas demonstrate hard patterning (Chapter 4). These connections may indicate the existence of segregated function, as well as connectivity, within multiple extrastriate areas in the cat. Such a continuation of multiple processing streams in extrastriate areas has been recently demonstrated in the monkey (Tootell and Born, 1992; DeYoe et al., 1994). Clearly, the present studies have only uncovered a small portion of the complexity that must exist in the visual cortex of the cat.

Some of the findings of this thesis are summarized in Figure 7.1. In this figure, the organization of parallel pathways in the cat, as elucidated in this study, are compared to an early view of the organization of parallel pathways in the visual system of the macaque monkey (Livingstone and Hubel, 1987b). This early, rather simplistic, version of parallel processing streams in primates has, with much further study, given way to an increasingly more complex view of the connections of cortical areas in primates, culminating in a diagram of connectivity that resembles a computer circuit board (Felleman and Van Essen, 1991). However, the earlier version was chosen for comparison here as an acknowledgement that studies of parallel pathways in the cat's visual cortex are still many years behind those in primates; with further study, similar "circuit diagrams" for the cat will undoubtedly become more complex as well.

Figure 7.1 A summary diagram showing the contributions of this study towards understanding the columnar organization of some of the inputs and outputs of cat visual cortical areas and a comparison with the columnar organization of some macaque monkey visual areas. Prior to this study, there was little evidence for a columnar organization of the parallel inputs and outputs of areas 17 and 18, and even less evidence for such an organization in area 19 (left panel; area 18 has been omitted from this diagram because of the similarity of its organization to that of area 17). Thus, the parallel inputs to area 17 were previously shown as becoming completely intermixed, and the parallel output pathways shown as being intermingled, in a homogenous layer 3. Likewise, a single pathway was previously shown connecting areas 17 and 19, and the cells in area 19 projecting to other areas were not thought to be segregated. This study has shown a columnar organization of the inputs and outputs of areas 17 and 19 (middle panel). The diagram for the monkey (right panel) was adapted from Livingstone and Hubel (1987b). Note the general similarity of the organization of the visual system in the two species. In both cat and monkey, multiple streams exist at all levels of the visual system, and these streams have different connections. Note that this figure is merely to show the general principles of parallel processing in these species, and not to indicate any homologies between visual areas in the two species. Question marks indicate projections which have not been established with certainty. The relationship of the input- and output-defined columns of area 19 is not yet known, and, thus, the projections of the different columns of area 19 are also marked with question marks.



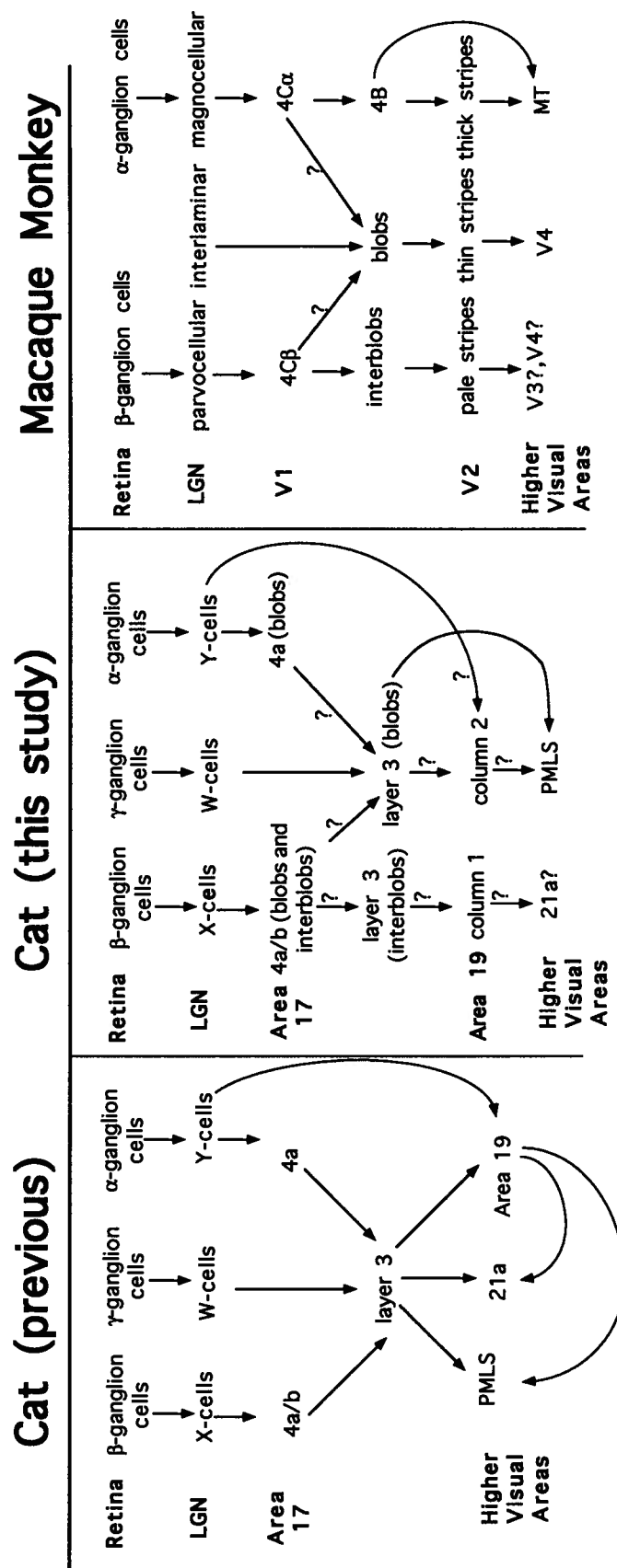


Figure 7.1

## REFERENCES

- Adams, J.C. (1981) Heavy metal intensification of DAB-based HRP reaction product. *J. Histochem. Cytochem.* 29:775.
- Albright, T.D. (1984) Direction and orientation selectivity of neurons in visual area MT of the macaque. *J. Neurophysiol.* 52:1106-1130.
- Anderson, P.A., J. Olavarria , and R.C. Van Sluyters (1988) The overall pattern of ocular dominance bands in cat visual cortex. *J. Neurosci.* 8:2183-2200.
- Beaulieu, C. , and M. Colonnier (1983) The number of neurons in the different laminae of the binocular and monocular regions of area 17 of the cat. *J. Comp. Neurol.* 217:337-344.
- Berardi, N., S. Bidti, A. Cattaneo, A. Fiorentini , and L. Maffei (1982) Correlation between the preferred orientation and spatial frequency of neurones in visual areas 17 and 18 of the cat. *J. Physiol.* 323:603-618.
- Berlucchi, G. , and G. Rizzolatti (1969) Binocularly driven neurons in visual cortex of split-chiasm cats. *Science* 159:308-310.
- Berman, N.E. , and B.R. Payne (1983) Alterations in connections of the corpus callosum following convergent and divergent strabismus. *Brain Res.* 274:201-212.
- Berson, D.M. (1985) Cat lateral suprasylvian cortex: Y-cell inputs and corticotectal projection. *J. Neurophysiol.* 53:544-556.
- Blasdel, G. , and J.S. Lund (1983) Termination of afferent axons in macaque striate cortex. *J. Neurosci.* 3:1389-1413.
- Bowling, D.B. , and C.R. Michael (1980) Projection patterns of single physiologically characterized optic tract fibres in cat. *Nature* 286:899-902.

- Bowling, D.B. , and C.R. Michael (1984) Terminal patterns of single, physiologically characterized optic tract fibres in the cat's lateral geniculate nucleus. *J. Neurosci.* 4:198-216.
- Boycott, B.B. , and H. Wässle (1974) The morphological types of ganglion cells of the domestic cat's retina. *J. Physiol.* 240:397-419.
- Boyd, J., and J. Matsubara (1992) Segregated processing streams in cat visual cortex? Relationship of patchy connectivity to an extrastriate area, cytochrome oxidase staining, and local connections. *Soc. Neurosci. Abstr.* 18:298.
- Boyd, J.D. , and J.A. Matsubara (1993) The C laminae of the cat lateral geniculate selectively target the cytochrome oxidase blobs. *Soc. Neurosci. Abstr.* 19:298.
- Boyd, J.D. , and J.A. Matsubara (1994) Modular organization of corticocortical inputs and outputs of area 19. *Soc. Neurosci. Abstr.* 20:1742.
- Brandt, H.M. , and A.V. Apkarian (1992) Biotin-Dextran - a sensitive anterograde tracer for neuroanatomic studies in rat and monkey. *J. of Neurosci. Meth.* 45:35-40.
- Bruce, L.L. , and B.E. Stein (1988) Transient projections from the lateral geniculate to the posteriomedial lateral suprasylvian visual cortex in kittens. *J. Comp. Neurol.* 278:287-302.
- Bullier, J. , and G. Henry H. (1979a) Laminar distribution of first-order neurons and afferent terminals in cat striate cortex. *J. Neurophysiol.* 47:1271-1281.
- Bullier, J. , and G.H. Henry (1979b) Neural path taken by afferent streams in striate cortex of the cat. *J. Neurophysiol.* 1264-1270.
- Bullier, J. , and G.H. Henry (1979c) Ordinal position of neurons in cat striate cortex. *J. Neurophysiol.* 42:1251-1263.

- Bullier, J. , and H. Kennedy (1983) Projection of the lateral geniculate nucleus onto cortical area V2 in the macaque monkey. *Exp. Brain Res.* 53:168-172.
- Bullier, J. , and H. Kennedy (1987) Axonal bifurcation in the visual system. *TINS* 10:205-210.
- Bullier, J., H. Kennedy , and W. Salinger (1984) Branching and laminar origin of projections between visual cortical areas in the cat. *J. Comp. Neurol.* 228:329-341.
- Callaway, E.M. , and L.C. Katz (1991) Effects of binocular deprivation on the development of clustered horizontal connections in cat striate cortex. *Proc. Natl. Acad. Sci., USA* 88:745-749.
- Camarda, R. , and G. Rizzolatti (1976) Visual receptive fields in the lateral suprasylvian area (Clare-Bishop) area of the cat. *Brain Res.* 101:427-443.
- Casagrande, V.A. (1994) A third parallel visual pathway to primate area V1. *TINS* 17:305-310.
- Casagrande, V.A. , and J.H. Kaas (1994) The afferent, intrinsic, and efferent connections of primary visual cortex in primates. In A. Peters and K.S. Rockland (eds.): *Cerebral Cortex*. New York: Plenum Press, pp. 201-259.
- Casagrande, V.A. , and T.T. Norton (1991) Lateral geniculate nucleus: a review of its physiology and function. In A.G. Leventhal (ed.): *The Neural Basis of Visual Function*. Houndmills, Basingstoke, Hampshire, and London, U.K.: The Macmillan Press, pp. 41-84.
- Chehil, S., K.M. Murphy , and C.C. Beaver (1992) Tangential distribution of cat-301 neurons in cat visual cortex. *Invest. Ophthalm. and Visual Sci.* (suppl) 1218.
- Clare, M.H. , and G.H. Bishop (1954) Responses from an association area secondarily activated from optic cortex. *J. Neurophysiol.* 17:271-277.
- Cleland, B.G., M.W. Dubin , and W.R. Levick (1971) Sustained and transient neurons in the cat's retina and lateral geniculate nucleus. *J. Physiol.* 217:473-496.

- Coleman, J. , and W.J. Clerici (1981) The organization of thalamic projections to visual cortex in opossum. *Brain, Behav., Evol.* 18:41-59.
- Condo, G.C. , and V.A. Casagrande (1990) Organization of cytochrome oxidase staining in the visual cortex of nocturnal primates (*Galago crassicaudatus* and *Galago senegalensis*): I. Adult patterns. *J. Comp. Neurol.* 293:632-645.
- Conley, M., D. Fitzpatrick , and I.T. Diamond (1984) The laminar organization of the lateral geniculate body and the striate cortex in the tree shrew (*Tupaia Glis*). *J. Neurosci.* 4:171-197.
- Cresho, H.S., L.M. Rasco, G.H. Rose , and G.J. Condo (1992) Blob-like pattern of cytochrome oxidase staining in ferret visual cortex. *Soc. Neurosci. Abstr.* 18:298.
- Crockett, D.P., S. Maslany, S.L. Harris , and M.D. Egger (1993) Enhanced cytochrome-oxidase staining of the cuneate nucleus in the rat reveals a modifiable somatotopic map. *Brain Res.* 612:41-55.
- Curcio, C.A. , and J.K. Harting (1978) Organization of pulvinar afferents to area 18 in the squirrel monkey: evidence for stripes. *Brain Res.* 143:155-161.
- Cusick, C.G., H.J.I. Gould , and J.H. Kaas (1984) Interhemispheric connections of visual cortex of owl monkeys (*Aotus trivigartus*). marmosets (*Callithrix jacchus*) and galagos (*Galago crassicaudatus*). *J. Comp. Neurol.* 230:311-336.
- Cusick, C.G. , and J.H. Kaas (1988) Surface view patterns of intrinsic and extrinsic cortical connections of area 17 in a prosimian primate. *Brain Res.* 458:383-388.
- Cusick, C.G. , and R.D. Lund (1981) The distribution of the callosal projection to the occipital visual cortex in rats and mice. *Brain Res.* 214:239-259.
- Cusick, C.G., M.G. MacAvoy , and J.H. Kaas (1985) Interhemispheric connections of cortical sensory areas in tree shrews. *J. Comp. Neurol.* 235:111-128.

- DeMonasterio, F.M. , and P. Gouras (1975) Functional properties of ganglion cells of the rhesus monkey retina. *J. Physiol.* 251:167-195.
- Desimone, R. , and S.J. Schein (1987) Visual properties of neurons in area V4 of the macaque: sensitivity to stimulus form. *J. Neurophysiol.* 57:835-868.
- DeYoe, E.A., D.J. Felleman, D.C. Van Essen , and E. McClendon (1994) Multiple processing streams in occipitotemporal visual cortex. *Nature* 371:151-154.
- DeYoe, E.A., S. Hockfield, H. Garren , and D.C. Van Essen (1990) Antibody labeling of functional subdivisions in visual cortex: Cat-301 immunoreactivity in striate and extrastriate cortex of the macaque monkey. *Visual Neurosci.* 5:67-81.
- DeYoe, E.A. , and D.C. Van Essen (1985) Segregation of efferent connections and receptive field properties in visual area V2 of the macaque. *Nature* 317:5861.
- DeYoe, E.A. , and D.C. Van Essen (1988) Concurrent processing streams in monkey visual cortex. *TINS* 11:219-226.
- Diamond, I.T., M. Conley, K. Itoh , and D. Fitzpatrick (1985) Laminar organization of geniculocortical projections in *Galago senegalensis* and *Aotus trivirgatus*. *J. Comp. Neurol.* 242:584-610.
- Diamond, I.T., D. Fitzpatrick , and D. Schmechel (1993) Calcium binding proteins distinguish large and small cells of the ventral posterior and lateral geniculate nuclei of the prosimian galago and the tree shrew (*Tupaia belangeri*). *Proc. Natl. Acad. Sci. USA.* 90:1425-1429.
- Diao, Y.-c., W.-g. Jia, N.V. Swindale , and M.S. Cynader (1990) Functional organization of the cortical 17/18 border region in the cat. *Exp. Brain Res.* 79:271-282.
- Donaldson, I.M.L. , and D. Whitteridge (1977) The nature of the boundary between cortical visual area II and III in the cat. *Proc. R. Soc. Lond. B.* 199:445-462.

- Dreher, B., A.G. Leventhal , and P.T. Hale (1980) Geniculate input to cat visual cortex: a comparison of area 19 with areas 17 and 18. *J. Neurophysiol.* 44:804-826.
- Dreher, B., A. Michalski, R.H. Ho, C.W. Lee , and W. Burke (1993) Processing of form and motion in area 21a of cat visual cortex. *Visual Neurosci.* 10:93-115.
- Dreher, B. , and A.J. Sefton (1979) Properties of neurons In cat's dorsal lateral geniculate nucleus: a comparison between medial interlaminar and laminated parts of the nucleus. *J. Comp. Neurol.* 183:47-64.
- Dyck, R.H. , and M.S. Cynader (1993a) Autoradiographic localization of serotonin receptor subtypes in cat visual cortex: transient regional, laminar, and columnar distributions during postnatal development. *J. Neurosci.* 13:4316-4338.
- Dyck, R.H. , and M.S. Cynader (1993b) An interdigitated columnar mosaic of cytochrome oxidase, zinc, and neurotransmitter-related molecules in cat and monkey visual cortex. *Proc. Nat'l Acad. Sci. USA* 90:9066-9069.
- Einstein, G. , and D. Fitzpatrick (1991) Distribution and Morphology of Area 17 Neurons That Project to the Cat's Extrastriate Cortex. *J Comp Neurol* 303:132-149.
- Elberger, A.J. (1993) Distribution of transitory corpus callosum axons projecting to developing cat visual cortex revealed by DiI. *J. Comp. Neurol.* 333:326-342.
- Engel, A.K., P. Konig, A.K. Kreiter , and W. Singer (1991) Interhemispheric Synchronization of Oscillatory Neuronal Responses in Cat Visual Cortex. *Science* 252:1177-1179.
- Enroth-Cugell, C. , and J.G. Robson (1966) The contrast sensitivity of retinal ganglion cells of the cat. *J. Physiol.* 187:517-552.
- Felleman, D.J. , and D.C. Van Essen (1991) Distributed hierarchical processing in the primate cerebral cortex. *Cerebral Cortex* 1:1-47.

- Ferrer, J.M.R., N. Kato , and D.J. Price (1992) Organization of association projections from area 17 to areas 18 and 19 and to suprasylvian areas in the cat's visual cortex. *J. Comp. Neurol.* 316:261-278.
- Ferrer, J.M.R., D.J. Price , and C. Blakemore (1988) The organization of corticocortical projections from area 17 to area 18 of the cat's visual cortex. *Proc. R. Soc. Lond. B* 223:77-98.
- Ferster, D. , and S. LeVay (1978) The axonal arborizations of lateral geniculate neurons in the striate cortex of the cat. *J. Comp. Neurol.* 182:923-944.
- Fitzpatrick, D., R.C. Carey , and I.T. Diamond (1980) The projection of the superior colliculus upon the lateral geniculate body in *Tupaia glis* and *Galago senegalensis*. *Brain Res.* 194:494-499.
- Fitzpatrick, D., K. Itoh , and I.T. Diamond (1983) The laminar organization of the lateral geniculate body and the striate cortex in the squirrel monkey (*Saimiri sciureus*). *J. Neurosci.* 3:673-702.
- Fitzpatrick, D. , and D. Raczkowski (1990) Innervation patterns of single physiologically identified geniculocortical axons in the striate cortex of the tree shrew. *Proc. Nat'l Acad. Sci. USA* 87:449-453.
- Florence, S.I., M. Comley , and V.A. Casagrande (1986) Ocular dominance projections and retinal projections in new world spider monkeys (*Ateles ater*). *J. Comp. Neurol.* 243:234-148.
- Freund, T.F., K.A.C. Martin, P. Somogyi , and D. Whitteridge (1985) Innervation of cat visual areas 17 and 18 by physiologically identified X- and Y-type thalamic afferents. II. Identification of postsynaptic targets by GABA immunocytochemistry and Golgi Impregnation. *J. Comp. Neurol.* 242:275-291.



- Friedlander, M.J., C.-S. Lin, L.R. Stanford , and S.M. Sherman (1981) Morphology of functionally identified neurons in lateral geniculate nucleus of the cat. *J. Neurophysiol.* 46:80-129.
- Friedlander, M.J., C.S. Lin , and M. Sherman (1979) Structure of physiologically identified X and Y cells in the cat's lateral geniculate nucleus. *Science* 204:1114-1116.
- Friedlander, M.J. , and K.A.C. Martin (1989) Development of Y-axon innervation of cortical area 18 in the cat. *J. Physiol.* 416:183-213.
- Garey, L.J. (1971) A light and electron microscopic study of the visual cortex of the cat and monkey. *Proc. R. Soc. Lond. B* 179:21-40.
- Gilbert, C.D. (1977) Laminar differences in receptive field properties of cells in cat primary visual cortex. *J. Physiol.* 268:391-421.
- Gilbert, C.D. , and J.P. Kelly (1975) The projection of cells in different layers of the cats visual cortex. *J. Comp. Neurol.* 163:81-106.
- Gilbert, C.D. , and T.N. Wiesel (1981) Projection bands in visual cortex. *Soc. Neurosci. Abstr.* 7:356.
- Gilbert, C.D. , and T.N. Wiesel (1983) Clustered intrinsic connections in cat visual cortex. *J. Neurosci.* 3:1116-1133.
- Gilbert, C.D. , and T.N. Wiesel (1989) Columnar specificity of intrinsic horizontal and corticocortical connections in cat visual cortex. *J. Neurosci.* 9:2432-2442.
- Girard, P., P.A. Salin , and J. Bullier (1992) Response selectivity of neurons in area MT of the macaque monkey during reversible inactivation of area V1. *J. Neurophysiol.* 67:1437-1446.

- Gizzi, M.S., E. Katz, R.A. Schmuer , and R.A. Movshon (1990) Selectivity for orientation and direction of motion of single neurons in cat striate and extrastriate visual cortex. *J. Neurosci.* 63:1529-1543.
- Gouras, P. (1968) Identification of cone mechanisms in monkey ganglion cells. *J. Physiol.* 199:533-547.
- Gouras, P. (1969) Antidromic responses of orthodromically identified ganglion cells in monkey retina. *J. Physiol.* 204:407-419.
- Grant, S. , and S. Shipp (1991) Visuotopic organization of the lateral suprasylvian area and of an adjacent area of the ectosylvian gyrus of cat cortex: a physiological and connectional study. *Visual Neurosci.* 6:315-338.
- Graybiel, A.M. , and D.M. Berson (1981) Families of related cortical areas in the extrastriate visual system: summary of an hypothesis. In C.N. Woolsey (ed.): *Multiple Visual Areas*. Clifton, N.J.: Humana Press, Inc., pp. 103-120.
- Guillemot, J.-P., L. Richer, M. Ptito , and F. Lepore (1993) Disparity coding in the cat: a comparison between areas 17-18 and area 19. *Prog. Brain Res.* 95:179-187.
- Guillery, R.W. (1970) The laminar distribution of retinal fibers in the dorsal lateral geniculate nucleus of the cat: a new interpretation. *J. Comp. Neurol.* 138:339-368.
- Guillery, R.W., E.E. Geisert, E.H. Polley , and C.A. Mason (1980) An analysis of the retinal afferents to the cat's medial interlaminar nucleus and to its rostral thalamic extension, the "geniculate wing". *J. Comp. Neurol.* 194:117-142.
- Guillery, R.W. , and M.D. Oberdorfer (1977) A study of fine and coarse retino-fugal axons terminating in the geniculate c laminae and in the medial interlaminar nucleus of the mink. *J. Comp. Neur.* 176:515-526.
- Harting, J.H., B.V. Updyke , and D.P. Van Lieshout (1992) Corticotectal projections in the cat: anterograde transport studies of twenty-five cortical areas. *J. Comp. Neurol.* 234:379-414.

- Harting, J.K., M.F. Huerta, T. Hashikawa , and D.P. van Lieshout (1991) Projection of the mammalian superior colliculus upon the dorsal lateral geniculate nucleus: organization of tectogeniculate pathways in nineteen species. *J. Comp. Neurol.* 304:275-306.
- Harvey, A.R. (1980) The afferent connexions and laminar distribution of cells in area 18 of the cat. *J. Physiol.* 302:483-505.
- Hata, Y. , and M.P. Stryker (1994) Control of thalamocortical afferent rearrangement by postsynaptic activity in developing visual cortex. *Science* 265:1732-1735.
- Hendrickson, A.E., J.R. Wilson , and M.P. Ogren (1978) Neuroanatomical organization of pathways between the dorsal lateral geniculate nucleus and visual cortex in old world and new world primates. *J. Comp. Neurol.* 182:123-136.
- Hendry, S.H.C., E.G. Jones, S. Hockfield , and R.D.G. McKay (1988) Neuronal populations stained with the monoclonal antibody cat-301 in the mammalian cerebral cortex and thalamus. *J. Neurosci.* 8:518-542.
- Hendry, S.H.C. , and T. Yoshioka (1994) A neurochemically distinct third channel in the macaque dorsal lateral geniculate nucleus. *Science* 264:575-577.
- Henry, G.H. (1988) Afferent Inputs, Receptive Field Properties and Morphological Cell Types in Different Laminae of the Striate Cortex. In A.G. Leventhal (ed.): *The Neural Basis of Visual Function*. Salt Lake City, Utah: MacMillan Press, pp. 223-245.
- Hickey, T.L. , and R.W. Guillery (1974) An autoradiographic study of retinogeniculate pathways in the cat and the fox. *J. Comp. Neurol.* 1156:239-254.
- Hitchcock, P.F. , and T.L. Hickey (1983) Morphology of c-laminae neurons in the dorsal lateral geniculate nucleus of the cat: a golgi impregnation study. *The Journal of Comparative Neurology* 220:137-146.

*References*

- Hockfield, S., R.D. McKay, S.H.C. Hendry, and E.G. Jones (1983) A surface antigen that identifies ocular dominance columns in the visual cortex and laminar features of the lateral geniculate nucleus. *Cold Spring Harbor Symp. Quant. Biol.* 48:877-889.
- Hoffmann, K.-P., J. Stone, and S.M. Sherman (1972) Relay of receptive-field properties in dorsal lateral geniculate nucleus of the cat. *J. Neurophysiol.* 35:518-531.
- Horn, A.K.E., and K.-P. Hoffman (1987) Combined GABA-immunocytochemistry and TMB-HRP histochemistry of pretectal nuclei projecting to the inferior olive in rats, cats and monkeys. *Brain Res.* 409:133-138.
- Horton, J.C. (1984) Cytochrome oxidase patches: a new cytoarchitectonic feature of monkey visual cortex. *Phil. Trans. R. Soc. Lond. B* 304:199-253.
- Horton, J.C., and D.H. Hubel (1981) Regular patchy distribution of cytochrome oxidase staining in primary visual cortex of macaque monkey. *Nature* 292:762-764.
- Hubel, D.H. (1988) *Eye, brain, and vision*. New York: W.H. Freeman and Company.
- Hubel, D.H., and M.S. Livingstone (1987) Segregation of form, color, and stereopsis in primate area 18. *Journal Neurosci.* 7:3378-3415.
- Hubel, D.H., and T.N. Wiesel (1962) Receptive fields, binocular interaction and functional architecture in the cat's visual cortex. *J. Physiol.* 160:106-154.
- Hubel, D.H., and T.N. Wiesel (1965) Receptive fields and functional architecture in two nonstriate visual areas (18 and 19) of the cat. *J. Neurophysiol.* 28:229-289.
- Hubel, D.H., and T.N. Wiesel (1967) Cortical and callosal connections concerned with the vertical meridian of visual fields in the cat. *J. Neurophysiol.* 30:1561-1573.
- Hubel, D.H., and T.N. Wiesel (1969a) Anatomical demonstration of columns in the monkey striate cortex. *Nature* 221:747-750.

- Hubel, D.H. , and T.N. Wiesel (1969b) Visual area of the lateral suprasylvian gyrus (Clare-Bishop area) of the cat. *J. Physiol.* 202:251-260.
- Hübener, M. , and J. Bolz (1992) Relationships between dendritic morphology and cytochrome oxidase compartments in monkey striate cortex. *J. Comp. Neurol.* 324:67-80.
- Humphery, A.L. , and A.E. Hendrickson (1983) Background and stimulus-induced patterns of high metabolic activity in the visual cortex (area 17) of the squirrel and macaque monkey. *J. Neurosci.* 3:345-358.
- Humphery, A.L., M. Sur, D.J. Uhlrich , and S.M. Sherman (1985a) Projection patterns of individual X- and Y-cell axons from the lateral geniculate nucleus to cortical area 17 in the cat. *J. Comp. Neurol* 233:159-189.
- Humphery, A.L., M. Sur, D.J. Uhlrich , and S.M. Sherman (1985b) Termination patterns of individual X- and Y-cell axons in the visual cortex of the cat: projections to area 18, to the 17/18 border region, and to both areas 17 and 18. *J. Comp. Neurol* 233:190-212.
- Illing, R.-B. , and H. Wässle (1979) Visualization of the HRP reaction product using the polarization microscope. *Neurosci. Lett.* 13:7-11.
- Illing, R.-B. , and H. Wässle (1981) The retinal projection to the thalamus in the cat: a quantitative investigation and a comparison with the retinotectal pathway. *J. Comp. Neurol.* 202:265-285.
- Innocenti, G.M. (1980) The primary visual pathway through the corpus callosum: morphological and functional aspects in the cat. *Arch. Ital. Biol.* 118:124-188.
- Innocenti, G.M. (1981) The development of interhemispheric connections. *TINS* 4:142-144.
- Innocenti, G.M. (1986) General organization of callosal connections in the cerebral cortex. In A. Peters and E.G. Jones (eds.): *Cerebral cortex*. Plenum Press, pp. 291-353.

- Innocenti, G.M. , and S. Clarke (1984) The organization of immature callosal connections. *J. Comp. Neurol.* 230:287-309.
- Innocenti, G.M. , and L. Fiore (1976) Morphological correlates of visual field transformation in the corpus calosum. *Neurosci. Lett.* 2:245-252.
- Irvin, G.E., T.T. Norton, M.A. Sesma , and V.A. Casagrande (1986) W-like response properties of interlaminar zone cells in the lateral geniculate nucleus of a primate (*Galago crassicaudatus* ). *Brain Res.* 362:254-270.
- Itoh, K., A. Konishi, S. Nomura, N. Mizuno, Y. Nakamura , and T. Sugimoto (1979) Application of coupled oxidation reaction to electron microscopic demonstration of horseradish peroxidase: cobalt-glucose oxidase method. *Brain Res.* 175:341-346.
- Jain, N., T.M. Preuss , and J.H. Kaas (1994) Subdivisions of the visual system labeled with the cat-301 antibody in tree shrews. *Visual Neurosci.* 11:731-741.
- Kaas, J.H. (1989) The evolution of complex sensory systems in mammals. *J. Exp. Biol.* 146:165-176.
- Kageyama, G.H. , and M. Wing-Riley (1986) Laminar and cellular localization of cytochrome oxidase in the cat striate cortex. *J. Comp. Neurol.* 245:137-159.
- Kageyama, G.H. , and M. Wong-Riley (1985) An analysis of the cellular localization of cytochrome oxidase in the lateral geniculate nucleus of the cat. *J. Comp. Neurol.* 242:338-357.
- Kageyama, G.H. , and M. Wong-Riley (1986) The localization of cytochrome oxidase in the LGN and striate cortex of postnatal kittens. *J. Comp. Neurol.* 243:182-194.
- Kalia, M. , and D. Whitteridge (1973) The visual areas in the splenial visual sulcus of the cat. *J. Physiol.* 232:275-283.

- Kaplan, E. (1991) The receptive field structure of retinal ganglion cells in cat and monkey. In A.G. Leventhal (ed.): *The Neural Basis of Visual Function*. London: Macmillan, pp. 10-40.
- Kennedy, H. , and C. Dehay (1988) Functional implications of the anatomical organization of the callosal projections of visual areas V1 and V2 in the macaque monkey. *Behav. Brain Res.* 29:225-236.
- Kennedy, H., C. Dehay , and J. Bullier (1986) Organization of the callosal connections of visual areas V1 and V2 in the macaque monkey. *J. Comp. Neurol.* 247:398-415.
- Kratz, K.E., S.V. Web , and S.M. Sherman (1978) Studies of the cat's medial interlaminar nucleus: a subdivision of the dorsal lateral geniculate nucleus. *J. Comp. Neurol.* 181:601-614.
- Krubitzer, L.A. , and J.H. Kaas (1989) Cortical integration of parallel pathways in the visual system of primates. *Brain Res.* 478:161-165.
- Krubitzer, L.A. , and J.H. Kaas (1993) The dorsomedial visual area of owl monkeys: connections, myeloarchitecture, and homologies in other primates. *J. Comp. Neurol.* 334:497-528.
- Kuffler, S.W. (1953) Discharge patterns and functional organization of mammalian retina. *J. Neurophysiol.* 16:37-68.
- Lachica, E.A., P.D. Beck , and V.A. Casagrande (1992) Parallel pathways in Macaque Monkey striate cortex: anatomically defined columns in layer III. *Proc. Natl. Acad. Sci. USA* 89:3566-3570.
- Lachica, E.A., P.D. Beck , and V.A. Casagrande (1993) Intrinsic connections of Layer-III of striate cortex in squirrel monkey and bush baby - correlations with patterns of cytochrome oxidase. *J. of Comp. Neurol.* 329:163-187.

- Lachica, E.A. , and V.A. Casagrande (1988) Development of primate retinogeniculate axon arbors. *Visual Neurosci.* 103-123.
- Lachica, E.A. , and V.A. Casagrande (1992) Direct W-Like Geniculate Projections to the Cytochrome Oxidase (CO) Blobs in Primate Visual Cortex - Axon Morphology. *J. Comp. Neurol.* 319:141-158.
- Law, M.I., K.R. Zahs , and M.P. Stryker (1988) Organization of primary visual cortex (Area 17) in the ferret. *J. Comp. Neurol.* 278:157-180.
- Lee, C., J.G. Malpeli, H.D. Schwark , and T.G. Weyand (1984) Cat medial interlaminar nucleus: retinotopy, relation to tapetum, and implications for scotopic vision. *J. Neurophysiol.* 52:848-869.
- Leporé, F. , and J.-P. Guillemot (1982) Visual receptive field properties of cells innervated through the corpus callosum in the cat. *Exp. Brain Res.* 46:413-424.
- Leporé, F., M. Ptito , and M. Lassonde (1986) Stereoperception on cats following section of the corpus callosum and/or the optic tract. *Exp. Brain Res.* 61:258-264.
- LeVay, S. (1988) The patchy intrinsic projections of visual cortex. *Prog. Brain Res.* 75:147-161.
- LeVay, S. , and C.D. Gilbert (1976) Laminar patterns of geniculocortical projection in the cat. *Brain Res.* 113:1-19.
- LeVay, S. , and S.B. Nelson (1991) Columnar Organization of the Visual Cortex. In A.G. Leventhal (ed.): *The Neural Basis of Visual Function*. Houndmills, Basingstoke, Hampshire, and London, U.K.: The Macmillan Press, pp. 266-315.
- Leventhal, A.G. (1979) Evidence that the different classes of relay cells of the cat's lateral geniculate nucleus terminate in different layers of the striate cortex. *Exp. Brain Res.* 37:349-372.



- Leventhal, A.G. (1982) Morphology and distribution of retinal ganglion cells projecting to different layers of the dorsal lateral geniculate nucleus in normal and siamese cats. *J. Neurosci.* 2:1024-1042.
- Leventhal, A.G., R.W. Rodieck , and B. Dreher (1981) Retinal ganglion cell classes in the old world monkey: morphology and central projections. *Science* 213:1139-1142.
- Leventhal, A.G., R.W. Rodieck , and B. Dreher (1985) Central projections of cat retinal ganglion cells. *J. Comp. Neurol.* 237:216-226.
- Liu, Y., Q. Gu , and M.S. Cynader (1993) An improved staining technique for cytochrome C oxidase. *J. Neurosci. Meth.* 49:181-184.
- Livingstone, M.S. , and D.H. Hubel (1983) Specificity of cortico-cortical connections in monkey visual sytsem. *Nature* 304:531-534.
- Livingstone, M.S. , and D.H. Hubel (1984) Anatomy and physiology of a color system in the primate visual cortex. *J. Neurosci.* 4:309-356.
- Livingstone, M.S. , and D.H. Hubel (1987a) Connections between layer 4B of area 17 and the thick cytochrome oxidase stripes of area 18 in the squirrel monkey. *J. Neurosci.* 7:3371-3377.
- Livingstone, M.S. , and D.H. Hubel (1987b) Psychophysical evidence for separate channels fro the perception of form, color, movement, and depth. *J. Neurosci.* 7:3416-3468.
- Livingstone, M.S. , and D.H. Hubel (1987c) Thalamic inputs to cytochrome oxidase rich regions in monkey visual cortex. *Proc. Natl. Acad. Sci. USA* 79:6098-6101.
- LLewellyn-Smith, I.J., J.B. Minson, A.P. Wright , and A.J. Hodgson (1990) Cholera toxin B-gold, a retrograde tracer that can be used in light and electron microscopic immunocytochemical studies. *J. Comp. Neurol.* 294:179-191.

## References

- Lorente de N6, R. (1943) Cerebral cortex: architecture, intracortical connections, motor projections. In J. Fulton (ed.): Physiology of the Nervous System. Oxford: Oxford University Press, pp. 274-301.
- Lund, J.S., G.H. Henry, C.L. Macqueen , and A.R. Harvey (1979) Anatomical organization of the primary visual cortex (area17) of the cat. A comparison with area 17 of the Macaque monkey. *J. Comp. Neurol.* 184:599-618.
- Lund, J.S., R.D. Lund, A.E. Hendrickson, A.H. Bunt , and A.F. Fuchs (1975) The origin of efferent pathways from the primary visual cortex, area 17, of the macaque monkey as shown by retrograde transport of horseradish peroxidase. *J. Comp. Neurol.* 164:287-304.
- Marshall, W.H., S.A. Talbot , and H.W. Ades (1943) Cortical response of the anesthetized cat to gross photic and electrical afferent stimulation. *J. Neurophysiol.* 6:1-15.
- Martin, K.A.C. (1988) From enzymes to visual perception: a bridge too far? *TINS* 11:380-387.
- Mason, R. (1978) Functional organization in the cat's pulvinar complex. *Exp. Brain Res.* 31:51-66.
- Maunsell, H.R. , and D.C. Van Essen (1983) The connections of the middle temporal visual area (MT) and their relationship to a cortical hierarchy. *J. Neurosci.* 3:2563-2586.
- Mesulam, M.M. (1978) Tetramethylbenzidine for horseradish peroxidase neurochemistry. *J. Histochem. Cytochem.* 26:106-117.
- Murphy, K.M., R.C. Van Sluyters , and D.G. Jones (1990) Cytochrome oxidase activity in cat visual cortex: is it periodic? *Soc. Neurosci. Abstr.* 16:292.
- Murphy, K.M., R.C. Van Sluyters , and D.G. Jones (1991) The organization of cytochrome oxidase blobs in the cat visual cortex. *Soc. Neurosci. Abstr.* 17:1088.
- O'Leary, J.L. (1941) Structure of the area striata of the cat. *J. Comp. Neurol.* 75:131-164.

## References

- Olavarria, J. , and V.M. Montero (1983) The pattern of visual callosal connections in the cat as revealed in tangential sections of the unfolded cortex. Soc. Neurosci. Abstr. 9:155.
- Olavarria, J. , and R.C. Van Sluyters (1985) Unfolding and flattening the cortex of gyrencephalic brains. J. Neurosci. Meth. 15:91-102.
- Olavarria, J.F. , and J.W. Lewis (1992) The distribution of callosal cells correlates with dense cytochrome oxidase stripes in V2 of the macaque monkey. Soc. Neurosci. Abstr. 18:293
- Otsuka, R. , and R. Hassler (1962) Über aufbau und gliederung der corticalen sehsphäre bei der katze. Archiv Psych. Z. Neurol. 203:212-234.
- Palmer, L.A., A.C. Rosenquist , and R.J. Tusa (1978) The retinotopic organization of lateral suprasylvian visual areas in the cat. J. Comp. Neurol. 177:237-256.
- Paolini, M., M.I. Sereno, R.J.A. Dobbins , and J.M. Allman (1994) Organization of extrastriate cortex in the primitive primates, *Cheirogaleus* and *Lemur*. Soc. Neurosci. Abstr. 20:427.
- Payne, B. (1990a) Representation of the ipsilateral visual field in the transition zone between areas 17 and 18 of the cat's cerebral cortex. Visual Neurosci. 4:445-474.
- Payne, B.R. (1990b) Function of the corpus callosum in the representation of the visual field in cat visual cortex. Visual Neurosci. 5:205-211.
- Payne, B.R. (1993) Evidence for visual cortical area homologs in cat and macaque monkey. Cerebral Cortex 3:1-25.
- Payne, B.R. , and D.F. Siwek (1991) Visual-field map in the callosal recipient zone at the border between areas 17 and 18 in the cat. Visual Neurosci. 7:221-236.
- Price, D.J. (1984) Patterns of cytochrome oxidase activity in areas 17, 18 and 19 of the visual cortex of cats and kittens. Exp. Brain Res. 159:1-9.

- Prusky, G.T., C. Shaw , and M.S. Cynader (1987) Nicotine receptors are located on lateral geniculate nucleus terminals in cat visual cortex. *Brain Res.* 412:131-138.
- Raczkowski, D., J.E. Hamos , and S.M. Sherman (1988) Synaptic circuitry of physiologically identified W-cells in the cat's dorsal lateral geniculate nucleus. *J. Neurosci.* 8:31-48.
- Raczkowski, D. , and A.C. Rosenquist (1983) Connections of the multiple visual cortical areas with the lateral posterior-pulvinar complex and adjacent thalamic nuclei in the cat. *J. Neurosci.* 3:1912-1942.
- Rauschecker, J.P., M.W. von Grünau , and C. Poulin (1987) Thalamo-cortical connections and their correlation with receptive field properties in the cat's lateral syprasylian cortex. *Exp. Brain Res.* 67:100-112.
- Ribak, C.E. , and A. Peters (1975) An autoradiographic study of the projections from the lateral geniculate body of the art. *Brain Res.* 93:341-368.
- Rodieck, R.W. (1992) The origin of parallel visual pathways in primates. *Invest. Ophthal. and Visual Sci.* (suppl) 900.
- Rodieck, R.W., K.F. Binmoeller , and J. Dineen (1985) Parasol and midget ganglion cells of the human retina. *J. Comp. Neurol.* 233:115-132.
- Rodieck, R.W. , and R.K. Brening (1983) Retinal ganglion cells: properties, types, genera, pathways and trans-species comparisons. *Brain Behav. Evol.* 23:121-164.
- Rosenquist, A.C. (1985) Connections of visual areas in the cat. In E.G. Jones and A. Peters (eds.): *Cerebral Cortex*. New York: Plenum Press, pp. 81-117.
- Rowe, M.H. , and B. Drehher (1982) Retinal W-cell projections to the medial interlaminar nucleus in the cat: implications for ganglion cell classifications. *J. Comp. Neurol.* 204:117-133.

- Saito, H.-A., K. Tanaka, Y. Fukada , and H. Oyamada (1988) Analysis of discontinuity in visual contours in area 19 of the cat. *J. Neurosci.* 8:1131-1143.
- Salin, P.A. (1989) Convergence and divergence in the afferent projections to cat area 17. *J. Comp. Neurol.* 283:486-512.
- Sanderson, K.J. (1971a) The projection of the visual field to the lateral geniculate and medial interlaminar nuclei in the cat. *J. Comp. Neurol.* 143:101-118.
- Sanderson, K.J. (1971b) Visual field projection columns and magnification factors in the lateral geniculate nucleus of the cat. *Exp. Brain Res.* 13:159-177.
- Sanides, D. , and K. Albus (1980) The distribution of interhemispheric projections in area 18 of the cat: coincidence with discontinuities of the representation of the visual field in the second visual area (V2). *Exp. Brain Res.* 38:237-240.
- Schein, S.J. , and R. Desimone (1990) Spectral properties of V4 neurons in the macaque. *J. Neurosci.* 10:3369-3389.
- Segraves, M.A. , and G.M. Innocenti (1985) Comparison of the distributions of ipsilaterally and contralaterally projecting corticocortical neurons in cat visual cortex using two fluorescent tracers. *J. Neurosci.* 5:2107-2118.
- Segraves, M.A. , and A.C. Rosenquist (1982) The distribution of the cells of origin of callosal projections in cat visual cortex. *Neurosci.* 2:1079-1089.
- Sereno, M.I. , and J.M. Allman (1991) Cortical visual areas in mammals. In A.G. Leventhal (ed.): *The Neural Basis of Visual Function*. London: Macmillan, pp. 160-172.
- Shapley, R. , and V.H. Perry (1986) Cat and monkey retinal ganglion cells and their visual functional roles. *TINS* 9:229-225.
- Shatz, C.J., S. Lindstrom , and T.N. Wiesel (1977) The distribution of afferents representing the right and left eyes in the cat's visual cortex. *Brain Res.* 131:103-116.

- Sherk, H. (1986) Location and connections of visual cortical areas in the cat's suprasylvian sulcus. *J. Comp. Neurol.* 247:1-31.
- Sherk, H. (1988) Retinotopic order and functional organization in a region of suprasylvian visual cortex: the Clare-Bishop area. *Prog. Brain Res.* 75:237-244.
- Sherk, H. , and K.A. Mulligan (1993) A reassessment of the lower visual field map in striate-recipient lateral suprasylvian cortex. *Visual Neurosci.* 10:131-158.
- Sherman, S.M. (1985) Functional organization of the W-, X-, and Y-cell pathway in the cat: a review and hypothesis. *Prog. Psychol. Physiol. Psychol.* 2:233-314.
- Sherman, S.M. , and P.D. Spear (1982) Organization of visual pathways in normal and visually deprived cats. *Physiol. Rev.* 62:739-855.
- Shipp, S. , and S. Grant (1991) Organization of reciprocal connections between area 17 and the lateral suprasylvian area of cat visual cortex. *Visual Neurosci.* 6:339-355.
- Shipp, S. , and S. Zeki (1989) The organization of connections between areas V5 and V1 in macaque monkey visual cortex. *Europ. J. Neurosci.* 1:310-332.
- Silverman, N.S. , and R.B.H. Tootell (1987) Modified technique for cytochrome oxidase histochemistry: increased staining intensity and compatibility with 2-deoxyglucose autoradiography. *J. Neurosci. Meth.* 19:1-10.
- Spear, P.D. (1991) Functions of extrastriate visual cortex in non-primate species. In A.G. Leventhal (ed.): *The Neural Basis of Visual Function*. Houndmills, Basingstoke, Hampshire, and London, U.K.: The Macmillan Press, pp. 339-370.
- Spear, P.D. , and T.P. Baumann (1975) Receptive-field characteristics of single neurons in lateral suprasylvian visual area of the cat. *J. Neurophysiol.* 38:1403-1420.

- Spear, P.D., M.A. McCall , and N. Tumosa (1989) W- and Y-cells in the C layers of the cat's lateral geniculate nucleus: normal properties and effects of monocular deprivation. *J. Neurophysiol.* 61:58-73.
- Stanford, L.R., J. Friedlander , and S.M. Sherman (1983) Morphological and physiological properties of geniculate W-cells of the cat: a comparison with X- and Y-cells. *Journal of Neurophysiology* 50:582-608.
- Stitchel, C.C., W. Singer, C.W. Heizmann , and A.W. Norman (1987) Immunohistochemical localization of calcium-binding proteins, parvalbumin and calbindin-D 28k, in the adult and developing visual cortex of cats: a light and electron microscopic study. *J. Comp. Neurol.* 262:563-577.
- Stone, J. (1983) *Parallel Processing in the Visual System: The Classification of Retinal Ganglion Cells and its Impact on the Neurobiology of Vision*. New York: Plenum Press.
- Stone, J.S., B. Dreher , and A. Leventhal (1979) Hierarchical and parallel mechanisms in the organization of visual cortex. *Brain Res. Rev.* 1:345-395.
- Sur, M., M. Esguerra, P.E. Garraghty, M.F. Kritzer , and S.M. Sherman (1987) Morphology of physiologically identified retinogeniculate X- and Y-axons in the cat. *J. Neurophysiol.* 58:1-32.
- Sur, M., D.O. Frost , and S. Hockfield (1988) Expression of a surface-associated antigen on Y-cells in the cat lateral geniculate nucleus is regulated by visual experience. *J. Neurosci.* 8:874-882.
- Symonds, L.L. , and A.C. Rosenquist (1984a) Corticocortical connections among visual areas in the cat. *J. Comp. Neurol.* 229:1-38.
- Symonds, L.L. , and A.C. Rosenquist (1984b) Laminar origins of visual corticocortical connections in the cat. *J. Comp. Neurol.* 229:39-47.

- Takeuchi, Y., G.V. Allen , and D.A. Hopkins (1985) Transnuclear transport and axon collateral projections of the mamillary nuclei in the rat. *Brain Res. Bull.* 14:453-468.
- Tieman, S.B. , and N. Tumosa (1983) [ $^{14}\text{C}$ ]2-deoxyglucose demonstration of the organization of ocular dominance in areas 17 and 18 of the normal cat. *Brain Res.* 267:35-46.
- Tong, L. (1991) Development of the projections from the dorsal lateral geniculate nucleus to the lateral suprasylvian visual area of cortex in the cat. *J. Comp. Neurol.* 314:526-533.
- Tong, L., R.E. Kalil , and P.D. Spear (1982) Thalamic projections to visual areas of the middle suprasylvian sulcus in the cat. *J. Comp. Neurol.* 212:103-117.
- Tootell, R.B., M.S. Silverman , and R.E. De Valois (1981) Spatial frequency columns in primary visual cortex. *Science* 813-816.
- Tootell, R.B., M.S. Silverman, R.L. De Valois , and G.H. Jacobs (1983) Functional organization of the second cortical visual areas in primates. *Science* 220:737-739.
- Tootell, R.B.H. , and R.T. Born (1992) Columnar systems related to blobs vs. interblobs in ten cortical areas. *Invest. Ophthalm. and Visual Sci. (suppl)* 33:1021.
- Tootell, R.B.H., M.S. Silverman, S.L. Hamilton, E. Switkes , and R.L. De Valois (1988) Functional anatomy of macaque striate cortex. V. Spatial frequency. *Journal Neurosci.* 8:1610-1624.
- Toyama, K., K. Mizobe, E. Akase , and T. Kaihara (1994) Neuronal responsiveness in areas 19 and 21a, and the posteromedial lateral suprasylvian cortex of the cat. *Exp. Brain Res.* 99:289-301.
- Tretter, F., M. Cynader , and W. Singer (1975) Cat parastriate cortex: a primary or secondary visual area? *J. Neurophysiol.* 38:1099-1113.
- Ts'o, D.Y. , and C.D. Gilbert (1988) The organization of chromatic and spatial interactions in the primate striate cortex. *J. Neurosci.* 8:1712-1727.



- Tusa, R.J., L.A. Palmer , and A.C. Rosenquist (1978) The retinotopic organization of area 17 (striate cortex) in the cat. *J. Comp. Neurol.* 177:213-236.
- Tusa, R.J., L.J. Palmer , and A.C. Rosenquist (1981) Multiple cortical visual areas: visual field topography in the cat. In C.N. Woolsey (ed.): *Multiple Visual Areas*. Clifton, N.J.: Humana Press, Inc., pp. 1-32.
- Tusa, R.J., A.C. Rosenquist , and L.A. Palmer (1979) Retinotopic organization of areas 18 and 19 in the cat. *J. Comp. Neurol.* 185:657-678.
- Updyke, B.V. (1981) Multiple representations of the visual field: corticothalamic and thalamic organization in the cat. In C.N. Woolsey (ed.): *Multiple Visual Areas*. Clifton, N.J.: Humana Press, Inc., pp. 83-101.
- Updyke, B.V. (1986) Retinotopic organization within the cat's posterior suprasylvian sulcus and gyrus. *J. Comp. Neurol.* 246:265-280.
- Van Essen, D.C., C.H. Anderson , and D.J. Felleman (1992) Information processing in the primate visual system: an integrated systems perspective. *Science* 255:419-423.
- Van Essen, D.C. , and J.L. Gallant (1994) Neural mechanisms of form and motion processing in the primate visual cortex. *Neuron* 13:1-10.
- Van Essen, D.C. , and J.H.R. Maunsell (1983) Hierarchical organization and functional streams in visual cortex. *TINS.* 6:370-376.
- Veenman, C.L., A. Reiner , and M.G. Honig (1992) Biotinylated dextran amine as an anterograde tracer for single-labeling and double-labeling studies. *J. Neurosci. Meth.* 41:239-254.
- Voigt, T., S. LeVay , and M.A. Stamnes (1988) Morphological and Immunocytochemical observations on the visual callosal projections in the cat. *J. Comp. Neurol.* 272:450-460.

- von Grünau, M.W., T.J. Zumbroich , and C. Poulin (1987) Visual receptive field properties in the posterior suprasylvian cortex of the cat: a comparison between the areas PMLS and PLLS. *Vision Res.* 27:343-356.
- Weber, J.T., M.F. Heurta, J.H. Kaas , and J.K. Harting (1983) The projections of the lateral geniculate nucleus of the squirrel monkey: studies of the interlaminar zones and the S layers. *J. Comp. Neurol.* 213:113-145.
- White, E.L. , and A. Keller (1987) Intrinsic circuitry involving the local axon collaterals of corticothalamic projection cells in mouse SmI cortex. *J. Comp. Neurol.* 262:13-26.
- Wieniawa-Narkiewicz, E., B.M. Wimbome , and G.H. Henry (1992) Area 21a in the cat and the detection of binocular orientation disparity. *Ophthal. Physiol. Opt.* 12:269-272.
- Wimbome, B.M. , and G.H. Henry (1992) Response characteristics of the cells of cortical area-21a of the cat with special reference to orientation specificity. *Journal of Physiology - London* 449:457-478.
- Wong-Riley, M. (1979) Changes in the visual system of monocularly sutured or enucleated cats demonstrable with cytochrome oxidase histochemistry. *Brain Res.* 171:11-28.
- Wong-Riley, M. , and D.A. Riley (1983) The effect of impulse blockage on cytochrome oxidase activity in the cat visual system. *Brain Res.* 261:185-193.
- Wong-Riley, M.T.T. (1994) Primate visual cortex: dynamic metabolic organization and plasticity revealed by cytochrome oxidase. In A. Peters and K.S. Rockland (eds.): *Cerebral Cortex*. New York: Plenum Press, pp. 141-200.
- Wong-Riley, M.T.T., S.C. Tripathi, T.C. Trusk , and D.A. Hoppe (1989) Effect of retinal impulse blockage on cytochrome oxidase-rich zones in the macaque striate cortex: I quantitative electron-microscopic (EM) analysis of neurons. *Visual Neurosci.* 2:483-497.
- Yin, T.C.T. , and M. Greenwood (1992) Visual response properties of neurons in the middle and lateral suprasylvian cortices of the behaving cat. *Exp. Brain Res.* 88:1-14.

- Zeki, S. (1977) Colour coding in the superior temporal sulcus of rhesus monkey visual cortex. *Proc. R. Soc. Lond. B* 197:195-223.
- Zeki, S. (1993) *A vision of the brain*. Boston: Blackwell Scientific Publications.
- Zeki, S. , and S. Shipp (1988) The functional logic of cortical connections. *Nature* 335:311-317.
- Zeki, S.M. (1973) Colour coding in rhesus monkey prestriate cortex. *Brain Res.* 53:422-427.
- Zeki, S.M. (1974) Functional organization of a visual area in the posterior bank of the superior temporal sulcus of the rhesus monkey. *J. Physiol.* 236:549-573.
- Zeki, S.M. (1975) The functional organization of projections from striate to prestriate visual cortex in the rhesus monkey. *Cold Spring Harb. Symp. Quant. Biol.* 40:591-600.
- Zumbroich, T.J. , and C. Blakemore (1987) Spatial and temporal selectivity in the suprasylvian visual cortex of the cat. *J. Neurosci.* 7:482-500.